

**Development of Mass Spectrometry Methods to Study
Protein-Ligand Interactions**

by

Yuyu Yao

A thesis submitted in partial fulfillment of the requirements for the degree of

Master of Science

Department of Chemistry

University of Alberta

© Yuyu Yao, 2016

Abstract

This thesis describes the development of mass spectrometry methods to study protein-ligand interactions in vitro. Liquid sample desorption electrospray ionization mass spectrometry (liquid sample DESI-MS) was first applied to quantify protein-carbohydrate interactions in aqueous ammonium acetate solutions. Protein-carbohydrate interactions were measured using liquid sample DESI-MS were found to be in good agreement with values measured by isothermal titration calorimetry (ITC) and the direct ESI-MS assay. The suitability of liquid sample DESI-MS for quantitative binding measurements carried out using solutions containing high concentrations of phosphate buffered saline (PBS) was also first explored. Binding of lysozyme to β -D-GlcNAc-(1 \rightarrow 4)- β -D-GlcNAc-(1 \rightarrow 4)-D-GlcNAc in aqueous solutions containing up to 1x PBS was successfully monitored using liquid sample DESI-MS; with ESI-MS the binding measurements were limited to concentrations less than \sim 0.02x PBS.

The influence of sulfolane on ESI-MS measurements of protein-ligand affinities was investigated. Having found evidence that sulfolane generally reduces the apparent affinity, a detailed study of the origin of the reduced affinity was carried out using ITC, circular dichroism (CD) and nuclear magnetic resonance (NMR) spectroscopy to establish how sulfolane affects the structure and stability of the protein-ligand complex in solution. Finally, binding measurements performed using liquid sample DESI-MS revealed that the introduction of sulfolane into the ESI solution results in protein supercharging without any loss in affinity.

Preface

This thesis is an original work by Yuyu Yao. The work described in Chapter 2 of this thesis has been published as: Yao, Y., Shams-Ud-Doha, K., Daneshfar, R., Kitova, E. N., Klassen, J. S.. Quantifying Protein-Carbohydrate Interactions Using Liquid Sample Desorption Electrospray Ionization Mass Spectrometry. *J Am Soc Mass Spectrom*, **2015**, 26, 98-106. I was responsible for data collection and analysis, as well as the manuscript composition. Km Shams-Ud-Doha contributed to control experiments of liquid sample DESI. Rambod Daneshfar assisted with instrument set-up and modifications. Elena N. Kitova contributed to manuscript edits. John S. Klassen was the supervisory author. The work described in Chapter 3 has been published as: Yao, Y., Richards, M. R., Kitova, E. N., Klassen, J. S.. Influence of Sulfolane on ESI-MS Measurements of Protein-Ligand Affinities. *J Am Soc Mass Spectrom*, **2016**, 27,498-506. I was responsible for all data collection and analysis, as well as the manuscript composition. Michele R. Richards assisted with the NMR data analysis. Elena N. Kitova contributed to manuscript edits. John S. Klassen was the supervisory author.

Acknowledgement

First of all, I wish to express my deepest gratitude to my supervisor, Professor John S. Klassen, for his valuable inspiration, guidance and support throughout my graduate study. I would like to thank my supervisor and defense committee members, Prof. Robert E. Campbell, Prof. Todd L. Lowary, Prof. Mark T. McDermott and Prof. Julianne M. Gibbs-Davis for their thoughtful and helpful comments into my research. I would like to thank Prof. Michael J. Serpe for his generous encouragement and help.

I also wish to sincerely thank Dr. Elena N. Kitova and Dr. Rambod Daneshfar for their useful advice, technical support and continued encouragement. I would like to give my special thanks to previous and present excellent colleagues in the Klassen group, Dr. Amr El-hawiet, Dr. Lan Liu, Dr. Lu Deng, Dr. Aneika C. Leney, Dr. Ling Han, Dr. Michele R. Richards, Dr. Emma-Dune Leriche, Hong Lin, Yixuan Zhang, Jingjing Zhang, Nobar Jalili, Sanaz Nikjah, Reza Rezaei Darestani, Xuxin Fan, Km Shams-Ud-Doha, Jun Li and Yajie Chen for their helpful advice and encouragement.

I wish to thank the valuable technical instruction and support received from Dr. Simon Ng and Dr. Pavel I. Kitov, Dr. Ryan T. McKay and Mark Miskolzie, and Dr. Jody Groenendyk for isothermal titration calorimetry, nuclear magnetic resonance, and surface plasmon resonance, respectively.

I wish to acknowledge the financial support from Department of Chemistry, University of Alberta.

Finally, I wish to thank my friends and parents for always being by my side.

Table of Contents

Chapter 1 Development of Mass Spectrometry Methods to Study Protein-Glycan Interactions	1
1.1 Introduction.....	1
1.2 Electrospray ionization mass spectrometry	3
1.2.1 Electrospray ionization.....	3
1.2.1.2 NanoESI.....	7
1.2.2 MS instrumentation	8
1.2.2.1 Hybrid quadrupole time of flight mass spectrometer	8
1.2.2.1.1 Quadrupole mass filter.....	9
1.2.2.1.2 Time of flight (TOF)	10
1.2.2.2 Fourier transform ion cyclotron resonance mass spectrometer (FTICR-MS)	11
1.3 Desorption electrospray ionization mass spectrometry (DESI-MS).....	15
1.3.1 Conventional DESI-MS.....	15
1.3.2 Liquid sample DESI	18
1.4 Direct ESI-MS binding assay.....	20
1.5 Potential defects of the direct ESI-MS binding assay.....	22
1.5.1 Non-uniform response factors	22
1.5.2 Nonspecific binding.....	23
1.5.3 In-source dissociation	26
1.6 The present work.....	28
1.7 Literature cited.....	30

Chapter 2 Quantifying Protein-Carbohydrate Interactions Using Liquid Sample Desorption Electrospray Ionization Mass Spectrometry	35
2.1 Introduction.....	35
2.2 Experimental section.....	37
2.2.1 Materials	37
2.2.2 Mass spectrometry.....	38
2.2.3 Isothermal titration calorimetry	40
2.2.4 Data analysis.....	41
2.3 Results and discussion	44
2.3.1 Binding of Lyz to L2 and L3	47
2.3.2 Binding of scFv to L4 and L5.....	50
2.3.3 Comparison of liquid sample DESI-MS and reactive liquid sample DESI-MS	53
2.3.4 Tolerance of liquid sample DESI-MS to non-volatile salts.....	55
2.4 Conclusions.....	59
2.5 Literature cited.....	60
Chapter 3 Influence of Sulfolane on ESI-MS Measurements of Protein-Ligand Affinities.....	63
3.1 Introduction.....	63
3.2 Experimental	66
3.2.1 Materials	66
3.2.2 Mass spectrometry.....	66
3.2.3 Isothermal titration calorimetry	68

3.2.4 Circular dichroism	68
3.2.5 NMR spectroscopy	68
3.2.6 Data analysis.....	69
3.2.6.1 Average charge state calculation	69
3.2.6.2 Association constants from ESI mass spectra.....	70
3.2.6.3 Determination of association constants for stepwise binding of L3 to CTB ₅	70
3.3 Results and discussion	71
3.3.1 Influence of sulfolane on protein-carbohydrate affinities	71
3.3.2 Influence of sulfolane on the (Lyz + L1) complex in solution.....	78
3.3.3 Supercharging and liquid sample DESI-MS	90
3.4 Conclusions.....	92
3.5 Literature cited.....	94
Chapter 4 Conclusions and Future Work	97
4.1 References.....	100
Bibliography	101

List of Tables

Table 2.1 Comparison of association constants (K_a) measured by liquid sample DESI-MS, ESI-MS and ITC for the interactions of L2 and L3 with Lyz and L4 and L5 with scFv in aqueous ammonium acetate solutions at pH 6.8 and 25 °C. ^a	49
---	----

List of Figures

Figure 1.1 Schematic representation of the electrospray ionization process. Adapted from reference 36.....	4
Figure 1.2 Summary of ESI models: (a) IEM: Small ion ejection from a charged nanodroplet; (b) CRM: Formation of a globular protein into the gas phase; (c) CEM: Ejection of an unfolded protein.....	6
Figure 1.3 Schematic representation of the Waters Synapt G2 nanoESI Q-IMS-TOF mass spectrometer, adapted from the Waters user's manual.	8
Figure 1.4 Schematic representation of the quadrupole in Waters Synapt G2 Q-IMS-TOF mass spectrometer.	9
Figure 1.5 Schematic diagrams of the Bruker Apex-II 9.4T FTICR mass spectrometer coupled with nanoESI source, adapted from the Bruker user's manual.	11
Figure 1.6 Illustration of the circular motion of a positive ion with charge q moving at velocity \mathbf{v} in the presence of a constant magnetic field, \mathbf{B} , which is pointing orthogonal to the plane of the motion. A downward Lorentz force is generated if the ion moves to the left, $\mathbf{F} = q(\mathbf{v} \times \mathbf{B})$, $q = ze$, which leads to the ion moves counterclockwise.	13
Figure 1.7 Illustration of excitation, image current detection and the production of mass spectrum by FTICR.....	14
Figure 1.8 Schematic representation of typical DESI instrument, adapted from reference 65.....	16
Figure 1.9 Schematic representation of the liquid sample DESI used in this study.	19
Figure 1.10 Cartoon representation of the formation of nonspecific protein-ligand interactions (false positive), adapted from reference 30.....	24

Figure 2.1 Representative liquid sample DESI mass spectra acquired in positive ion mode for aqueous ammonium acetate (20 mM) solutions containing (a) Lyz (10 μ M), and (b) scFv (10 μ M). The ESI spray solution was 50/50 water/acetonitrile. 40

Figure 2.2 Representative liquid sample DESI mass spectra acquired in positive ion mode for aqueous ammonium acetate (20 mM, pH 6.8 and 25 $^{\circ}$ C) solutions containing Ubq (10 μ M), Lyz (10 μ M) and L1 at (a) 15 μ M or (b) 40 μ M concentrations. The ESI spray solution was 50/50 water/acetonitrile..... 43

Figure 2.3 ITC data measured for the binding of Lyz (0.087 mM) to L2 (2.0 mM) in aqueous ammonium acetate (50 mM, pH 6.8 and 25 $^{\circ}$ C) solutions. 45

Figure 2.5 Representative (a), (c) liquid sample DESI and (b), (d) ESI mass spectra acquired in positive ion mode for aqueous ammonium acetate (20 mM, pH 6.8 and 25 $^{\circ}$ C) solutions containing Lyz (10 μ M), L2 (15 μ M) and Ubq (5 μ M) ((a) and (b)) or Lyz (10 μ M), L3 (15 μ M) and Ubq (5 μ M) ((c) and (d)). For the liquid sample DESI-MS measurements, the ESI spray solution was 50/50 water/acetonitrile..... 48

Figure 2.6 Representative (a), (c) liquid sample DESI and (b), (d) ESI mass spectra acquired in positive ion mode for aqueous ammonium acetate (20 mM, pH 6.8 and 25 $^{\circ}$ C) solutions containing scFv (10 μ M), L4 (15 μ M) and Lyz (5 μ M) ((a) and (b)) or scFv (10 μ M), L5 (40 μ M) and Lyz (5 μ M) ((c) and (d)). For the liquid sample DESI-MS measurements, the ESI spray solution was 50/50 water/acetonitrile..... 51

Figure 2.7 Representative reactive liquid sample DESI mass spectrum acquired in positive ion mode for an aqueous ammonium acetate (20 mM, pH 6.8 and 25 $^{\circ}$ C) solution containing Lyz (10 μ M) and Ubq (5 μ M) and an ESI spray solution (50/50 water/acetonitrile) that contained L2 (50 μ M). The flow rates of both the sample and ESI

spray solution were $5 \mu\text{L min}^{-1}$. All other instrumental conditions were identical to those used for the liquid sample DESI measurements. 54

Figure 2.8 Representative (a), (b) and (c) liquid sample DESI and (e), (f) and (g) ESI mass spectra acquired for aqueous solutions (pH 7.4 and 25 °C) containing Lyz (40 μM) and L2 (30 μM) in 20 mM ammonium acetate and 0.1x PBS ((a) and (d)), 0.5X PBS ((b) and (e)) and 1x PBS ((c) and (f)). For the liquid sample DESI-MS measurements, the ESI spray solution was 50/50 water/acetonitrile..... 56

Figure 2.9 ITC data measured for the binding of Lyz (0.128 mM) to L2 (2.0 mM) in 1x PBS (pH 7.4 and 25 °C)..... 57

Figure 3.1 Representative ESI mass spectra acquired in positive ion mode for aqueous ammonium acetate (50 mM) solutions of Lyz (10 μM), L1 (15 μM) and P_{ref} (Ubq, 5 μM) with (a) 0% sulfolane and (b) 2% sulfolane, or scFv (10 μM), L2 (15 μM) and P_{ref} (Lyz, 5 μM), with (c) 0% sulfolane and (d) 2% sulfolane. Nonspecific sulfolane adducts are labelled as “S”..... 73

Figure 3.2 Representative ESI mass spectra acquired in positive ion mode for aqueous ammonium acetate (50 mM) solutions of CTB₅ (5 μM), L3 (5 μM) and P_{ref} (scFv, 3 μM) with (a) 0% sulfolane and (b) 2% sulfolane, or Gal3-C (10 μM), L4 (10 μM) and P_{ref} (Ubq, 5 μM) with (c) 0% sulfolane and (d) 2% sulfolane. Nonspecific sulfolane adducts are labelled as “S”..... 74

Figure 3.3 Plot of average charge state (*ACS*) of the (Lyz + L1) ions observed from ESI mass spectra acquired for aqueous ammonium acetate (50 mM) solutions of Lyz (10 μM), L1 (15 μM) and Ubq (5 μM) with 0 – 10% sulfolane. Also shown are the association

constants (K_a) for the (Lyz + L1) interaction measured by ESI-MS and isothermal titration calorimetry (ITC).....	75
Figure 3.4 ITC profiles obtained for the binding of Lyz (0.2 mM) to L1 (2.0 mM) in aqueous ammonium acetate (50 mM, pH 6.8 and 25 °C) solution containing 2% (v/v) sulfolane. Raw data are shown in the top panel, in the lower panel integrated data (black squares) and fitting curve (solid red line) obtained using Origin 8.0 and a single site binding model, are presented. The inset in the lower panel shows best fit parameters: stoichiometry (N), association constant ($K \equiv K_a$) and enthalpy of association (ΔH). The entropy of association (ΔS) was calculated from the free energy ($\Delta G = -RT \ln K$) and enthalpy values ($\Delta G = \Delta H - T\Delta S$).....	79
Figure 3.6 ITC profiles obtained for the binding of Lyz (0.2 mM) to L1 (2.0 mM) in aqueous ammonium acetate (50 mM, pH 6.8 and 25 °C) solution containing 10% (v/v) sulfolane. Raw data are shown in the top panel, in the lower panel integrated data (black squares) and fitting curve (solid red line) obtained using Origin 8.0 and a single site binding model, are presented. The inset in the lower panel shows best fit parameters as described in Figure 3.4	81
Figure 3.7 CD spectra acquired for an aqueous phosphate buffer (20 mM, pH 7.0) solutions of Lyz (56 μ M) and sulfolane (0-20%).....	82
Figure 3.8 Natural abundance ^1H - ^{15}N gHSQC NMR spectrum for Lyz in 10% (v/v) D_2O - H_2O . Backbone NH signals were assigned based on comparisons with literature values (reference 51 and 52).....	83
Figure 3.9 Natural abundance ^1H - ^{15}N gHSQC NMR spectra were obtained for lysozyme in 10% (v/v) D_2O - H_2O with varying concentrations of sulfolane – 0, 2, 5, and 10% (v/v).	

Backbone NH signals for lysozyme in 10% (v/v) D ₂ O–H ₂ O were assigned based on comparisons with literature values (reference 51 and 52).	84
Figure 3.10 Natural abundance ¹ H– ¹⁵ N gHSQC NMR spectrum for denatured lysozyme in 8M urea and 10% (v/v) D ₂ O–H ₂ O.	85
Figure 3.11 a) ¹ H NMR spectrum of L1 in D ₂ O. b) ¹ H NMR spectrum of L1 in 2% (v/v) sulfolane–D ₂ O.	86
Figure 3.12 TROESY spectra of L1 in D ₂ O (green) and L1 in 2 % (v/v) sulfolane-D ₂ O (blue).	87
Figure 3.13 Natural abundance ¹ H– ¹⁵ N gHSQC NMR spectrum for Lyz (black) and lysozyme with the tetrasaccharide ligand L1 (blue) in 10% (v/v) D ₂ O–H ₂ O. Backbone NH signals were assigned based on comparisons with literature values (reference 51 and 52).	88
Figure 3.14 Natural abundance ¹ H– ¹⁵ N gHSQC NMR spectra were obtained for Lyz with L1 in 10% (v/v) D ₂ O–H ₂ O with varying concentrations of sulfolane – 0, 2, 5, and 10% (v/v). Backbone NH signals for Lyz in 10% (v/v) D ₂ O–H ₂ O were assigned based on comparisons with literature values (reference 51 and 52).	89
Figure 3.15 Liquid sample DESI mass spectra acquired in positive ion mode for aqueous ammonium acetate (20 mM) solutions of Lyz (10 μM), L1 (15 μM) and Ubq (5 μM) using an ESI spray solvent (ACN:H ₂ O=50:50, v/v) containing (a) 0% sulfolane and (b) 0.5% sulfolane.	91

List of Abbreviations

<i>Ab</i>	Abundance of gas-phase ions
<i>Ab_{app}</i>	Apparent abundance of gas-phase ions
Abe	Abequose
<i>ACS</i>	Average charge state
BIRD	Blackbody infrared radiative dissociation
CaR	Catch-and-release
CEM	Chain ejection model
CD	Circular dichroism
CID	Collision induced dissociation
CRM	Charge residue model
CTB ₅	Cholera toxin B subunit homopentamer
Da	Dalton
DC	Direct current
DESI	Desorption electrospray ionization
ECD	Electron capture dissociation
ELISA	Enzyme-linked immunosorbent assay
ESI	Electrospray ionization
ESI-MS	Electrospray ionization mass spectrometry
ETD	Electron transfer dissociation
FTICR	Fourier transform ion cyclotron resonance
Fuc	Fucose
Gal	Galactose

Gal-3C	The C-terminal fragment of human galectin-3
GalNAc	N-acetylgalactosamine
Glc	Glucose
GlcNAc	N-acetylglucosamine
H	Hydrogen
H-bond	Hydrogen bond
HEPES	4-(2-hydroxyethyl)-1-piperazineethanesulfonic acid
HMOs	Human milk oligosaccharides
HPLC	High performance liquid chromatography
i.d.	Inner diameter
IEM	Ion evaporation model
IMS	Ion mobility separation
IS	Internal standard
ITC	Isothermal titration calorimetry
K_a	Association constant
$K_{a,app}$	Apparent association constant
L	Ligand
Lyz	Lysozyme
m/z	Mass-to-charge ratio
<i>m</i> -NMA	3-nitrobenzoic acid
Man	Mannose
MS	Mass spectrometry
MW	Molecular weight

nanoESI	Nanoflow electrospray ionization
N	Nitrogen
Neu	Neuraminic acid
Neu5Ac	N-Acetylneuraminic acid
NMR	Nuclear magnetic resonance
O	Oxygen
o.d.	Outside diameter
P	Protein
PBS	Phosphate buffered saline
PL	Protein-ligand complex
P _{ref}	Reference protein
Pt	Platinum
Q-IMS-TOF	Quadrupole-ion mobility separation time-of-flight
<i>R</i>	Abundance ratio
<i>RF</i>	Response factor
RF	Ratio frequency
S/N	Signal to noise ratio
scFv	Single chain variable fragment
SPR	Surface plasmon resonance spectroscopy
TOF	Time of flight
Tris	Tris(hydroxymethyl) aminomethane
TWIMS	Travelling wave ion mobility spectrometry
Ubq	Ubiquitin

v/v

Volume per volume

Chapter 1

Development of Mass Spectrometry Methods to Study Protein-Glycan Interactions

1.1 Introduction

Protein-ligand interactions play essential roles in many physiological and pathological events, including cell-cell communication, signal transduction, immune response, and host-pathogen interactions.¹⁻⁶ The non-covalent interaction of proteins and glycan is primarily driven by hydrogen bond (H-bond) networking and van der Waals force.⁷ In order to obtain a fundamental understanding of many important cellular processes, to instruct drug discovery, and to develop effective new therapeutics, it is extremely important to characterize structural information, thermodynamic and kinetic parameters of protein-glycan interactions. There are a certain number of well-established analytical methods available to study protein-glycan interactions in vitro, each method possesses particular strengths and weaknesses. Several methods are introduced below, which are extensively used for detection and characterization of protein-carbohydrate interactions, including isothermal titration calorimetry (ITC),⁸ surface plasmon resonance (SPR),⁹ nuclear magnetic resonance (NMR) spectroscopy,¹⁰ and enzyme-linked immunosorbent assay (ELISA).¹¹

ITC is generally considered as the “gold standard” method for studying non-covalent interactions of biological complexes, such as protein-carbohydrate interactions. It is the only method that can directly and accurately provide thermodynamic data (e.g. Gibbs free energy, enthalpy, and entropy) of protein-carbohydrate interactions from a single experiment, as well as association constant (K_a).¹²⁻¹³ Conventional ITC instruments consume relative large quantities (~mg) of raw materials, exhibit low sensitivity, and low

throughput (~3 measurements / day). Meanwhile, Nano ITC instruments were developed with improved sensitivity and lower sample consumption.¹⁴

SPR is one of the most widely used methods to study protein-carbohydrate interactions and is able to provide kinetic insights of interested interactions with high sensitivity and low sample consumption (~ng). It can provide not only K_a data, but also the association and dissociation rate constants.¹⁵⁻¹⁹ However, one of the binding partners needs to be immobilized on the SPR sensor chip, which may alter the nature of interactions.

NMR is also a popular technique to study protein-carbohydrate interactions, because NMR could provide geometry information of protein-carbohydrate interactions at atomic level, as well as the strength of interactions.²⁰⁻²² Unfortunately, several factors limit applications of NMR, such as molecular weights (<40 kDa),²² amount of sample (~mg), and throughput capacity (~1 measurement / day).

ELISA is a reliable competitor of favored methods used for studying protein-carbohydrate interactions, because its simplicity, sensitivity and low cost.²³⁻²⁴ In conventional ELISA, however, the immobilization and modification to binding partners may not be able to reflect their true nature of interactions, and large immobilization surface area could be a potential factor to produce nonspecific binding and increase background noise.²⁴

Recently, electrospray ionization mass spectrometry (ESI-MS) has emerged as a powerful method for detecting protein-carbohydrate complexes in solution and measuring the affinities of the interactions *in vitro*.²⁵⁻³⁰ The ESI-MS measurements are fast and can often be completed within few minutes, the amount of sample consumed is low (~pmol), and there is no requirement for labeling or immobilization, which makes the assay very

versatile.³⁰ Moreover, the direct ESI-MS assay is the only technique that directly measures binding stoichiometry.³⁰

Desorption electrospray ionization mass spectrometry (DESI-MS) and liquid sample DESI-MS were developed through last decade and are becoming powerful tools to study protein-carbohydrate interactions.³¹⁻³² (Liquid sample) DESI-MS possesses all ESI-MS advantages, and analyzes sample with low or no pre-treatment.³¹⁻³⁵

This thesis mainly focuses on the development of mass spectrometry methods to study protein-glycan interactions. Before I start to describe those strategies that have been studied, it is necessary to give an overview of ionization methods and mechanisms, as well as instrumentations, associated with those studies described in following chapters.

1.2 Electrospray ionization mass spectrometry

1.2.1 Electrospray ionization

Several ionization methods were developed before ESI-MS, including electron ionization, chemical ionization, etc., but none of them could overcome the challenge of analyte fragmentation.³⁶ Therefore, these methods are not able to precisely detect and measure the molecular weight of biological macromolecules, such proteins. Two decades ago, Fenn and co-workers introduced a new ionization method: electrospray ionization (ESI), which is recognized as a soft ionization technique, to ionize intact macromolecules (proteins) by multiple charging without fragmentation.³⁷ In addition, weak noncovalent interactions could be preserved during ionization process,³⁸ which is an ideal technique to study noncovalent interaction between protein and ligand for mass spectrometry.

The ESI mechanism was described by Kebarle and co-workers in detail.³⁹ Following are several important stages involved in the ESI process to bring ionic species from solution into gas phase.

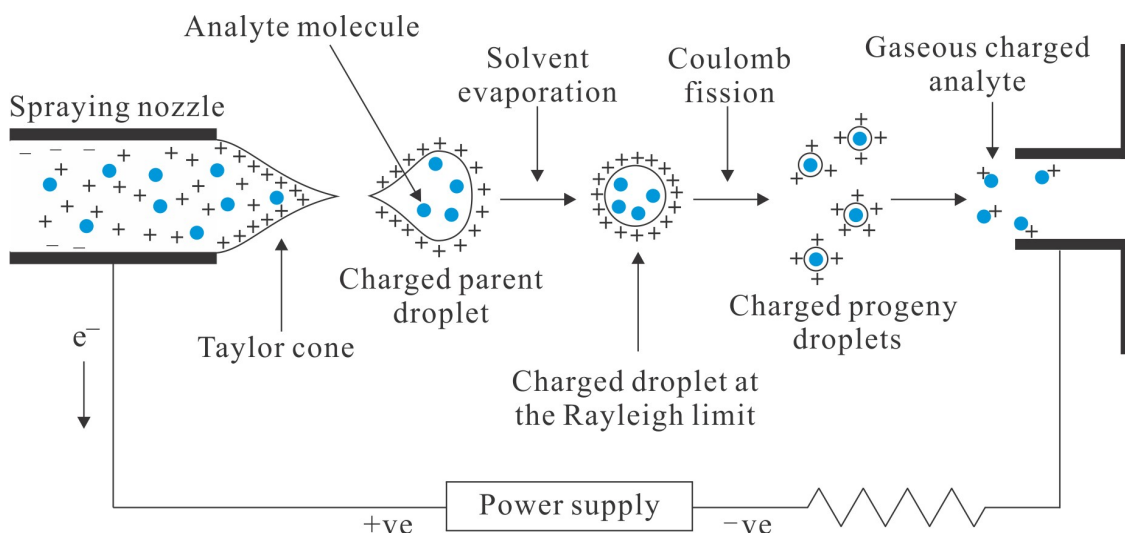


Figure 1.1 Schematic representation of the electrospray ionization process. Adapted from reference 36.

(a) Production of charged droplets

As shown in Figure 1.1, the schematic diagram describes the ESI process in the position ion mode. A high voltage (\sim kV) is applied to the capillary and separating charged electrolytes in solution. The positive charged ions drift to the liquid surface, while the negative charged ions drift away to the anode. The accumulation of positive ions leads to the formation of a liquid cone, which is so-called Taylor cone,⁴⁰ and generated by the electrical field competing with the resistance of the liquid surface tension. Under sufficient electric field, the Taylor cone becomes unstable and emits charged droplets that containing

analyte molecules.⁴⁰ The initial parent droplets usually have radii in the micrometer scale.³⁹

(b) Solvent evaporation and shrinkage of charged droplets

Along with the solvent evaporation, initial parent droplets are shrinking to smaller size, which is increasing the electric field of droplets while the charges stay same on the same droplet. In most cases, ambient gas, such as air, provides the thermal energy required for solvent evaporation. The droplet size becomes smaller during evaporation and the charge density on the droplet increases until the “Rayleigh limit”,⁴¹ the limit indicates that the surface tension of the droplet could bear with the maximum extent of the Coulombic repulsion caused by surface charges. Once this limit is exceeded and broke, droplets would undergo Coulomb fission that releases a jet of smaller and charged progeny droplets. Evaporation and fission events were repeated to create final generation of ESI nanodroplets, which have radii within few nanometers.³⁹

(c) Production of gas-phase ions

These very small and highly charged droplets would then form gas-phase ions, which may undergo different ionization models, such as ion evaporation model (IEM), charged residue model (CRM), and chain ejection model (CEM).^{37, 39, 42-44}

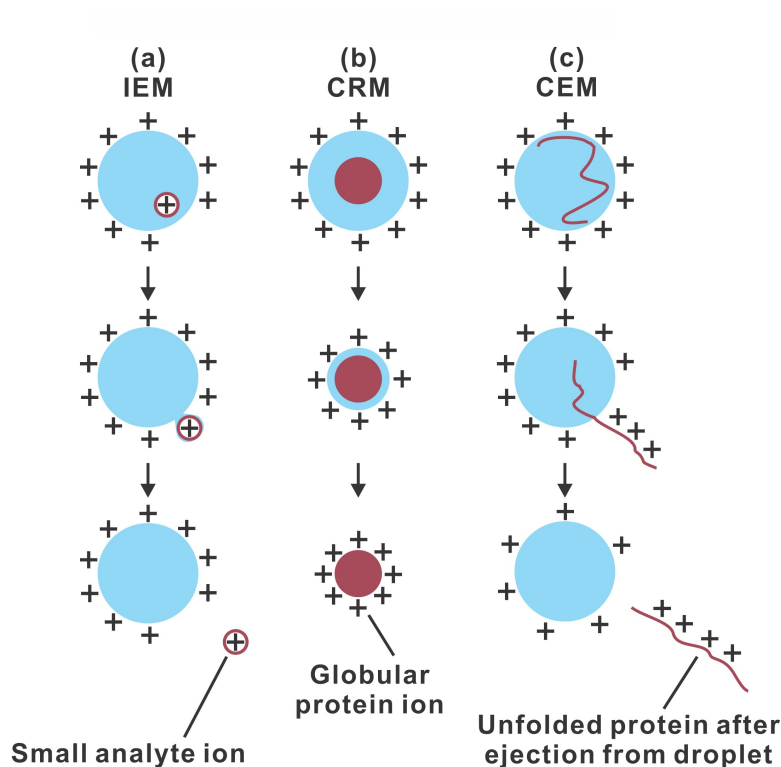


Figure 1.2 Summary of ESI models: (a) IEM: Small ion ejection from a charged nanodroplet; (b) CRM: Formation of a globular protein into the gas phase; (c) CEM: Ejection of an unfolded protein.

(i) The ion evaporation model (IEM):⁴⁵ small (organic or inorganic) ions in bulk solution would like to be transferred into gas phase via IEM model.⁴⁵⁻⁵¹ Because the high electric field in highly charged nanodroplets ($R \leq 10$ nm) is sufficient to cause to eject small solvated ions from droplets. In addition, small analyte ions prefer to be close to the droplet surface, which in turn assists the IEM ejection.

(ii) The charged residue model (CRM):⁵² For large globular species (e.g. natively folded proteins), it is widely accepted that CRM plays a major role in the ESI process.⁵² During CRM, nanodroplets containing a single analyte molecule evaporate to dryness, and

the charges on the droplet are transferred to the analyte ion.^{39,53} Meanwhile, Rayleigh limit applies to the whole ionization process. Therefore, the final number of charges pass onto the analyte ion may smaller than the number of charges on the vanishing nanodroplet, where the charge reduction can undergo IEM to eject solvated proteins and small ions.⁴⁴

(iii) The chain ejection model (CEM):⁵⁴⁻⁵⁵ It is believed that unfolded proteins undergo ionization process via CEM. Unfolding process alters the characteristics of proteins from compact and hydrophilic to be extended and hydrophobic, which leads unfolded proteins to migrate to the droplet surface.⁵⁶ Following, the unfolded peptide chain gets ejected from the droplet.⁴⁴ Therefore, the CEM is considered, in some extent, as similar to the IEM, whereas it is completely different from the CRM.

1.2.1.2 NanoESI

In the present work, nanoESI was performed in all ESI-MS measurements using narrow glass tips with an emitter tip opening within only a few microns. NanoESI has the same ionization mechanisms of ESI, but it operates at lower solution flow (10-50 $\mu\text{L}/\text{min}$) rates and emits smaller droplets than conventional ESI (1-10 $\mu\text{L}/\text{min}$).⁵⁷ Thus, only a small amount ($\sim\text{pmol}$) of sample is required per analysis,⁵⁸ which is a very important feature to quantity limited biological molecules. In addition, the smaller droplets from nanoESI undergo less evaporation/fission events, and have shorter lifetimes than those droplets from conventional ESI, which may help preserve the original solution composition during the ionization process. Furthermore, nanoESI can minimize nonspecific interactions that occur during ESI process since there will be less analyte molecules per droplet.⁵⁹⁻⁶⁰ These important features of nanoESI make it more favorable for studying non-covalent protein complexes directly by MS.

1.2.2 MS instrumentation

In the present study, nanoESI combined with hybrid quadrupole time of flight mass spectrometer and Fourier transform ion cyclotron resonance (FTICR) mass spectrometer were used. Besides, there are several other different types of mass analyzers included in this study, such as ion trap, quadrupole and magnetic sector.

1.2.2.1 Hybrid quadrupole time of flight mass spectrometer

Shown in Figure 1.3 is the schematic representation of the Synapt G2 quadrupole ion mobility separation time-of-flight (Q-IMS-TOF) mass spectrometer (Waters UK Ltd., Manchester, UK), equipped with a nanoflow ESI (nanoESI) source was used (Chapter 2, 3 & 4). Gaseous analyte ions are produced from buffered solutions by nanoESI source performed at ambient pressure by applying a high voltage (+/- 1000 V) to a platinum (Pt) wire inserted into the solution inside the glass tip.

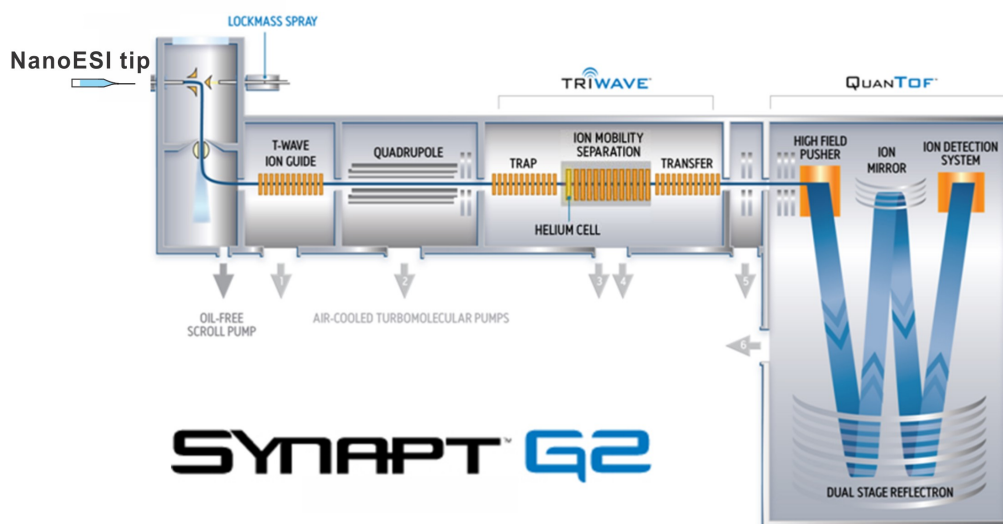


Figure 1.3 Schematic representation of the Waters Synapt G2 nanoESI Q-IMS-TOF mass spectrometer, adapted from the Waters user's manual.

The Waters Synapt G2 nanoESI Q-IMS-TOF mass spectrometer was used, because of its wide mass range and high sensitivity. Since the IMS feature was not used in this study, therefore, only a brief overview of the quadrupole and TOF components in this instrument is given below.

1.2.2.1.1 Quadrupole mass filter

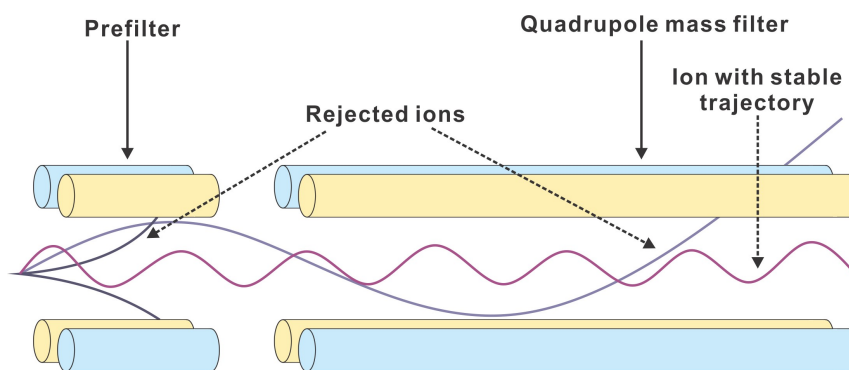


Figure 1.4 Schematic representation of the quadrupole in Waters Synapt G2 Q-IMS-TOF mass spectrometer.

The quadrupole consists of four cylindrical metal rods, which are precisely positioned in a radial array and the diametrically opposed rods are paired. A direct current (DC) potential and a radiofrequency (RF) potential, 180° out of phase, are applied to each pair of rods.⁶¹ Based on the specific voltage and frequency applied, ions of particular mass-to-charge (m/z) ratio can be selected and transit through the entire length of the rods, while other ions that outside the m/z range would hit the rods and be expelled. By turning off the DC voltages and only operating in the RF mode, the quadrupole can also be a broad bandpass filter that transmits and guides ions over a wide m/z range to the following components of the instrument. In this Synapt G2 mass spectrometer, the quadrupole

consists of two parts, a quadrupole prefilter and a quadrupole mass filter (Figure 1.4). The use of prefilter could minimize the effects of fringing fields at the entrance of quadrupole, and, therefore, increase the absolute sensitivity.

1.2.2.1.2 Time of flight (TOF)

For the time of flight (TOF) analyzer, the physical property that is measured during an analysis is the flight time of ions.⁶² The m/z values are determined by measuring the time that the ions take to move through a field-free region (flight tube) between the source and the detector, according to eq 1.1:

$$\sqrt{m/z} = t \left(\frac{\sqrt{2eV_s}}{L} \right) \quad (1.1)$$

Where m is the mass of the ion, z is the charge state of the ion, e is the elementary charge, V_s is the acceleration potential, t is the flight time and L is the length of the flight tube. This equation indicates that m/z can be calculated from measuring the flight time (t). The higher the mass of an ion, the slower it will reach the detector. There are two types of TOF analyzers, which are linear TOF analyzer and reflectron TOF analyzer. However, due to initial energy distribution, ions of the same m/z would reach the detector at different times in the linear TOF analyzer.

The reflectron TOF analyzer is used in Waters Synapt G2 mass spectrometer, because the reflectron TOF analyzer can compensate the energy distribution of ions by using successive sets of electric grids of increasing potential which deflects the ions and reverses their flight direction sending them back through the flight tube. Therefore, ions of the same m/z will pierce into the field at different depths, e.g. ions with more kinetic energy and faster velocity will penetrate the field more deeply than those ions with lower kinetic

energy. As a consequence, these faster ions spend more time in the reflectron and will arrive at the detector at the same time as the slower ions at the same m/z . This effect has improved mass resolution, especially in the range of 10,000 – 20,000 with minimal loss in sensitivity.

1.2.2.2 Fourier transform ion cyclotron resonance mass spectrometer (FTICR-MS)

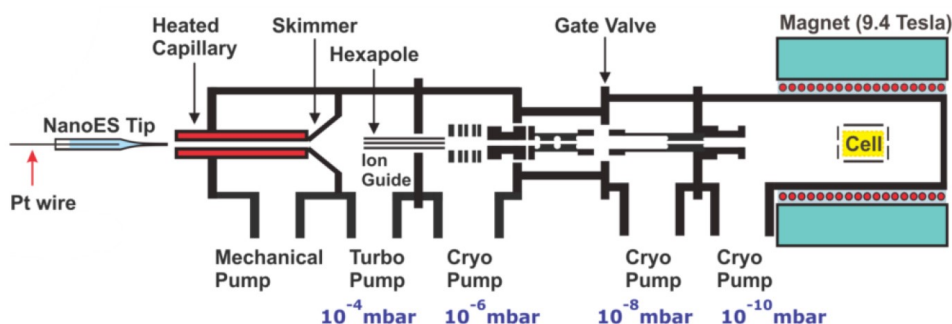


Figure 1.5 Schematic diagrams of the Bruker Apex-II 9.4T FTICR mass spectrometer coupled with nanoESI source, adapted from the Bruker user's manual.

Shown in Figure 1.5 is a schematic diagram of the Bruker Apex-II 9.4T FTICR mass spectrometer coupled with nanoESI source. Small droplets produced from nanoESI tip are transmitted through a heated metal capillary for completion of ionization process to form gaseous ions. Then these gaseous ions are transmitted through a skimmer and accumulated in the hexapole for a preset time period to enhance the signal-to-noise (S/N) ratio. After accumulation, analyte ions will be ejected from the hexapole and accelerated by a high voltage through the fringing field of a 9.4T superconducting magnet. Then these ions will be decelerated and trapped by a combinational manipulation of electric and magnetic field in FTICR cell for detection. Very low base pressure ($\sim 5 \times 10^{-10}$ mbar) is maintained by the differential pumping system.

FTICR-MS was used in this study for its high resolving power and mass accuracy. The general operating principles of FTICR have been described in many reviews.⁶³⁻⁶⁴ Only a brief overview is therefore given here. There are three pairs of plates (trapping, excitation and detection) in the ICR cell, which is located inside a spatial uniform static superconducting high field magnet and cooled by liquid helium and liquid nitrogen. When the ions enter into the magnetic field, they become circular motions in a plane perpendicular to the field (see Figure 1.6) according to the Lorentz force law (eq. 1.2)

$$\omega_c = \frac{qB}{m} = \frac{zeB}{m} \quad (1.2)$$

Where ω_c is the cyclotron frequency, q is the charge of the ion ($q = z \cdot e$, where z and e are the charge and the elementary charge, respectively), B is the magnetic field strength and m is the mass of the ion. Because $\omega_c = 2\pi f$, so the results in radian per second has to be divided by 2π to obtain the cyclotron frequency in Hertz (f). An important feature of equation 1.2 is that all ions of a same m/z rotate at the same frequency, which is independent of their velocities. The insensitivity of the cyclotron frequency to the kinetic energy of an ion directly leads to the ultra-high resolution achieved by FTICR-MS.

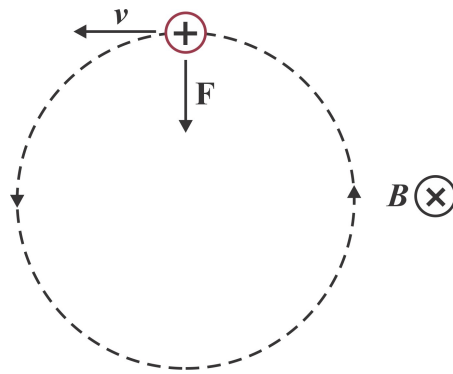


Figure 1.6 Illustration of the circular motion of a positive ion with charge q moving at velocity \mathbf{v} in the presence of a constant magnetic field, \mathbf{B} , which is pointing orthogonal to the plane of the motion. A downward Lorentz force is generated if the ion moves to the left, $\mathbf{F} = q (\mathbf{v} \times \mathbf{B})$, $q = ze$, which leads to the ion moves counterclockwise.

Measurable signal will not be generated if ions keep moving in cyclotron orbits in a static magnetic field. In order to make it detectable for ions trapped in the ICR cell, a packet of ions with same m/z needs to be excited by applying an oscillating electrical field (e.g. AC signal generator). If the frequency of the applied electrical field is same as the ω_c of ions, these ions will absorb energy and then increase their orbital radius while keep a constant cyclotron frequency. Shown in Figure 1.7 is the spiral trajectory of the excited ions that have the same m/z and ω_c .

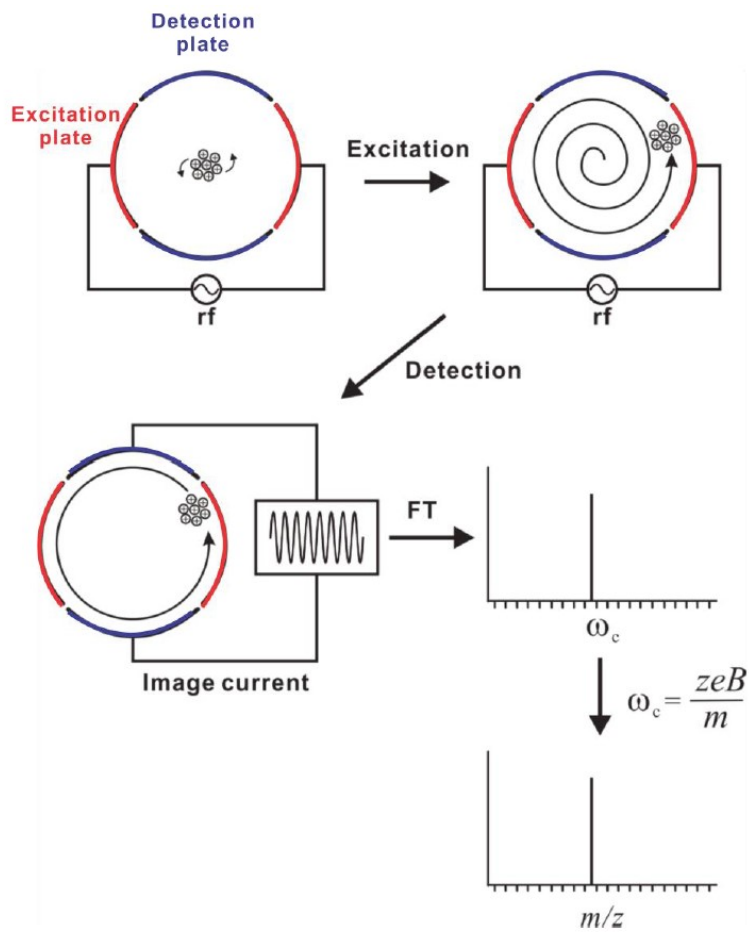


Figure 1.7 Illustration of excitation, image current detection and the production of mass spectrum by FTICR.

When the coherently orbiting excited ions passing another opposing pair of detection electrodes of the cell, which is also parallel to the magnetic axis, they produce an alternating current, called image current (Figure 1.7). The amplitude of this image current is proportional to the amount of ions in the analyzer ICR cell, while the frequency of the alternating current is same as the cyclotron frequency of ions. FT transforms the detected image current into the frequency domain signal from time domain signal, and then a mass spectrum could be generated since the ω_c is m/z related (eq 1.2). Analyte ions can be

detected without collision to the electrodes after the signal is amplified; therefore, the detection method is nondestructive, which allows for improvement of sensitivity and versatility of FTICR. Meanwhile, the ω_c can be measured at very high precision, and the mass accuracy of FTICR-MS can achieve 1 ppm. The amazing resolving power of FTICR-MS is normally able to achieve hundreds of thousands at the broad band mode, which is measuring the full width at half maximum (FWHM) of peaks on mass spectrum. The higher the magnetic field is used and the longer the acquisition time is obtained, the higher resolving power will be. The acquisition time is the time used for detection phase. Longer acquisition time results in larger dataset size and higher resolution in spectrum. In order to avoid the collision of analyte ions with gas particles and the deactivation of analyte ions, high vacuum (10^{-10} mbar) is crucial in the FT cell.

1.3 Desorption electrospray ionization mass spectrometry (DESI-MS)

1.3.1 Conventional DESI-MS

Desorption electrospray ionization (DESI) was introduced by Graham Cooks and co-workers from Purdue University in 2004.⁶⁵ DESI-MS requires minimal or no sample preparation.⁶⁵ Through last decade, DESI has become a popular and powerful ambient ionization method, because, at a certain extent, of its robustness and -applicability to extensive analyte types, as well as the low cost to build a DESI source.⁶⁶ Due to similar ionization mechanism, mass spectra obtained from DESI-MS are very similar to those yielded by ESI-MS. In addition, DESI-MS capable of all the attractive characteristics of ESI-MS (i.e., sensitivity, selectivity, and speed of analysis), therefore, DESI-MS has been increasingly applied to directly identify explosives, pharmaceutical compounds, proteins

and a range of biological materials.⁶⁷ Thus, it is important to understand the ionization processes in DESI.

A brief mechanistic overview of DESI is described below. Shown in Figure 1.8 is schematic representation of typical DESI instrument.

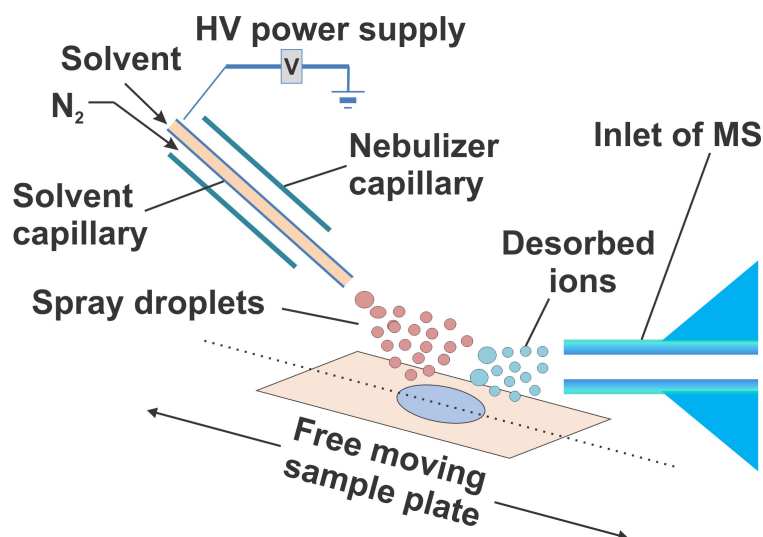


Figure 1.8 Schematic representation of typical DESI instrument, adapted from reference 65.

The production of gaseous analyte ions from typical DESI instrument takes place in four major steps via so-called “droplet pick-up” mechanism.⁶⁸

(1) Formation of a high-speed jet of charged ESI droplets

The high-speed jet of charged ESI droplets is generated by a high voltage applied to a solvent solution, which is commonly a mixture of H₂O and organic solvent,⁶⁹ along with a nebulizing sheath gas. The solvent spray consists of droplets with sizes ranging from 1 to 10 microns and velocities more than 100 m/s that depend on the capillary diameter, the applied voltage, composition and flow rate of the solvent, and the sheath gas velocity.⁷⁰⁻⁷¹

The primary solvent droplets start to lose velocity once they have been made due to

collisions with ambient atmospheric molecules. However, the distance, traveled by primary droplets from the emission at the end of solvent capillary to the collision at the sample surface is usually within few millimeters. Therefore, the primary droplet diameters and velocities are nearly the same as their initial values when they arriving at the sample surface.⁷¹

(2) Creation of a thin liquid layer on sample surface

When the solvent spray impacts the sample surface, a thin liquid film is formed. The solvent accumulated at the sample surface undergoes secondary droplet emission and the process of solvent evaporation under the strong sheath gas flow. Therefore, equilibrium is achieved on the sample surface between the deposition and vanishing of solvent, which plays an important role in stable and reproducible analysis.⁷²

(3) Dissolution and desorption of analytes from solid phase into liquid phase

The dissolution of analyte takes place between the thin liquid layer and the sample surface. The analyte solubility plays a crucial role during ambient dissolution and extraction process. The signal on DESI mass spectra is positive correlation to the solubility of analytes.^{66,69,73} Meanwhile, primary droplets impacting the thin liquid film result in the production of secondary droplets containing analytes, which is the desorption process. Thus, solid sample dried on the surface is successfully transferred to secondary droplets flying to the mass spectrometer inlet.⁷⁴

(4) Production of secondary droplets containing analytes

Secondary droplets are generated by the momentum transfer from the high-speed primary droplets, and are composed of liquid from both the primary spray and the thin liquid film. However, the geometric parameters in the DESI instruments, such as the

distance of the solvent capillary tip to the sample surface and the sheath gas velocity, can affect desorption process and the production of secondary droplets.⁶⁸ High gas flow rate improves evaporation of droplets, which can be compensated, at some extent, by increasing the solvent flow rate. Therefore, optimum combination of instrumental parameters can effectively wet the sample surface and produce secondary droplets with sufficient energy to arrive the inlet of MS. These highly charged secondary droplets undergo the same ionization process as those droplets produced by ESI (e.g., IEM and CRM) to generate gaseous analyte ions for detection.⁷⁵⁻⁷⁶

1.3.2 Liquid sample DESI

Due to the ineffective desorption of proteins from the sample surface, conventional DESI could not obtain decent instrumental response of proteins.⁷⁷⁻⁷⁹ In order to overcome this shortcoming, liquid sample DESI can be employed to study proteins. It has been reported previously that up to 150 kDa proteins were successfully detected using liquid sample DESI and noncovalent interaction of protein-ligand complex was preserved during DESI process.⁸⁰ Therefore, it is interesting to investigate the ability of DESI in quantifying protein-ligand interactions. Shown in Figure 1.9 is the schematic representation of the liquid sample DESI.

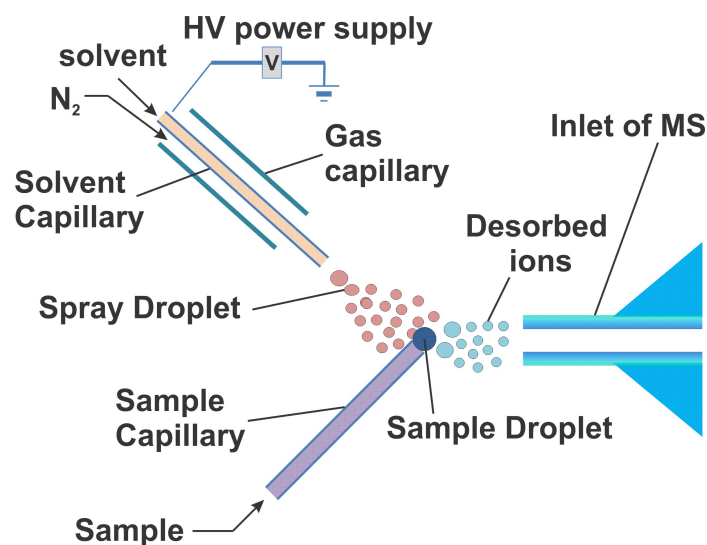


Figure 1.9 Schematic representation of the liquid sample DESI used in this study.

In liquid sample DESI, instead of drying sample onto a surface, sample solution is delivered by the sample capillary (Chapter 2 and Chapter 3). The ionization mechanism of liquid sample DESI is the same (droplet pick-up) mechanism of conventional DESI discussed previously, except the step of dissolution of dried sample into solution phase.

Conventional DESI demonstrated its ability in minimal sample preparation and tolerance of matrix and non-volatile salts presented in sample. Similarly, liquid sample DESI may overcome the significant drawback of the ESI-MS assay, which is typically carried out using aqueous ammonium acetate solutions,⁵⁰ and it suffers from general incompatibility with nonvolatile “physiological” buffers, such as phosphate buffered saline (PBS), citrate, HEPES and Tris-HCl. Such buffers are often needed to keep the protein stable in solution and to minimize protein aggregation.³⁶ In addition, liquid sample DESI has been shown to produce multiply charged gaseous ions of proteins and non-covalent protein complexes without inducing significant unfolding of the protein.⁸⁰ Therefore, the goal of the Chapter 2 is to assess the reliability of liquid sample DESI for the

quantification of protein-carbohydrate binding in aqueous ammonium acetate solutions and the tolerance of assay to the presence nonvolatile buffers.

1.4 Direct ESI-MS binding assay

In the direct ESI-MS binding assay, the protein-ligand binding equilibrium is determined by quantifying the relative abundances (*Ab*) of the free and ligand-bound protein ions in the gas phase by ESI-MS.^{30, 81-82} For a solution containing single binding site protein P and a specific ligand L the reaction between P and L is expressed as eq 1.3:



When the reaction equilibrium is reached, the association constant (*K_a*) can be calculated from equilibrium concentrations of species in solution, eq 1.4:

$$K_a = \frac{[PL]_{eq}}{[P]_{eq}[L]_{eq}} \quad (1.4)$$

Here $[PL]_{eq}$ is the equilibrium concentration of PL complex, $[P]_{eq}$ is the equilibrium concentration of free P, and $[L]_{eq}$ is the equilibrium concentration of L in solution. *K_a* can be calculated from initial concentrations of P and L in solution, and the concentration ratio of PL to free P in solution at the equilibrium (eqs 1.5 – 1.8). The ratio (*R*) of the relative abundances of gaseous PL and P ions measured by ESI-MS is expected to be equal to the ratio of the concentrations of PL and free P in solution at the equilibrium.⁸³

$$[P]_0 = [P]_{eq} + [PL]_{eq} \quad (1.5a)$$

$$[L]_0 = [L]_{eq} + [PL]_{eq} \quad (1.5b)$$

$$R = \frac{Ab(PL)}{Ab(P)} = \frac{[PL]_{eq}}{[P]_{eq}} \quad (1.6)$$

$$[\text{PL}]_{\text{eq}} = \frac{R[\text{P}]_0}{1+R} \quad (1.7)$$

$$K_a = \frac{R}{[\text{L}]_0 - \frac{R}{1+R}[\text{P}]_0} \quad (1.8)$$

When the protein (or protein assembly) have q ($q > 1$) binding sites, there are q reactions existing in solution:



...



Here, only the simplest case is described, where all q binding sites are all equivalent with identical binding affinities. Therefore, K_a values for each reaction can be derived as eqs 1.12 from eqs 1.10 – 1.11:

$$[\text{P}]_0 = [\text{P}]_{\text{eq}} + [\text{PL}]_{\text{eq}} + [\text{PL}_2]_{\text{eq}} \cdots + [\text{PL}_q]_{\text{eq}} \quad (1.10a)$$

$$[\text{L}]_0 = [\text{L}]_{\text{eq}} + [\text{PL}]_{\text{eq}} + 2[\text{PL}_2]_{\text{eq}} \cdots + q[\text{PL}_q]_{\text{eq}} \quad (1.10b)$$

$$K_i = K_a (q - i + 1)/i \quad (1.11)$$

$$K_i = \frac{[\text{PL}_i]_{\text{eq}}}{[\text{PL}_{(i-1)}]_{\text{eq}} [\text{L}]_{\text{eq}}} \quad (1.12)$$

where $[\text{P}]_0$ and $[\text{L}]_0$ are initial concentrations of multiple binding sites protein P and its specific ligand L, respectively. $[\text{P}]_{\text{eq}}$, $[\text{L}]_{\text{eq}}$, $[\text{PL}]_{\text{eq}}$, $[\text{PL}_2]_{\text{eq}}$, $[\text{PL}_{(i-1)}]_{\text{eq}}$, $[\text{PL}_q]_{\text{eq}}$ are equilibrium concentrations of free P, free L, and differently bound protein complexes,

respectively. And i is the number of bound ligands. An average K_a can be determined from each reaction binding constant.

Practically, R value in ESI-MS binding measurements is typically limited to the range from approximately 0.05 to 20, and to concentrations of P and L concentration between 0.1 – 1000 μM . Therefore, the reliable K_a values from direct ESI-MS binding assay are ranging from $\sim 10^3$ to 10^7 M^{-1} .⁵⁰ In addition, very strong interactions (large K_a values) can be studied using competitive binding assay.

1.5 Potential defects of the direct ESI-MS binding assay

The direct ESI-MS has few limitations. Any physical or chemical process that affects the abundance ratio of bound and unbound proteins during ESI process and ion transportation will lead to incorrect K_a values and, potentially, incorrect binding stoichiometry. There are three universal error sources associated with ESI-MS measurements: (1) non-uniform response factors, (2) nonspecific binding, and (3) in-source dissociation, which are briefly described below.

1.5.1 Non-uniform response factors

Due to ionization and detection efficiencies, the abundances of free protein and bound protein complex ions in gas phase measured by ESI-MS are associated with their solution concentrations by response factors (RF), eq 1.13:

$$\frac{[\text{PL}]_{\text{eq}}}{[\text{P}]_{\text{eq}}} = \frac{Ab(\text{PL})/RF_{\text{PL}}}{Ab(\text{P})/RF_{\text{P}}} = RF_{\text{P/PL}} \frac{Ab(\text{PL})}{Ab(\text{P})} \quad (1.13)$$

where RF_{PL} and RF_{P} are the response factors of PL and free P , respectively, and the $RF_{\text{P/PL}}$ is the ratio of RF_{P} to RF_{PL} , which is also referred as the relative response factor. Although the absolute RF values relate to many factors, such as the size, structure and surface

properties of PL and free P, the solution composition and instrumental parameters, similar RF values of PL and free P (i.e., $RF_{P/PL} \approx 1$) are expected in cases where the size of ligand L is small compared to the size of protein, thereby PL and free P have similar size and surface properties.⁸⁴⁻⁸⁹

A number of strategies have been developed to reduce the effects of non-uniform response factors on the determination of binding affinity constants. One approach was to adjust $RF_{P/PL}$ values of an appropriate binding model to interpret with experimental titration data.^{13, 90-92} As this method requires fitting multiple adjustable parameters of a binding model to its titration data, therefore, high quality experimental data are demanding in order to derive reliable K_a values.⁹¹ Meanwhile, it is crucial to realize the underlying assumption to use this approach: $RF_{P/PL}$ is independent of concentration in the range that would be investigated. Another strategy is to employ usage of an internal standard (IS), which has similar properties (e.g. MW and surface activity) to the target analyte P and does not bind to L specifically.⁹² This method is favored because the abundance of the IS ions can reflect the fluctuations of $RF_{P/PL}$ in concentrations, instability in the ESI or other factors.

1.5.2 Nonspecific binding

It was shown previously that, during the ESI process, free L can form so-called nonspecific complexes with P (and specific PL complexes), as the ESI droplets evaporate to dryness.^{26, 93} The extent of nonspecific ligand binding is sensitive to the concentration of free L and, consequently, is more prevalent when measuring low affinity interactions because high L concentrations are needed to produce detectable concentrations of the PL

complexes.⁹³ The formation of nonspecific PL interactions changes to the measured abundances of the P and PL ions and, thereby, introduces error into the R and K_a values.

Shown in Figure 1.10 is the cartoon of the formation of nonspecific protein-ligand interaction during ESI process. This phenomenon can be understood through the CRM of ESI (section 1.2.1).

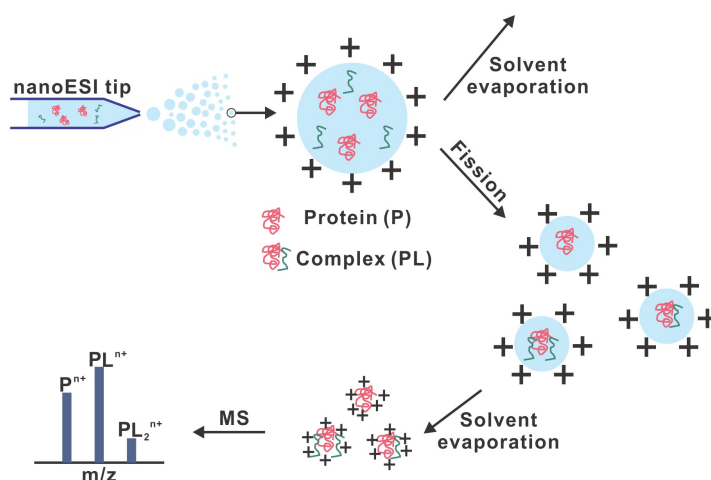


Figure 1.10 Cartoon representation of the formation of nonspecific protein-ligand interactions (false positive), adapted from reference 30.

According to the CRM model, initial parent droplets are shrinking to smaller size during solvent evaporation until they reach the Rayleigh limit, beyond which point parent droplets undergo Coulomb fission to release a jet of smaller and multiple charged progeny droplets. These nanodroplets contain different content of analyte molecules, and yield gaseous analyte ions after solvent evaporation. If two or more analyte molecules are present in a nanodroplet, nonspecific complexes can be formed due to nonspecific intermolecular interactions occurring ionization process. Therefore, L can nonspecifically bind to P and PL in the presence of high concentration of L in solution, which mystify the

true binding stoichiometry of P and L in bulk solution and lead false positive error into K_a values measured by ESI-MS.

The extent of nonspecific complex formation can be reduced by lowering the initial concentration of ligand. However, nonspecific binding may be unavoidable when high concentration of ligand is used to produce detectable signal of weakly interacted protein-ligand complexes. Fortunately, several strategies have been reported to effectively correct nonspecific binding occurring on ESI mass spectra.⁹³⁻⁹⁴ The reference protein method is a very straightforward and effective method to quantitatively correct ESI mass spectra for nonspecific binding.⁹³ The method involves the addition of reference protein (P_{ref}), which does not interact specifically with P or L, to the solution. Generally, the distribution of nonspecific bound molecules on mass spectra is very close to a Poisson process, which suggests that the nonspecific binding event of ligand to protein is a random process and has same effect on all protein species in solution phase. The presence of nonspecific binding is established from the appearance of ions corresponding to P_{ref} bound to one or more molecules of L, i.e., $P_{ref}L_q$ complexes. Therefore, the fraction abundance of nonspecifically bound and unbound P_{ref} can provide a quantitative measurement of the nonspecific binding contributed in the apparent intensities of free and specifically bound proteins. For one binding site proteins, the contribution of nonspecific binding to the apparent (measured) abundances of P ($Ab_{app}(P)$) and PL ($Ab_{app}(PL)$) can be accounted for using eqs 1.14a and 1.14b:

$$Ab(P) = Ab_{app}(P) / f_0 \quad (1.14a)$$

$$Ab(PL) = [Ab_{app}(PL) - f_1 Ab(P)] / f_0 \quad (1.14b)$$

where f_0 is the fraction of free P and f_l the fraction of P bound nonspecifically to one molecule of L. These fractions can be determined from the measured abundances of free and ligand-bound forms of P_{ref} , eqs 1.15a and 1.15b:

$$f_0 = Ab(P_{\text{ref}})/[Ab(P_{\text{ref}})+Ab(P_{\text{ref}}L)] \quad (1.15a)$$

$$f_l = Ab(P_{\text{ref}}L)/[Ab(P_{\text{ref}})+Ab(P_{\text{ref}}L)] \quad (1.15b)$$

Similarly, the “true” abundance of a protein with multiple binding sites (PL_q) can be calculated from the measured abundance of PL_q and $P_{\text{ref}}L_q$ species using the following eqs 1.16a and 1.16b:

$$Ab(PL_q) = [Ab_{\text{app}}(PL_q) - f_l Ab(PL_{q-1}) - \dots - f_q Ab(P)] / f_0 \quad (1.16a)$$

$$f_q = Ab(P_{\text{ref}}L_q) / [Ab(P_{\text{ref}}) + Ab(P_{\text{ref}}L) + \dots + Ab(P_{\text{ref}}L_q)] \quad (1.16b)$$

where f_q is the fraction of P bound nonspecifically to q molecules of L. Notably, this method has been successfully applied to correct for nonspecific interactions of neutral and charged molecules, such as carbohydrates, amino acids, peptides and divalent metal ions, to proteins during ESI-MS measurements.^{93, 95-97}

1.5.3 In-source dissociation

When using ESI-MS to study noncovalent protein-ligand interactions, the in-source collision-induced dissociation generally results in reducing abundance of PL complex ions.⁹³ As a consequence, the R value, which is the ratio of abundances of the ligand-bound protein to free protein, becomes smaller, and the magnitude of K_a value decreases. In an undesirable case, PL complex ions influenced by in-source dissociation may not be able to survive enough to obtain detectable signals.⁹⁸ Generally, weak protein-ligand interactions are more sensitive to ion source parameters, especially the particular voltage differences in high pressure regions, which can regulate internal energy of complex ions and alter the R

value. Besides the gas-phase stability of the PL complex being studied, it is also very important to choose proper configurations of the ion source and instrumental parameters, which play essential roles in in-source dissociation.

In order to reduce in-source dissociation of gaseous complex ions, therefore, low source temperatures (i.e., drying gas and sampling capillary), low voltages across lens elements, and short accumulation time are crucial for obtaining more reliable binding constants with minimal false negative error. However, these conditions often reduce signal intensities. Instrumental parameters must be thereby adjusted to minimize dissociation of complex ions, and obtain mass spectra with decent S/N at the same time. Besides, there are other ways, such as addition of small organic molecules (i.e., imidazole²⁷ and amino acids⁹⁹) into ESI solutions and introduction of solvent vapors (i.e., sulfur hexafluoride¹⁰⁰, water and organic solvents¹⁰¹) into the ion source. For instance, Konermann and co-workers reported that they could not detect any signal for the trypsin (Tryp) – benzamidine (Benz) complex ions using direct ESI-MS assay.¹⁰² Few years later, Klassen and co-workers demonstrated that addition of imidazole could stabilize (Tryp-Benz) complex ions in gas phase, and the measured K_a is $2.1 \times 10^4 \text{ M}^{-1}$ using ESI-MS, which is consistent with reference values.²⁷ The stabilization effect of imidazole is believed due to the enhanced evaporation cooling by dissociation of imidazole from PL ions during ionization process, which decreases internal energy of gaseous PL ions and, therefore, reduces dissociation of PL complex ions.²⁷ Recently, Chen and co-workers reported that adding amino acids into ESI solutions could stabilize non-covalent protein complexes during ionization in high source temperatures ($\sim 400 \text{ }^\circ\text{C}$).⁹⁹ However, in case of in-source dissociation, low source temperatures and low potentials are essential for obtaining more protein-ligand complex

ions in gas phase. Therefore, the effects of amino acid additives on stabilizing protein-ligand complex ions may need to be reconsidered in low source temperature.

1.6 The present work

The work described in this thesis focuses on the development of mass spectrometry methods to study protein-glycan interactions.

The goal of Chapter 2 was to assess the reliability of liquid sample DESI for the quantification of protein-carbohydrate binding in aqueous ammonium acetate solutions and the tolerance of assay to the presence nonvolatile buffers. The affinities of tri- and tetrasaccharide ligands for lysozyme (Lyz), a glycosyl hydrolase, and a single chain variable fragment (scFv) of a monoclonal antibody were measured by liquid sample DESI-MS and the results compared with those measured using ITC and the direct ESI-MS assay. The suitability of liquid sample DESI-MS for quantitative binding measurements carried out using solutions containing high concentration of PBS was also explored. Binding measurements were performed on solutions of Lyz and a trisaccharide ligand in varying concentrations of PBS and the results compared to those obtained using ITC and ESI-MS.

Chapter 3 describes an investigation of the influence of sulfolane on ESI-MS measurements of protein-ligand affinities *in vitro*. With this in mind, ESI-MS binding measurements were carried out on four protein-carbohydrate complexes in the presence and absence of sulfolane. The interactions between lysozyme (Lyz) and the tetrasaccharide ligand β -D-GlcNAc-(1 \rightarrow 4)- β -D-GlcNAc-(1 \rightarrow 4)- β -D-GlcNAc-(1 \rightarrow 4)-D-GlcNAc (**L1**), a single chain variable fragment (scFv) of the monoclonal antibody Se155-4 and the

trisaccharide ligand α -D-Gal-(1 \rightarrow 2)-[α -D-Abe-(1 \rightarrow 3)]- α -D-Man-OCH₃ (**L2**), cholera toxin B subunit homopentamer and the GM1 pentasaccharide β -D-Gal-(1 \rightarrow 3)- β -D-GalNAc-(1 \rightarrow 4)-[α -D-Neu5Ac-(2 \rightarrow 3)]- β -D-Gal-(1 \rightarrow 4)- β -D-Glc (**L3**) and a fragment of galectin 3 and the tetrasaccharide ligand α -L-Fuc-(1 \rightarrow 2)- β -D-Gal-(1 \rightarrow 3)- β -D-GlcNAc-(1 \rightarrow 3)- β -D-Gal-(1 \rightarrow 4)- β -D-Glc (**L4**) served as model systems for this study. Having found evidence that sulfolane generally reduces the apparent affinity, a detailed study of the origin of the reduced affinity was undertaken using the Lyz-**L1** interaction as a model. Measurements were carried out using isothermal titration calorimetry (ITC), circular dichroism (CD) and nuclear magnetic resonance (NMR) spectroscopy to establish how sulfolane affects the structure and stability of the protein-tetrasaccharide complex in solution. Finally, the effect of sulfolane on protein-ligand affinity measurements carried out using liquid sample DESI-MS was explored.

1.7 Literature cited

1. Zhao, Y.Y., et al., *Cancer Sci.* **2008**, *99*, 1304-1310.
2. Varki, A., *Glycobiology.* **1993**, *3*, 97-130.
3. Dwek, R.A., *Biochem Soc Trans.* **1995**, *23*, 1-25.
4. Saxon, E., Bertozzi, C.R., *Annu Rev Cell Dev Bi.* **2001**, *17*, 1-23.
5. Taniguchi, N., et al., *Curr Opin Struct Biol.* **2006**, *16*, 561-566.
6. Dennis, J.W., Granovsky, M., Warren, C.E., *Bioessays.* **1999**, *21*, 412-421.
7. Ho, J.G.S., et al., *Proc Natl Acad Sci U S A.* **2005**, *102*, 18373-18378.
8. Leavitt, S., Freire, E., *Curr Opin Struct Biol.* **2001**, *11*, 560-566.
9. Patching, S.G., *Biochim Biophys Acta.* **2014**, *1838*, 43-55.
10. Fernandez-Alonso, M.D., et al., *Curr Protein Pept Sc.* **2012**, *13*, 816-830.
11. Chiodo, F., et al., *PloS one.* **2013**, *8*, e73027.
12. Saboury, A.A., *J Iran Chem Soc.* **2006**, *3*, 1-21.
13. Wilcox, J.M., Rempel, D.L., Gross, M.L., *Anal Chem.* **2008**, *80*, 2365-2371.
14. Utsuno, K., Uludag, H., *Biophys J.* **2010**, *99*, 201-207.
15. Daghestani, H.N., Day, B.W., *Sensors.* **2010**, *10*, 9630-9646.
16. De Crescenzo, G., et al., *Cell Mol Bioeng.* **2008**, *1*, 204-215.
17. Karlsson, R., *J Mol Recognit.* **2004**, *17*, 151-161.
18. Schuck, P., *Annu Rev Bioph Biom.* **1997**, *26*, 541-566.
19. Homola, J., *Anal Bioanal Chem.* **2003**, *377*, 528-539.
20. Shuker, S.B., et al., *Science.* **1996**, *274*, 1531-1534.
21. Zech, S.G., et al., *J Am Chem Soc.* **2004**, *126*, 13948-13953.
22. Wishart, D., *Curr Pharm Biotechno.* **2005**, *6*, 105-120.

23. Larsen, K., et al., *Carbohydr Res.* **2006**, *341*, 1209-1234.
24. Chiodo, F., et al., *PloS one.* **2013**, *8*, e73027.
25. Kitova, E.N., Bundle, D.R., Klassen, J.S., *J Am Chem Soc.* **2002**, *124*, 9340-9341.
26. Wang, W., Kitova, E.N., Klassen, J.S., *Anal Chem.* **2005**, *77*, 3060-3071.
27. Sun, J.X., Kitova, E.N., Klassen, J.S., *Anal Chem.* **2007**, *79*, 416-425.
28. Liu, L., et al., *J Am Chem Soc.* **2009**, *131*, 15980-15981.
29. El-Hawiet, A., et al., *Glycobiology.* **2011**, *21*, 1217-1227.
30. Kitova, E.N., et al., *J Am Soc Mass Spectrom.* **2012**, *23*, 431-441.
31. Liu, P.Y., et al., *Anal Chem.* **2013**, *85*, 11966-11972.
32. Yao, Y.Y., et al., *J Am Soc Mass Spectrom.* **2015**, *26*, 98-106.
33. Miao, Z., Chen, H., *J Am Soc Mass Spectrom.* **2009**, *20*, 10-19.
34. Ferguson, C.N., et al., *Anal Chem.* **2011**, *83*, 6468-6473.
35. Moore, B.N., Hamdy, O., Julian, R.R., *Int J Mass Spectrom.* **2012**, *330-332*, 220-225.
36. Banerjee, S., Mazumdar, S., *Int J Anal Chem.* **2012**, *2012*, 282574.
37. Fenn, J.B., et al., *Science.* **1989**, *246*, 64-71.
38. Przybylski, M., Glocker, M.O., *Angew Chem.* **1996**, *35*, 807-826.
39. Kebarle, P., Verkerk, U.H., *Mass Spectrom Rev.* **2009**, *28*, 898-917.
40. Wu, X., Oleschuk, R.D., Cann, N.M., *Analyst.* **2012**, *137*, 4150-4161.
41. Rayleigh, L., *Phil Mag.* **1882**, *14*, 184-186.
42. Cech, N.B., Enke, C.G., *Mass Spectrom Rev.* **2001**, *20*, 362-387.
43. Nguyen, S., Fenn, J.B., *Proc Natl Acad Sci U S A.* **2007**, *104*, 1111-1117.
44. Konermann, L., et al., *Anal Chem.* **2013**, *85*, 2-9.
45. Iribarne, J.V., Thomson, B.A., *J Chem Phys.* **1976**, *64*, 2287-2294.

46. Kebarle, P., Tang, L., *Anal Chem.* **1993**, *65*, 972A-986A.
47. Thomson, B., Iribarne, J., *J Chem Phys.* **1979**, *71*, 4451-4463.
48. Cole, R.B., *J Mass Spectrom.* **2000**, *35*, 763-772.
49. De La Mora, J.F., *Anal Chim Acta.* **2000**, *406*, 93-104.
50. Kebarle, P., *J Mass Spectrom.* **2000**, *35*, 804-817.
51. Olumee, Z., Callahan, J.H., Vertes, A., *J Phys Chem A.* **1998**, *102*, 9154-9160.
52. Dole, M., et al., *J Chem Phys.* **1968**, *49*, 2240-2249.
53. Iavarone, A.T., Williams, E.R., *J Am Chem Soc.* **2003**, *125*, 2319-2327.
54. Ahadi, E., Konermann, L., *J Phys Chem B.* **2012**, *116*, 104-112.
55. Konermann, L., Rodriguez, A.D., Liu, J., *Anal Chem.* **2012**, *84*, 6798-6804.
56. Yue, X., Vahidi, S., Konermann, L., *J Am Soc Mass Spectrom.* **2014**, *25*, 1322-1331.
57. Wilm, M., Mann, M., *Anal Chem.* **1996**, *68*, 1-8.
58. Joensson, H.N., et al., *Angew Chem.* **2009**, *48*, 2518-2521.
59. Karas, M., Bahr, U., Dulcks, T., *Fresenius J Anal Chem.* **2000**, *366*, 669-676.
60. Juraschek, R., Dulcks, T., Karas, M., *J Am Soc Mass Spectrom.* **1999**, *10*, 300-308.
61. Hoffmann, E. d., Stroobant, V., *Mass Spectrometry : Principles and Applications. 3rd ed.*, Wiley: 2007.
62. Guilhaus, M., et al., *Mass Spectrom Rev.* **2000**, *19*, 65-107.
63. Marshall, A.G., et al., *Mass Spectrom Rev.* **1998**, *17*, 1-35.
64. Marshall, A.G., Hendrickson, C.L., *Int J Mass Spectrom.* **2002**, *215*, 59-75.
65. Takats, Z., et al., *Science.* **2004**, *306*, 471-473.
66. Badu-Tawiah, A., et al., *J Am Soc Mass Spectrom.* **2010**, *21*, 572-579.
67. Ifa, D.R., et al., *Analyst.* **2010**, *135*, 669-681.

68. Takats, Z., et al., *J Mass Spectrom.* **2005**, *40*, 1261-1275.
69. Green, F.M., et al., *Analyst.* **2010**, *135*, 731-737.
70. Olumee, Z., et al., *J Phys Chem A.* **1998**, *102*, 9154-9160.
71. Venter, A., et al., *Anal Chem.* **2006**, *78*, 8549-8555.
72. Zivolic, F., et al., *J Mass Spectrom.* **2010**, *45*, 411-420.
73. Douglass, K.A., Venter, A.R., *J Mass Spectrom.* **2013**, *48*, 553-560.
74. Costa, A.B., Cooks, R.G., *Chem Commun.* **2007**, 3915-3917.
75. Thomson, B., Iribarne, J., *J Chem Phys.* **1979**, *71*, 4451-4463.
76. Mack, L.L., et al., *J Chem Phys.* **1970**, *52*, 4977-4986.
77. Shin, Y.S., et al., *Anal Chem.* **2007**, *79*, 3514-3518.
78. Heaton, K., et al., *J Archaeol Sci.* **2009**, *36*, 2145-2154.
79. Myung, S., et al., *J Phys Chem B.* **2006**, *110*, 5045-5051.
80. Ferguson, C.N., et al., *Anal Chem.* **2011**, *83*, 6468-6473.
81. El-Hawiet, A., et al., *Biochemistry.* **2012**, *51*, 4244-4253.
82. Daniel, J.M., et al., *Int J Mass Spectrom.* **2002**, *216*, 1-27.
83. Wang, W., et al., *Methods in enzymology.* **2003**, *362*, 376-397.
84. Soya, N., et al., *Glycobiology.* **2009**, *19*, 1224-1234.
85. Kitova, E.N., et al., *Glycobiology.* **2007**, *17*, 1127-1137.
86. El-Hawiet, A., et al., *Glycobiology.* **2011**, *21*, 1217-1227.
87. Yanes, O., et al., *Nat Protoc.* **2007**, *2*, 119-130.
88. Jecklin, M.C., et al., *Anal Chem.* **2009**, *81*, 408-419.
89. Yanes, O., et al., *Mol Cell Proteomics.* **2005**, *4*, 1602-1613.
90. Chitta, R.K., et al., *J Am Soc Mass Spectrom.* **2005**, *16*, 1031-1038.

91. Gabelica, V., et al., *J Mass Spectrom.* **2003**, *38*, 491-501.
92. Mathur, S., et al., *Phys Chem Chem Phys.* **2007**, *9*, 6187-6198.
93. Sun, J., et al., *Anal Chem.* **2006**, *78*, 3010-3018.
94. Kitova, E.N., et al., *Anal Chem.* **2011**, *83*, 5160-5167.
95. Sun, J., et al., *Anal Chem.* **2007**, *79*, 8301-8311.
96. Sun, N., et al., *J Am Soc Mass Spectrom.* **2010**, *21*, 472-481.
97. Deng, L., et al., *Anal Chem.* **2010**, *82*, 2170-2174.
98. El-Hawiet, A., et al., *J Am Soc Mass Spectrom.* **2010**, *21*, 1893-1899.
99. Zhang, H., et al., *Anal Chem.* **2015**, *87*, 7433-7438.
100. Bagal, D., et al., *Anal Chem.* **2009**, *81*, 7801-7806.
101. DeMuth, J.C., et al., *Rapid Commun Mass Spectrom.* **2015**, *29*, 973-981.
102. Clark, S.M., Konermann, L., *Anal Chem.* **2004**, *76*, 7077-7083.

Chapter 2

Quantifying Protein-Carbohydrate Interactions Using Liquid Sample Desorption Electrospray Ionization Mass Spectrometry*

2.1 Introduction

Non-covalent interactions between proteins and carbohydrates on the surfaces of cell, present as either part of membrane glycoproteins or glycolipids, are involved in many normal and pathological cellular processes, including catalysis, signaling and molecular recognition.¹ Studies of protein-carbohydrate interactions in vitro can provide fundamental insights into these important processes and guide the development of diagnostics and therapeutics for a variety of infections and diseases. There exist a number of analytical methods for the detection and characterization of protein-carbohydrate interactions. For example, glycan microarrays are now commonly used to screen libraries of carbohydrates for specific interactions with proteins,² while isothermal titration calorimetry (ITC),³ surface plasmon resonance (SPR),⁴ nuclear magnetic resonance (NMR) spectroscopy⁵ and enzyme-linked immunosorbent assays (ELISA)⁶ are extensively used to quantify the thermodynamics (and in some instances the kinetics) of protein-carbohydrate binding. In recent years, electrospray ionization mass spectrometry (ESI-MS) has emerged as a powerful method for detecting protein-carbohydrate complexes in solution and measuring the affinities of the interactions.⁷⁻¹⁸

In the direct ESI-MS binding assay, the protein-ligand binding equilibrium is determined by quantifying the relative abundances of the free and ligand-bound protein

* A version of this chapter has been published: Yao, Y., Shams-Ud-Doha, K., Daneshfar, R., Kitova, E. N., Klassen, J. S., *J Am Soc Mass Spectrom.*, 2015, 26, 98-106.

ions in the gas phase.¹¹⁻¹³ The measurements are fast and can often be completed within a few minutes, the amount of sample consumed is low, typically picomoles of protein and nano- to picomoles of ligand, and there is no requirement for labeling or additional reagents, which makes the assay very versatile. Moreover, the direct ESI-MS assay is the only technique that directly measures binding stoichiometry. This feature is particularly beneficial to the study of protein-carbohydrate interactions, as many carbohydrate-binding proteins are composed of multiple subunits and possess multiple ligand binding sites. The ESI-MS assay also affords the opportunity to measure, simultaneously, the binding of multiple, distinct ligands, and is, therefore, well suited to carbohydrate library screening.¹⁶

A drawback of the ESI-MS assay, which is typically carried out using aqueous ammonium acetate solutions,¹⁹ is that it suffers from general incompatibility with nonvolatile “physiological” buffers, such as phosphate buffered saline (PBS), citrate, HEPES and Tris-HCl. Such buffers are often needed to keep the protein stable in solution and to minimize protein aggregation.²⁰ Several strategies have been proposed to allow ESI-MS analysis of solutions containing physiological buffers at relevant concentrations, including the use of high concentrations of ammonium acetate²¹ or carrying out ESI in the presence of a high velocity gas.²² A possible alternative approach involves separating the sample from the ESI process through the use of desorption electrospray ionization (DESI)²³⁻²⁵ or liquid sample DESI.²⁶⁻²⁹ In liquid sample DESI-MS, the liquid sample is ionized through collisions with charged droplets produced by ESI.^{26-27, 30} The ESI solution is typically a mixture of water and an organic solvent, such as acetonitrile or methanol.²⁸ Despite this, liquid sample DESI has been shown to produce multiply charged gaseous ions of proteins and non-covalent protein complexes without inducing significant unfolding of

the protein.²⁸ A variation of liquid sample DESI, known as reactive liquid sample DESI, was recently described and used to screen a library of compounds for specific binding to a target protein and to quantify the interactions.²⁷ In this approach, the ligands are introduced (consecutively) into the ESI spray solvent, rather than to the sample solution, which contained the target protein. The advantage of reactive liquid sample DESI is that the premixing of protein with ligands can be avoided.²⁷

The goal of the present study was to assess the reliability of liquid sample DESI for the quantification of protein-carbohydrate binding in aqueous ammonium acetate solutions and the tolerance of assay to the presence nonvolatile buffers. The affinities of tri- and tetrasaccharide ligands for lysozyme (Lyz), a glycosyl hydrolase, and a single chain variable fragment (scFv) of a monoclonal antibody were measured by liquid sample DESI-MS and the results compared with those measured using ITC and the direct ESI-MS assay.³¹⁻³³ The suitability of liquid sample DESI-MS for quantitative binding measurements carried out using solutions containing high concentrations of PBS was also explored. Binding measurements were performed on solutions of Lyz and a trisaccharide ligand in varying concentrations of PBS and the results compared to those obtained using ITC and ESI-MS.

2.2 Experimental section

2.2.1 Materials

Ubiquitin (Ubq, MW 8565 Da), lysozyme (from chicken egg white, Lyz, MW 14310 Da) and maltotriose (**L1**, MW 504.44 Da) were purchased from Sigma-Aldrich Canada (Oakville, Canada) and β -D-GlcNAc-(1 \rightarrow 4)- β -D-GlcNAc-(1 \rightarrow 4)-D-GlcNAc (**L2**, MW 627.59 Da) and

β -D-GlcNAc-(1 \rightarrow 4)- β -D-GlcNAc-(1 \rightarrow 4)- β -D-GlcNAc-(1 \rightarrow 4)-D-GlcNAc (**L3**, MW 830.27 Da) were purchased from Dextra Science and Technology Centre (United Kingdom). The single chain variable fragment of Se155-4 (scFv, MW 26539 Da) was produced and purified as described previously³⁴⁻³⁵ and α -D-Galp-(1 \rightarrow 2)-[α -D-Abep-(1 \rightarrow 3)]- α -D-Manp-OCH₃ (**L4**, MW 486.50 Da) and β -D-Glcp-(1 \rightarrow 2)-[α -D-Abep-(1 \rightarrow 3)]- α -D-Manp-OCH₃ (**L5**, MW 486.50 Da) were gifts from Prof. D. Bundle (University of Alberta). Stock solutions of each protein (in 50 mM ammonium acetate) and oligosaccharide (in deionized water) were prepared, and stored at -20 °C until needed. A 10X PBS stock solution (NaCl (1.37 M), KCl (27 mM), Na₂HPO₄ (0.1 M) and KH₂PO₄ (18 mM), pH 7.4) was prepared and stored at 4 °C until needed. Sample solutions for ESI- and liquid sample DESI-MS analysis were prepared from the stock solutions of protein and oligosaccharide. Unless otherwise indicated, the sample solutions contained 20 mM ammonium acetate. In a limited number of experiments, PBS was added, at the concentrations indicated.

2.2.2 Mass spectrometry

All of the ESI- and liquid sample DESI-MS measurements were carried out in positive ion mode using a Synapt G2 quadrupole-ion mobility separation-time-of-flight (Q-IMS-TOF) mass spectrometer (Waters UK Ltd., Manchester, UK) equipped with a 8k quadrupole mass filter. All data were processed using MassLynx software (v4.1). For the ESI-MS measurements, nanoflow ESI (nanoESI) tips, produced from borosilicate capillaries (1.0 mm o.d., 0.68 mm i.d.) and pulled to ~5 μ m using a P-1000 micropipette puller (Sutter Instruments, Novato, CA, USA), were used. A platinum wire was inserted into the nanoESI tip and a Capillary voltage of 1.0 – 1.3 kV was applied to initiate the spray.

A Cone voltage of 30 V was used and the source block temperature was maintained at 60 °C. The Trap and Transfer ion guides were maintained at 5 V and 2 V, respectively, and the argon pressure in these regions was 2.22×10^{-2} mbar and 3.36×10^{-2} mbar, respectively. For the liquid sample DESI-MS measurements, a modified OMNI SPRAY Ion Sources 2-D OS-6205 (Prosolia Inc., Indianapolis, IN, USA) was used. The liquid sample solution was delivered through a silica capillary (360 nm o.d., 100 nm i.d.) at a flow rate of 5-10 $\mu\text{L h}^{-1}$ using a syringe pump (Chemyx Syringe Pumps Fusion 100, Chemyx Inc, Stafford, TX, USA). The end of the silica capillary was positioned between the ESI tip and inlet of the mass spectrometer. The ESI solution flow rate was between 2 and 4 $\mu\text{L min}^{-1}$. Capillary and Cone voltages of 3.0 – 3.5 kV and 30 V, respectively, were used and the pressure of the N_2 nebulizing gas was 60 – 70 psi. The source block temperature was the same as for the ESI-MS measurements.

Prior to carrying out the liquid sample DESI-MS protein-carbohydrate binding measurements, several different spray solvent compositions were tested (deionized water, 20 mM ammonium acetate, 50/50 v/v water/methanol, 20/80 v/v water/acetonitrile, 50/50 v/v water/acetonitrile and 80/20 v/v water/acetonitrile) for the analysis of aqueous ammonium acetate solutions of Lyz or scFv, the two model carbohydrate-binding proteins used in this study. Ultimately, it was found that a 50/50 water/acetonitrile solution gave mass spectra with the highest signal-to-noise ratios. Shown in Figure 2.1 are representative liquid sample DESI mass spectra acquired in positive ion mode for aqueous ammonium acetate (20 mM) solutions containing Lyz (10 μM) or scFv (10 μM).

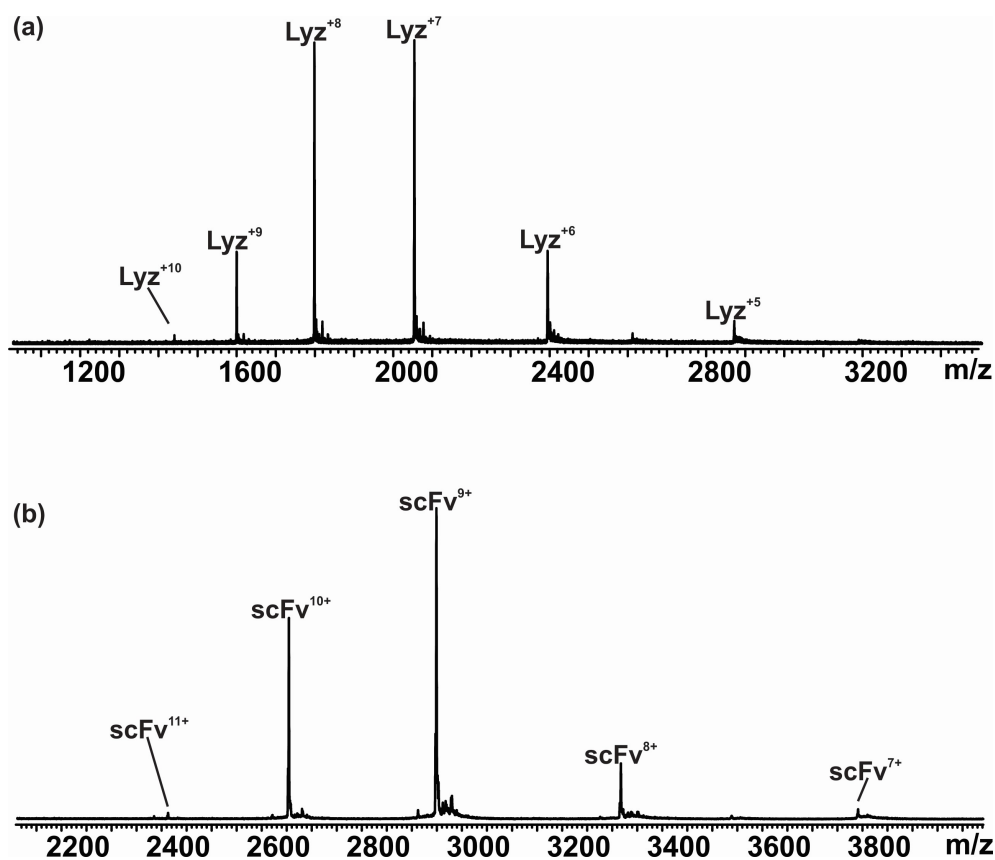


Figure 2.1 Representative liquid sample DESI mass spectra acquired in positive ion mode for aqueous ammonium acetate (20 mM) solutions containing (a) Lyz (10 μM), and (b) scFv (10 μM). The ESI spray solution was 50/50 water/acetonitrile.

It can be seen that liquid sample DESI-MS produced abundant signal corresponding to the protonated ions of Lyz (Figure 2.1a) and scFv (Figure 2.1b). A 50/50 water/acetonitrile solution was used as the spray solvent for all of the liquid sample DESI-MS binding measurements reported in this study.

2.2.3 Isothermal titration calorimetry

The ITC measurements were carried out using a VP-ITC (MicroCal, Inc. USA). For each ITC experiment, the Lyz solution (0.1 - 0.2 mM) in the sample cell was titrated with a

solution of **L2** or **L3** (2 mM); both the protein and ligand solutions were aqueous ammonium acetate (50 mM, pH 6.8) or PBS (1x, pH 7.4) at 25 °C.

2.2.4 Data analysis

The general procedure for determining association constants (K_a) for protein-ligand interactions from ESI mass spectra has been described in detail elsewhere and only a brief description is given for the case where the protein has single ligand binding site.^{18, 36-37} The assay relies on the detection and quantification of the gas-phase ions of free and ligand-bound protein. The concentration ratio (R) of the ligand-bound protein (PL) to free protein (P) in solution is taken to be equal to the total abundance (Ab) of P and PL ions as measured by ESI-MS, eq 1. It follows that K_a can be calculated from eq 2:

$$R = \frac{\sum Ab(PL)}{\sum Ab(P)} = \frac{[PL]_{eq}}{[P]_{eq}} \quad (1)$$

$$K_a = \frac{R}{[L]_o - \frac{R[P]_o}{1+R}} \quad (2)$$

where $[P]_o$ and $[L]_o$ are the initial protein and ligand concentrations, respectively.

It was shown previously that, during the ESI process, free L can form so-called nonspecific complexes with P (and specific PL complexes), as the ESI droplets evaporate to dryness.³⁶⁻³⁷ The extent of nonspecific ligand binding is sensitive to the concentration of free L and, consequently, is more prevalent when measuring low affinity interactions because high L concentrations are needed to produce detectable concentrations of the PL complexes.³⁷ The formation of nonspecific PL interactions changes to the measured abundances of the P and PL ions and, thereby, introduces error into the R and K_a values. The reference protein method was developed to quantitatively correct ESI mass spectra

for nonspecific binding.³⁷ The method involves the addition of reference protein (P_{ref}), which does not interact with P or L, to the solution. The presence of nonspecific binding is established from the appearance of ions corresponding to P_{ref} bound to one or more molecules of L, i.e., $P_{\text{ref}}L_x$ complexes. As described in detail elsewhere, the contribution of nonspecific binding to the apparent (measured) abundances of P ($Ab_{\text{app}}(P)$) and PL ($Ab_{\text{app}}(PL)$) can be accounted for using eqs 3a and 3b:

$$Ab(P) = Ab_{\text{app}}(P) / f_0 \quad (3a)$$

$$Ab(PL^{n+}) = \{Ab_{\text{app}}(PL^{n+}) - f_l Ab(P^{n+})\} / f_0 \quad (3b)$$

where f_0 is the fraction of free P and f_l the fraction of P bound nonspecifically to one molecule of L. These fractions can be determined from the measured abundances of free and ligand-bound forms of P_{ref} , eqs 4a and 4b:

$$f_0 = Ab(P_{\text{ref}}) / \{Ab(P_{\text{ref}}) + Ab(P_{\text{ref}}L)\} \quad (4a)$$

$$f_l = Ab(P_{\text{ref}}L) / \{Ab(P_{\text{ref}}) + Ab(P_{\text{ref}}L)\} \quad (4b)$$

To test the reliability of the reference protein method for correcting liquid sample DESI mass spectra for the occurrence of nonspecific carbohydrate-protein binding, control experiments were carried out on solutions containing a pair of proteins (Lyz and Ubq) and **L1**, which does not bind to either protein in solution.³¹⁻³² Shown in Figure 2.2 are liquid sample DESI mass spectra acquired in positive ion mode for aqueous 20 mM ammonium acetate solutions of Lyz (10 μM) and Ubq (10 μM) and **L1** at concentration of 15 μM (Figure 2.2a) or 40 μM (Figure 2.2b).

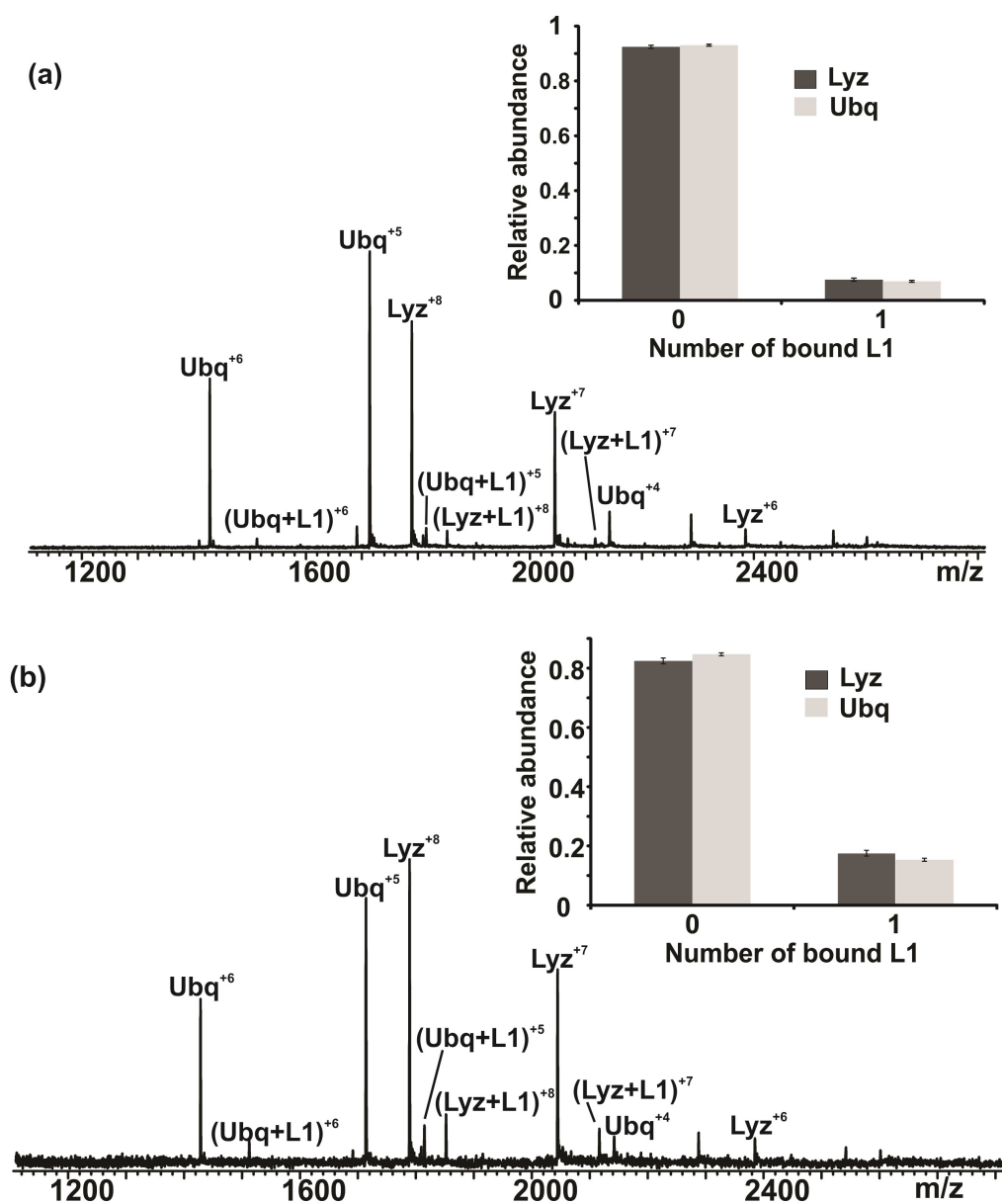


Figure 2.2 Representative liquid sample DESI mass spectra acquired in positive ion mode for aqueous ammonium acetate (20 mM, pH 6.8 and 25 °C) solutions containing Ubq (10 μM), Lyz (10 μM) and L1 at (a) 15 μM or (b) 40 μM concentrations. The ESI spray solution was 50/50 water/acetonitrile.

It can be seen that, in addition to the protonated ions of Lyz (at charge states +6 to +9) and Ubq (at charge states +4 to +6), ions corresponding to nonspecific complexes with **L1** are evident at both concentrations. Shown in the insets of Figures 2.2a and 2.2b are the normalized abundances of Lyz and Ubq in their free and bound (to **L1**) forms. Notably, the distributions of both proteins are identical, within experimental error, at both concentrations of **L1**. These results confirm that the extent of nonspecific carbohydrate binding during the liquid sample DESI process is the same for the two proteins and, further, supports the use of the reference protein method for correcting liquid sample DESI mass spectra for nonspecific carbohydrate-protein binding.

2.3 Results and discussion

To test the reliability of liquid sample DESI-MS for quantifying protein-carbohydrate interactions, the affinities of the tri- and tetrassachride ligands, **L2** and **L3** for Lyz, and the trisaccharide ligands **L4** and **L5** for scFv were measured. The affinities of **L4** and **L5** for scFv were previously measured in this laboratory using the direct ESI-MS assay and found to be $1.2 \times 10^5 \text{ M}^{-1}$ and $(5.0 \pm 1.0) \times 10^3 \text{ M}^{-1}$,³⁸⁻³⁹ respectively. The affinities of **L2** and **L3** for Lyz have been measured using several different biophysical techniques. Values of $1.1 \times 10^5 \text{ M}^{-1}$ (**L2**) and $1.8 \times 10^5 \text{ M}^{-1}$ (**L3**) were obtained using fluorescence-based assay.⁴⁰ Quantitative ESI-MS studies have also been carried out by Oldham and coworkers who measured affinities of $1.0 \times 10^5 \text{ M}^{-1}$ (**L2**) and $1.2 \times 10^5 \text{ M}^{-1}$ (**L3**).³¹ Zenobi and coworkers found somewhat lower values (ranging from $2 \times 10^4 \text{ M}^{-1}$ to $5 \times 10^4 \text{ M}^{-1}$) for **L2**.³³ Given the range of the reported values for **L2**, the affinities of **L2** and **L3** for Lyz in aqueous ammonium acetate (50 mM, pH 6.8 and

25 °C) were measured using ITC, which is widely regarded as the gold standard method for quantifying the thermodynamics of protein-carbohydrate interactions. Shown in Figures 2.3 and 2.4 are the raw and integrated ITC data measured for binding of Lyz to **L2** and **L3**, respectively.

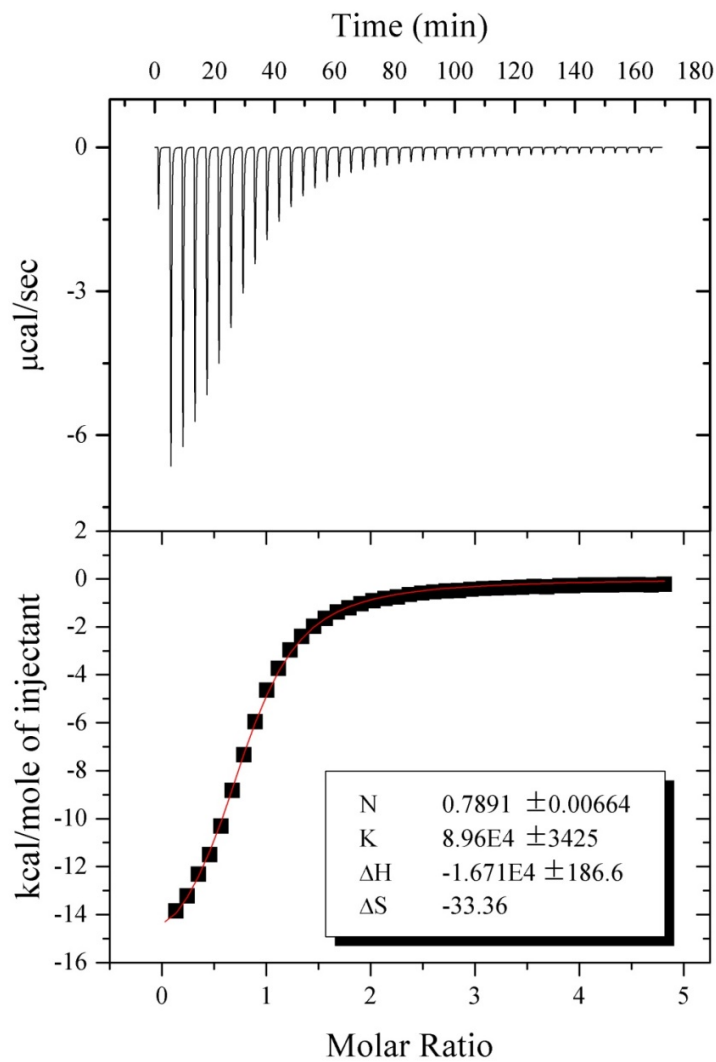


Figure 2.3 ITC data measured for the binding of Lyz (0.087 mM) to **L2** (2.0 mM) in aqueous ammonium acetate (50 mM, pH 6.8 and 25 °C) solutions.

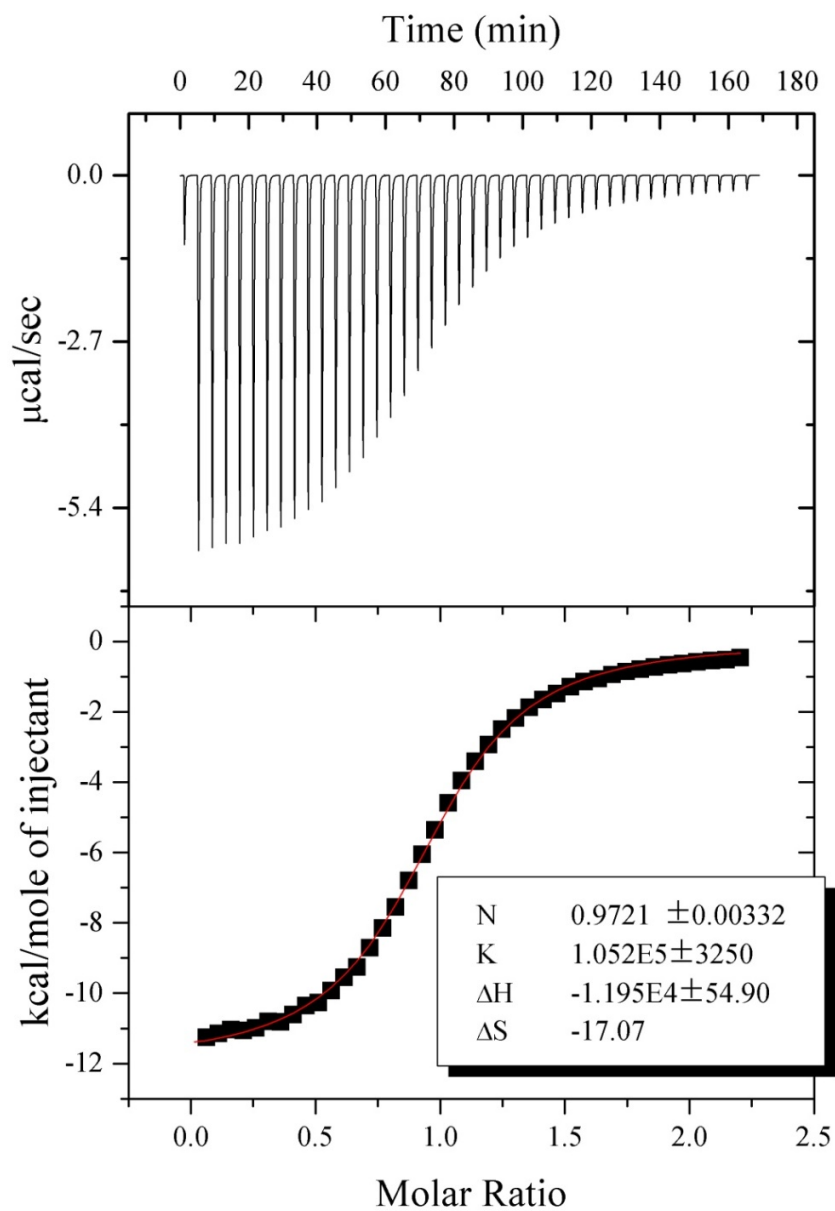


Figure 2.4 ITC data measured for the binding of Lyz (0.202 mM) to L3 (2.0 mM) in aqueous ammonium acetate (50 mM, pH 6.8 and 25 °C) solutions.

According to the best fit of a 1:1 binding model to the ITC data, the affinities of **L2** and **L3** for Lyz are $(9.0 \pm 0.3) \times 10^4 \text{ M}^{-1}$ and $(1.1 \pm 0.1) \times 10^5 \text{ M}^{-1}$, respectively. These results are in good agreement with the values obtained using the fluorescence-based assay⁴⁰ and those reported by Oldham and coworkers.³¹

2.3.1 Binding of Lyz to L2 and L3

The affinities of **L2** and **L3** for Lyz in aqueous ammonium acetate (20 mM, pH 6.8 and 25 °C) were measured at three different ligand concentrations. Shown in Figures 2.5a and 2c are representative liquid sample DESI mass spectra acquired for solutions of Lyz (10 μM) with **L2** (15 μM) or **L3** (15 μM), respectively. Ubq (5 μM), which served as P_{ref} , was added to both solutions. For comparison purposes, ESI mass spectra were also acquired for these solutions (Figures 2.5b and 2.5d). From Figures 2.5a and 2.5c, it can be seen that liquid sample DESI produces ions corresponding to free Lyz and ligand-bound Lyz (i.e., the (Lyz + **L2**) or (Lyz + **L3**) complexes), at charge states +6 to +8, as well as free Ubq at charge states +4 and +5. Ion signal corresponding to the nonspecific (Ubq + **L2**) or (Ubq + **L3**) complexes was negligible. Similar results were obtained for solutions containing **L2** or **L3** at two other concentrations, 5 μM and 10 μM (data not shown). The K_a values, representing the average of the values obtained by liquid sample DESI-MS at the three ligand concentrations, are $(1.0 \pm 0.1) \times 10^5 \text{ M}^{-1}$ (**L2**) and $(9.9 \pm 0.6) \times 10^4 \text{ M}^{-1}$ (**L3**) (Table 2.1).

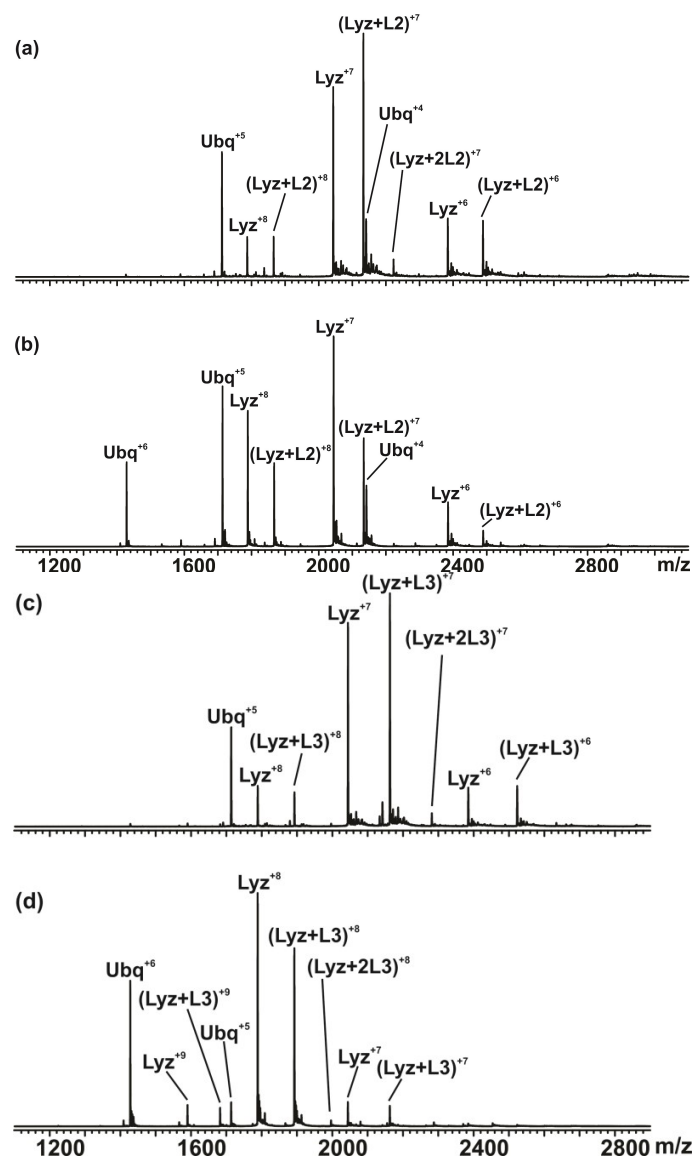


Figure 2.5 Representative (a), (c) liquid sample DESI and (b), (d) ESI mass spectra acquired in positive ion mode for aqueous ammonium acetate (20 mM, pH 6.8 and 25 °C) solutions containing Lyz (10 μM), **L2** (15 μM) and Ubq (5 μM) ((a) and (b)) or Lyz (10 μM), **L3** (15 μM) and Ubq (5 μM) ((c) and (d)). For the liquid sample DESI-MS measurements, the ESI spray solution was 50/50 water/acetonitrile.

Table 2.1 Comparison of association constants (K_a) measured by liquid sample DESI-MS, ESI-MS and ITC for the interactions of **L2** and **L3** with Lyz and **L4** and **L5** with scFv in aqueous ammonium acetate solutions at pH 6.8 and 25 °C.^a

Protein	Ligand	K_a (liquid sample	K_a	K_a (ITC)/M ⁻¹
		DESI-MS)/M ⁻¹	(ESI-MS)/M ⁻¹	
Lyz	L2	$(1.0 \pm 0.1) \times 10^5$	$(8.0 \pm 0.5) \times 10^4$	$(9.0 \pm 0.3) \times 10^4$
Lyz	L3	$(9.9 \pm 0.6) \times 10^4$	$(6.3 \pm 0.5) \times 10^4$	$(1.1 \pm 0.1) \times 10^5$
scFv	L4	$(7.6 \pm 0.1) \times 10^4$	$(6.6 \pm 0.3) \times 10^4$ $(1.2 \times 10^5)^b$	
scFv	L5	$(5.7 \pm 0.2) \times 10^3$	$(5.0 \pm 0.1) \times 10^3$	

a. Errors correspond to one standard deviation obtained from triplicate measurements. b.

Value taken from ref. 38.

The ESI mass spectra obtained for aqueous ammonium acetate (20 mM) solutions of Lyz (10 μ M), Ubq (5 μ M), and **L2** (15 μ M) or **L3** (15 μ M) (Figures 2.5b and 2.5d, respectively) are qualitatively similar to the liquid sample DESI mass spectra, although the average charge states (*ACS*) of Lyz are slightly higher than those observed with liquid sample DESI (*ACS* 6.98 (Figure 2.5a), 7.43 (Figure 2.5b), 7.02 (Figure 2.5c), 7.98 (Figure 2.5d)). The lower *ACS* values measured with liquid sample DESI-MS may be due to a subtle enhancement in the extent of proton transfer from the protein ions to acetonitrile in the gas phase. Acetonitrile has a relatively low gas phase basicity (178.8 kcal mol⁻¹), compared to ammonia (195.7 kcal mol⁻¹),⁴¹ but is present at a high concentration in the spray solvent (~9.6 M) and is expected to be present at relatively

high concentrations in the spray droplets. The resulting acetonitrile vapour could affect proton transfer from the gaseous Lyz ions. Support for this explanation can be found in an observed decrease in *ACS* measured for Lyz when carrying out ESI in the presence of acetonitrile vapour (data not shown), a phenomenon also observed by Oldham and coworkers.⁴⁴⁻⁴⁵ The average K_a values obtained by ESI-MS at the three ligand concentrations are $(8.0 \pm 0.5) \times 10^4 \text{ M}^{-1}$ (**L2**) and $(6.3 \pm 0.5) \times 10^4 \text{ M}^{-1}$ (**L3**) (Table 2.1). Notably, the absolute affinities measured by liquid sample DESI-MS for **L2** and **L3** agree within a factor of 2 with the values determined from the ESI-MS measurements. More importantly, the liquid sample DESI-MS values are in excellent agreement with the affinities determined by ITC.

2.3.2 Binding of scFv to L4 and L5

The affinities of **L4** and **L5** for scFv in aqueous ammonium acetate (20 mM, pH 6.8 and 25 °C) were also measured at three different ligand concentrations. Shown in Figures 2.6a and 2.6c are representative liquid sample DESI mass spectra acquired for solutions of scFv (10 μM) with **L4** (15 μM) or **L5** (40 μM), respectively. Lyz (5 μM), which served as P_{ref} , was added to both solutions. For comparison purposes, ESI mass spectra were also acquired for these solutions (Figures 2.6b and 2.6d). In Figures 2.6a and 2.6c, ion signal corresponding to protonated free scFv and the (scFv + **L4**) or (scFv + **L5**) complexes, at charge states +8 to +10, as well as free Lyz and the (Lyz + **L4**) or (Lyz + **L5**) complexes, at charge states +6 to +9, is evident. The appearance of ion signal for the (Lyz + **L4**) and (Lyz + **L5**) complexes indicates the occurrence of nonspecific carbohydrate-protein binding during ion formation.

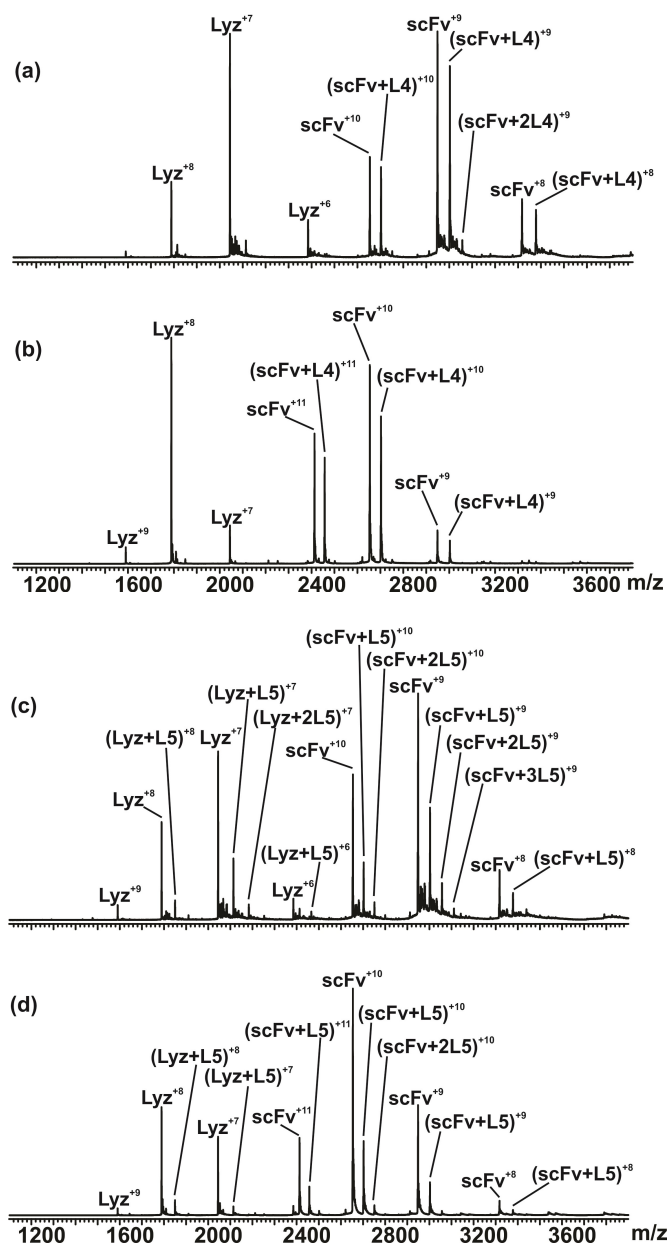


Figure 2.6 Representative (a), (c) liquid sample DESI and (b), (d) ESI mass spectra acquired in positive ion mode for aqueous ammonium acetate (20 mM, pH 6.8 and 25 °C) solutions containing scFv (10 μ M), L4 (15 μ M) and Lyz (5 μ M) ((a) and (b)) or scFv (10 μ M), L5 (40 μ M) and Lyz (5 μ M) ((c) and (d)). For the liquid sample DESI-MS measurements, the ESI spray solution was 50/50 water/acetonitrile.

Similar results were obtained for solutions at two other concentrations of **L4** (5 and 10 μM) and **L5** (20 and 30 μM). Following correction of the mass spectra for nonspecific binding, average K_a values of $(7.6 \pm 0.1) \times 10^4 \text{ M}^{-1}$ (**L4**) and $(5.7 \pm 0.2) \times 10^4 \text{ M}^{-1}$ (**L5**) were determined (Table 2.1). The ESI mass spectra measured for solutions of scFv (10 μM), Lyz (5 μM) with **L4** (15 μM) or **L5** (40 μM) (Figures 2.6b and 2.6d, respectively) are similar to the corresponding liquid sample DESI mass spectra (Figures 2.6a and 2.6c). However, the extent of nonspecific binding is less in the case of ESI - there was no significant signal corresponding to the nonspecific (Lyz + **L4**) complex and significantly less (Lyz + **L5**) detected. The reduced occurrence of nonspecific binding may be due to the small droplets produced with the nanoESI tips, compared to those formed in liquid sample DESI.⁴² The smaller nanoESI droplets will contain fewer ligand molecules and, therefore, produce less nonspecific binding, compared to the larger ESI droplets used for liquid sample DESI-MS. Following correction for nonspecific ligand binding, the affinities of **L4** and **L5** are found to be $(6.6 \pm 0.3) \times 10^4 \text{ M}^{-1}$ and $(5.0 \pm 0.1) \times 10^3 \text{ M}^{-1}$, respectively. Importantly, the affinities measured by liquid sample DESI-MS for **L4** and **L5** are in good agreement with the values determined using the direct ESI-MS assay.

Taken together, the results obtained for these model carbohydrate binding proteins demonstrate that absolute affinities for protein-carbohydrate interactions can be accurately quantified using liquid sample DESI-MS. These findings further indicate that the lifetime of the ESI droplets that produce gaseous protein ions in liquid sample DESI-MS are sufficiently short that neither the presence of a high concentration of organic solvent in the ESI spray solution, nor the inevitable dilution of the sample

(protein and ligand) solution by the solvent spray results in a measurable shift in the binding equilibrium.

2.3.3 Comparison of liquid sample DESI-MS and reactive liquid sample DESI-MS

It is also interesting to compare the affinity of **L2** for Lyz measured by liquid sample DESI-MS with the value determined by Loo and coworkers using reactive liquid sample DESI-MS.²⁷ Notably, the value measured using reactive liquid sample DESI-MS, $5.9 \times 10^3 \text{ M}^{-1}$, is eighteen times smaller than the value determined by liquid sample DESI-MS (and ITC). It has been suggested that the short time available for protein and ligand mixing in reactive liquid sample DESI (estimated to be $<2 \text{ ms}$) might be insufficient for equilibration of the binding reaction.⁴³ To help rule out other alternative explanations, in particular the possibility of in-source dissociation, reactive liquid sample DESI-MS was carried in the present study to measure the affinity of **L2** for Lyz. The experimental and instrumental conditions were identical to those used for the liquid sample DESI measurements described above, with the exception that **L2** was absent in the sample solution but present in the spray solvent. Shown in Figure 2.7 is a representative reactive liquid sample DESI mass spectrum acquired for an aqueous ammonium acetate (20 mM) solution of Lyz (10 μM) and Ubq (5 μM); the spray solvent was a 50/50 water/acetonitrile solution containing **L2** (50 μM).

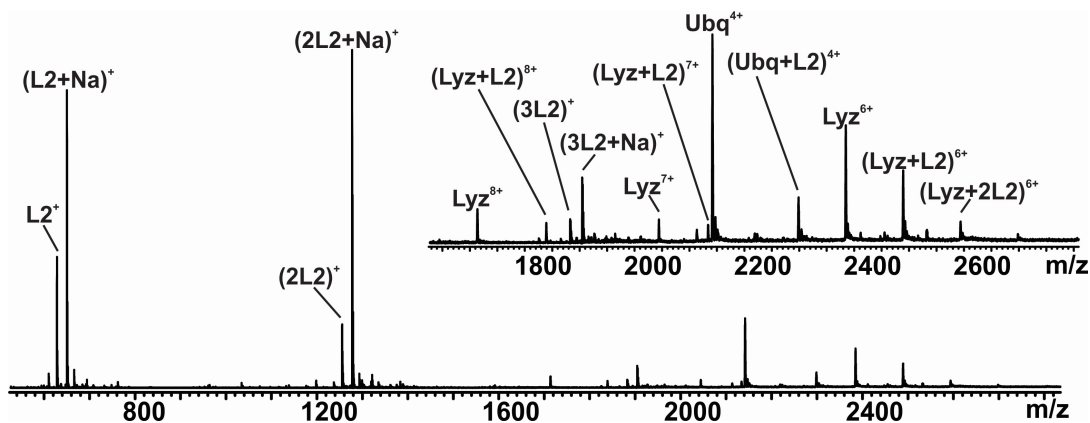


Figure 2.7 Representative reactive liquid sample DESI mass spectrum acquired in positive ion mode for an aqueous ammonium acetate (20 mM, pH 6.8 and 25 °C) solution containing Lyz (10 μ M) and Ubq (5 μ M) and an ESI spray solution (50/50 water/acetonitrile) that contained **L2** (50 μ M). The flow rates of both the sample and ESI spray solution were 5 μ L min^{-1} . All other instrumental conditions were identical to those used for the liquid sample DESI measurements.

Ion signal corresponding to protonated and sodiated **L2** monomer, dimer and trimer was detected, along with protonated ions of Lyz and (**Lyz + L2**), at charge states +6 to +8, and Ubq and (**Ubq + L2**), at charge state +4. Following correction for nonspecific carbohydrate-protein binding, the K_a value was determined to be $(7.9 \pm 0.4) \times 10^3 \text{ M}^{-1}$, which is similar to the value reported by Loo and coworkers.²⁷ Given that the instrumental conditions were identical to those used for the liquid sample DESI-MS measurements, it can be concluded that the lower affinity is not due to artifacts associated with instrumental conditions, such as in-source dissociation of the protein-carbohydrate complexes. This finding further supports the suggestion that the lower affinity is, in fact,

a kinetic artifact owing to the insufficient time in the droplets for the protein-ligand binding equilibrium to be established.²⁰

2.3.4 Tolerance of liquid sample DESI-MS to non-volatile salts

The influence of non-volatile salts on the performance of liquid sample DESI-MS for protein-carbohydrate binding measurements was assessed by through binding measurements performed on Lyz and **L2** in aqueous solutions containing varying concentrations of PBS. Shown in Figures 2.8a-2.8c are representative liquid sample DESI mass spectra acquired for aqueous solutions of ammonium acetate (20 mM), Lyz (40 μ M), **L2** (30 μ M) and 0.1x PBS, 0.5x PBS or 1x PBS. For comparison purposes, ESI mass spectra were also acquired for these solutions (Figures 2.8d-2.8f). At PBS concentrations up to 1x, abundant signal corresponding to protonated ions of Lyz and (**Lyz + L2**) at charge states +7 to +9 was detected. However, adducts corresponding to the attachment of Na^+ , NaCl , K^+ and KCl were also evident and their abundances increased with increasing PBS concentration. The K_a values determined at each PBS concentration are $(1.0 \pm 0.1) \times 10^5 \text{ M}^{-1}$ (0.1x), $(5.0 \pm 0.2) \times 10^4 \text{ M}^{-1}$ (0.5x) and $(4.1 \pm 0.2) \times 10^4 \text{ M}^{-1}$ (1x). The value at 0.1x PBS is similar to the one measured in aqueous ammonium acetate (20 mM), however, the values at the higher PBS concentrations are about a factor of two smaller. A similar phenomenon was reported by Oldham and coworkers, who proposed that alkali metal ions may destabilize Lyz-ligand complexes in the gas phase.⁴⁵ To establish whether the lower values measured at higher PBS concentrations were reflective of an actual decrease in affinity, ITC was used to measure K_a in a solution of 1x PBS (Figure 2.9).

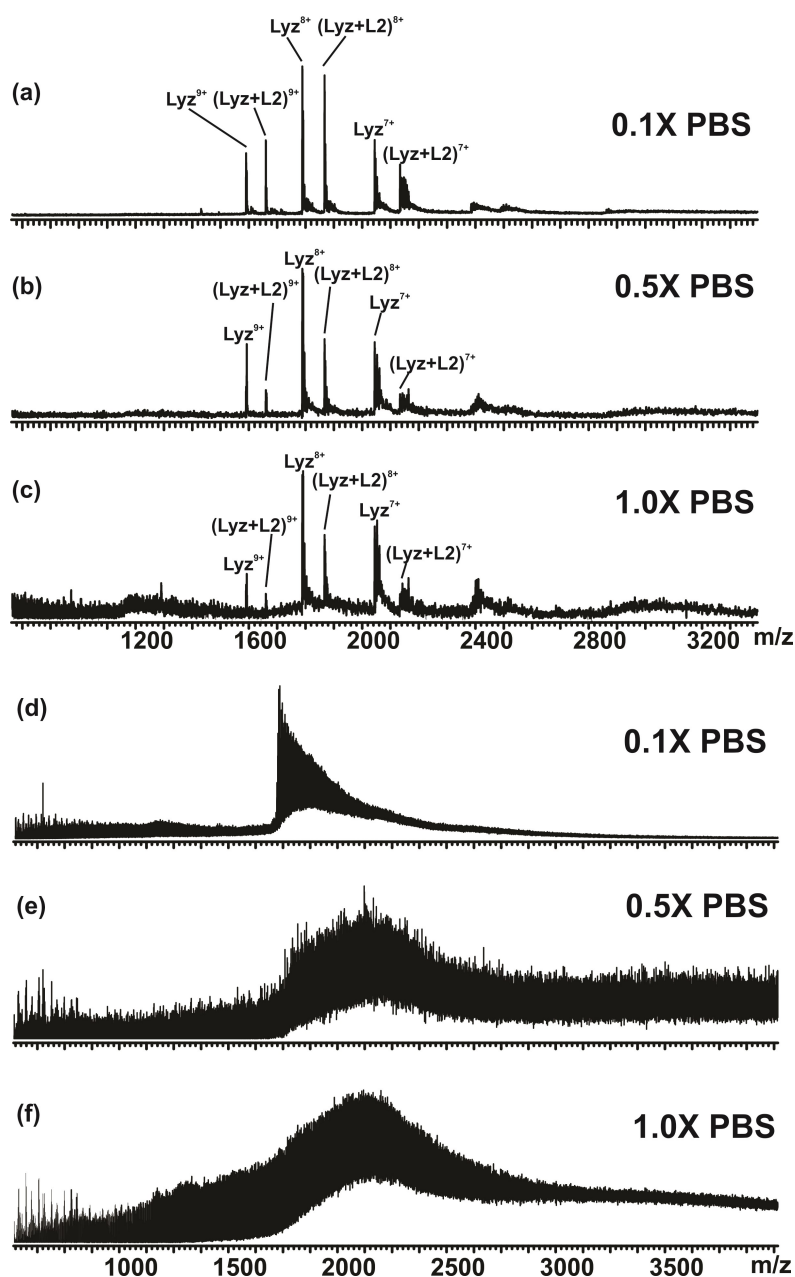


Figure 2.8 Representative (a), (b) and (c) liquid sample DESI and (e), (f) and (g) ESI mass spectra acquired for aqueous solutions (pH 7.4 and 25 °C) containing Lyz (40 μM) and L2 (30 μM) in 20 mM ammonium acetate and 0.1x PBS ((a) and (d)), 0.5x PBS ((b) and (e)) and 1x PBS ((c) and (f)). For the liquid sample DESI-MS measurements, the ESI spray solution was 50/50 water/acetonitrile.

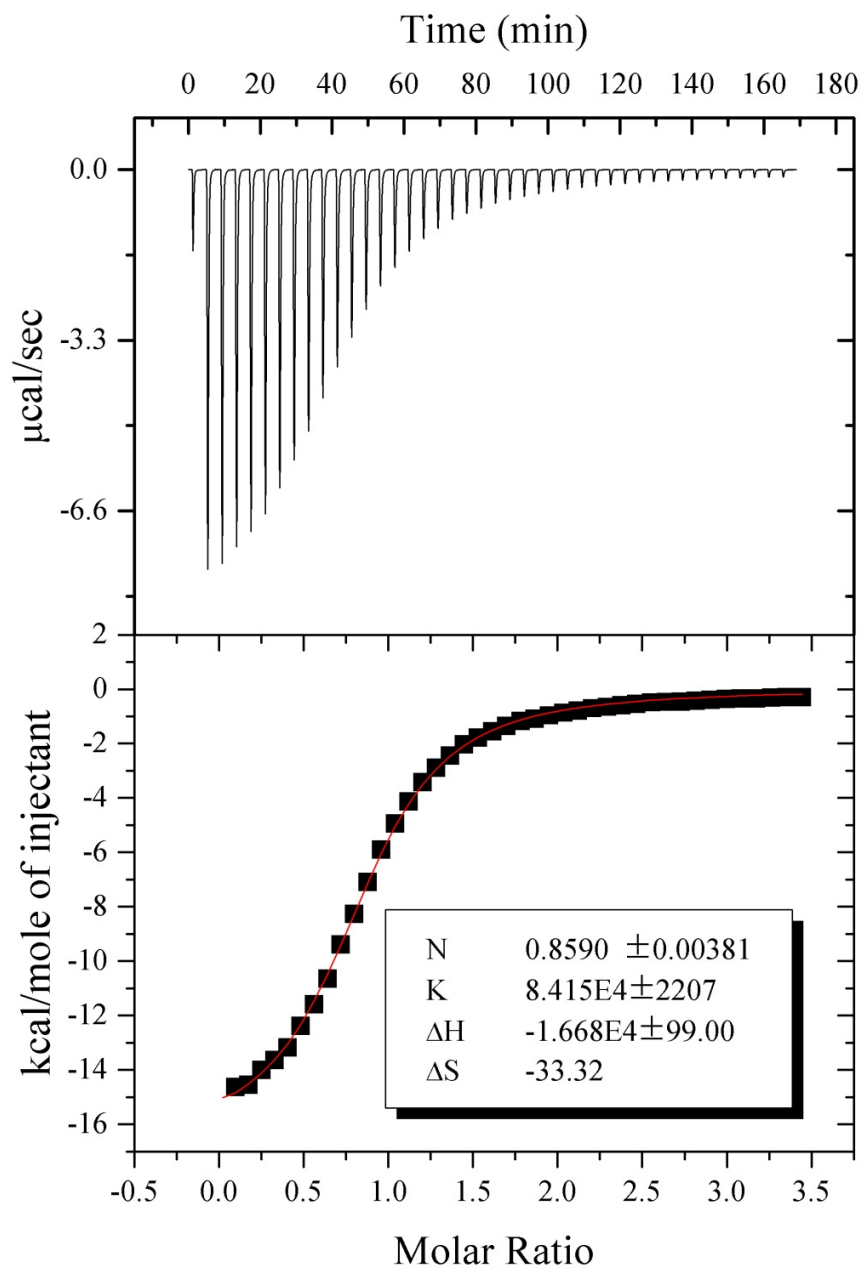


Figure 2.9 ITC data measured for the binding of Lyz (0.128 mM) to L2 (2.0 mM) in 1x PBS (pH 7.4 and 25 °C).

Notably, the ITC-derived value of $(8.4 \pm 0.2) \times 10^4 \text{ M}^{-1}$ confirmed that the interaction between **L2** and Lyz is slightly weakened at high PBS concentrations, although the magnitude of the effect is not as pronounced as suggested by the liquid sample DESI-MS measurements. Nevertheless, the affinity measured by liquid sample DESI-MS for the 1x solution agrees within a factor of two of the ITC value, indicating that liquid sample DESI-MS can be used to quantify protein-carbohydrate interactions in solutions containing relatively high concentrations of nonvolatile salts. The situation is very different in the case of the ESI mass spectra, which reveal the presence of significant nonspecific adducts (Figures 2.8d-2.8f). In fact, even for the 0.1x PBS solution, it was not possible to positively identify ions corresponding to the (Lyz + **L2**) complex, making it impossible to quantify the binding interaction. Further investigation revealed that the direct ESI-MS binding measurements were restricted to PBS concentrations of less than ~0.02x.

The differences in the appearances of the liquid sample DESI and ESI mass spectra can be rationalized by considering the differences in the initial composition of the droplets in each case. In the ESI-MS experiments, the initial droplets will contain concentrations of buffer that are similar to that found in bulk solution, with some enrichment in cations (Na^+ and K^+) expected as a result of the applied electric field.¹⁹ As a result of solvent evaporation, the concentration of buffer components in the droplets will further increase, with the highest concentrations found in the offspring droplets produced late in the ESI process.¹⁹ In contrast, in liquid sample DESI-MS, the initial ESI droplets are devoid of buffer and contain only water and acetonitrile. It is only through

collisions with the sample solution that buffer components are transferred to the ESI droplets. Consequently, the overall concentration of PBS in the droplets of liquid sample DESI that lead to the formation of gaseous protein ions is expected to be significantly lower than in the case of the direct ESI-MS measurements.

2.4 Conclusions

In summary, the application of liquid sample DESI-MS for quantifying protein-carbohydrate interactions in aqueous solutions is described. Notably, the affinities of tri- and tetrasaccharide ligands for Lyz and scFv measured using liquid sample DESI-MS are found to be in good agreement with values measured by ITC and the direct ESI-MS assay. It is also found that the reference protein method, which was originally developed to correct ESI mass spectra for the occurrence of nonspecific ligand-protein binding, can be used to correct liquid sample DESI mass spectra for nonspecific carbohydrate binding. The tolerance of liquid sample DESI-MS for quantitative binding measurements carried out using solutions containing high concentrations of PBS was also explored. The binding between Lyz and a trisaccharide ligand was successfully measured with liquid sample DESI-MS at concentrations up to 1x PBS. In contrast, direct ESI-MS binding measurements were limited to PBS concentrations less than ~ 0.02 x PBS.

2.5 Literature cited

1. Bewley, C.A., *Protein-carbohydrate Interactions in Infectious Diseases*. RSC Publishing: Cambridge, UK, **2006**
2. Disney, M.D., Seeberger, P.H., *Chem Biol.* **2004**, *11*, 1701-1707.
3. Leavitt, S., Freire, E., *Curr Opin Struct Biol.* **2001**, *11*, 560-566.
4. Frostell, Å., et al., *Methods in molecular biology.* **2013**, *1008*, 139-165.
5. Zech, S.G., et al., *J Am Chem Soc.* **2004**, *126*, 13948-13953.
6. Orosz, F., Ovadi, J., *J Immunol Methods.* **2002**, *270*, 155-162.
7. El-Hawiet, A., et al., *Anal Chem.* **2013**, *85*, 7637-7644.
8. Lin, H., et al., *J Am Soc Mass Spectrom.* **2014**, *25*, 104-110.
9. Han, L., et al., *Glycobiology.* **2013**, *23*, 276-285.
10. El-Hawiet, A., et al., *Anal Chem.* **2012**, *84*, 3867-3870.
11. El-Hawiet, A., et al., *Biochemistry.* **2012**, *51*, 4244-4253.
12. Daniel, J.M., et al., *Int J Mass Spectrom.* **2002**, *216*, 1-27.
13. Kitova, E.N., et al., *J Am Soc Mass Spectrom.* **2012**, *23*, 431-441.
14. El-Hawiet, A., et al., *J Am Soc Mass Spectrom.* **2010**, *21*, 1893-1899.
15. Deng, L., et al., *Anal Chem.* **2010**, *82*, 2170-2174.
16. El-Hawiet, A., et al., *Anal Chem.* **2012**, *84*, 50-58.
17. Loo, J.A., *Mass Spectrom Rev.* **1997**, *16*, 1-23.
18. Wang, W., et al., *Anal Chem.* **2003**, *75*, 4945-4955.
19. Kebarle, P., *J Mass Spectrom.* **2000**, *35*, 804-817.
20. Banerjee, S., Mazumdar, S., *Int J Anal Chem.* **2012**, *2012*, 282574.
21. Sterling, H.J., et al., *J Am Soc Mass Spectrom.* **2010**, *21*, 1045-1049.

22. Yang, P., et al., *Anal Chem.* **2005**, *77*, 6174-6183.
23. Takats, Z., et al., *Science.* **2004**, *306*, 471-473.
24. Shin, Y.S., et al., *Anal Chem.* **2007**, *79*, 3514-3518.
25. Lu, X., et al., *J Am Soc Mass Spectrom.* **2014**, *25*, 454-463.
26. Miao, Z., Chen, H., *J Am Soc Mass Spectrom.* **2009**, *20*, 10-19.
27. Liu, P., et al., *Anal Chem.* **2013**, *85*, 11966-11972.
28. Ferguson, C.N., et al., *Anal Chem.* **2011**, *83*, 6468-6473.
29. Moore, B.N., et al., *Int J Mass Spectrom.* **2012**, *330-332*, 220-225.
30. Takats, Z., et al., *J Mass Spectrom.* **2005**, *40*, 1261-1275.
31. Veros, C.T., Oldham, N.J., *Rapid Commun Mass Spectrom.* **2007**, *21*, 3505-3510.
32. Sun, N., et al., *J Am Soc Mass Spectrom.* **2010**, *21*, 472-481.
33. Jecklin, M.C., et al., *J Am Soc Mass Spectrom.* **2008**, *19*, 332-343.
34. Zdanov, A., et al., *Proc Natl Acad Sci U S A.* **1994**, *91*, 6423-6427.
35. Rademacher, C., et al., *J Am Chem Soc.* **2007**, *129*, 10489-10502.
36. Wang, W., et al., *Anal Chem.* **2005**, *77*, 3060-3071.
37. Sun, J., et al., *Anal Chem.* **2006**, *78*, 3010-3018.
38. Daneshfar, R., et al., *J Am Chem Soc.* **2004**, *126*, 4786-4787.
39. Kitova, E.N., et al., *J Am Soc Mass Spectrom.* **2014**, *25*, 1908-1916.
40. Schindler, M., et al., *Biochemistry.* **1977**, *16*, 423-431.
41. Hunter, E.P., Lias, S.G., *J Phys Chem Ref Data.* **1998**, *27*, 413-656.
42. Venter, A., et al., *Anal Chem.* **2006**, *78*, 8549-8555.
43. Miao, Z., et al., *J Am Soc Mass Spectrom.* **2010**, *21*, 1730-1736.
44. Hopper, J.T., et al., *Anal Biochem.* **2012**, *421*, 788-790.

45. Hopper, J.T., Oldham, N.J., *Anal Chem.* **2011**, *83*, 7472-7479.

Chapter 3

Influence of Sulfolane on ESI-MS Measurements of Protein-Ligand Affinities[†]

3.1 Introduction

The direct electrospray ionization mass spectrometry (ESI-MS) assay is a valuable tool for detecting and quantifying non-covalent protein-ligand interactions *in vitro*.¹ In addition to its speed, sensitivity and selectivity, the assay is free of any requirements of immobilization or labeling of either the protein or the ligand, making it a highly versatile binding assay. Moreover, the method is well suited for screening libraries of compounds to simultaneously identify and quantify the highest affinity ligands.² And when implemented using a catch-and-release (CaR) format (i.e., CaR-ESI-MS), the assay enables the screening of libraries against high molecular weight (MW) protein assemblies, such as viral capsid protein particles, for which the protein-ligand complexes are difficult to analyze directly by ESI-MS.³ A semi-quantitative ESI-MS assay suitable for screening natural compound libraries at unknown concentrations, such as mixtures of human milk oligosaccharides isolated from breast milk, against target proteins to identify interactions and rank their affinities was also recently described.⁴

While these ESI-MS assays allow for the detection and quantification of protein-ligand interactions *in vitro*, they do not, on their own, provide insight into the location or nature of the interactions. There is evidence that intermolecular interactions are largely preserved upon transfer of protein-ligand complexes from solution to the gas phase using ESI from studies of several protein-ligand complexes using the blackbody infrared radiative

[†] A version of this chapter has been published: Yao, Y., Richards, M. R., Kitova, E. N., Klassen, J. S., *J Am Soc Mass Spectrom.*, 2016, 27,498-506.

dissociation/functional group replacement strategy.⁵⁻¹⁰ Consequently, one possible strategy for localizing ligand binding sites involves so-called “top-down” MS using electron-mediated activation methods, such as electron capture dissociation (ECD) and electron transfer dissociation (ETD). With this approach, the identification of peptide fragments retaining the ligand serves to localize the binding site(s). To date, binding sites of several protein–ligand complexes,¹¹⁻¹⁷ including α -synuclein-spermine,¹⁵ adenylate kinase-ATP¹⁶ and anterior gradient-2-PTTIYY hexapeptide interactions,¹⁷ were identified using this approach.

In order for such a top-down approach to be effective for ligand localization, there must be extensive fragmentation of the protein-ligand complex ions in the gas phase. One of the limitations of the electron-mediated dissociation methods is the low efficiency of the electron transfer/capture processes.^{12, 17-22} Because electron capture cross sections increase quadratically with charge state, the efficiency of the process can be improved by increasing the charge state of the gaseous complex.¹² As shown by a number of different laboratories, the charge states of proteins and protein complexes in ESI can be significantly increased through the use of so-called “supercharging reagents”, such as 3-nitrobenzoic acid (*m*-NBA) and sulfolane.²³⁻²⁷ The mechanisms responsible for enhanced charging induced by supercharging agents have been extensively studied.²³⁻²⁹ In a recent review, Loo and co-workers concluded that efficient positive ion supercharging reagents must be weak Brønsted bases, soluble in aqueous solution and be less (or similarly) volatile as the solvent.³⁰ They also advanced the hypothesis that high concentrations of the supercharging reagent in the ESI progeny droplets reduce the extent of acidic residue ionization, which effectively results in an increase in the protonation state of the gaseous protein ions.³⁰

While there have been many reported examples of protein supercharging in ESI-MS, there have been relatively few studies of the effects of supercharging agents on the structures and stabilities of multiprotein and protein-ligand complexes. Loo and coworkers reported that the supercharging of several protein-ligand and multiprotein complexes using *m*-NBA was accompanied with little or no change their native structures and non-covalent interactions.²⁴ More recently, it was shown by the same group that the use of sulfolane in reactive liquid sample desorption ESI (DESI)-MS can produce supercharging without destabilizing protein-ligand complexes.³¹ However, studies have also shown that the structures and interactions of other protein complexes are susceptible to supercharging agents. For example, heme loss from myoglobin was observed upon addition of *m*-NBA or sulfolane to solution.²⁵⁻²⁷

The goal of the present study is to investigate the influence of sulfolane on ESI-MS measurements of protein-ligand affinities *in vitro*. With this in mind, ESI-MS binding measurements were carried out on four protein-carbohydrate complexes in the presence and absence of sulfolane. The interactions between lysozyme (Lyz) and the tetrasaccharide ligand β -D-GlcNAc-(1 \rightarrow 4)- β -D-GlcNAc-(1 \rightarrow 4)- β -D-GlcNAc-(1 \rightarrow 4)-D-GlcNAc (**L1**), a single chain variable fragment (scFv) of the monoclonal antibody Se155-4 and the trisaccharide ligand α -D-Gal-(1 \rightarrow 2)-[α -D-Abe-(1 \rightarrow 3)]- α -D-Man-OCH₃ (**L2**), cholera toxin B subunit homopentamer and the GM1 pentasaccharide β -D-Gal-(1 \rightarrow 3)- β -D-GalNAc-(1 \rightarrow 4)-[α -D-Neu5Ac-(2 \rightarrow 3)]- β -D-Gal-(1 \rightarrow 4)- β -D-Glc (**L3**) and a fragment of galectin 3 and the tetrasaccharide ligand α -L-Fuc-(1 \rightarrow 2)- β -D-Gal-(1 \rightarrow 3)- β -D-GlcNAc-(1 \rightarrow 3)- β -D-Gal-(1 \rightarrow 4)- β -D-Glc (**L4**) served as model systems for this study. Having found evidence that sulfolane generally

reduces the apparent affinity, a detailed study of the origin of the reduced affinity was undertaken using the Lyz-L1 interaction as a model. Measurements were carried out using isothermal titration calorimetry (ITC), circular dichroism (CD) and nuclear magnetic resonance (NMR) spectroscopy to establish how sulfolane affects the structure and stability of the protein-tetrasaccharide complex in solution. Finally, the effect of sulfolane on protein-ligand affinity measurements carried out using liquid sample DESI-MS was explored.

3.2 Experimental

3.2.1 Materials

Ubiquitin (Ubq, MW 8565 Da), lysozyme from chicken egg white (Lyz, MW 14310 Da), cholera toxin B subunit homopentamer from *Vibrio cholera* (CTB₅, MW 58 kDa) were purchased from Sigma-Aldrich Canada (Oakville, Canada). The C-terminal fragment (residues 107-250) of human galectin-3 (Gal-3C, MW 16340 Da) and single chain variable fragment (scFv, MW 26539 Da) of the monoclonal antibody Se155-4 were produced and purified as described previously.³²⁻³³ The tetrasaccharide **L1** (MW 830.3 Da) was purchased from Dextra Science and Technology Centre (Reading, UK); the trisaccharide **L2** (MW 486.5 Da) was a gift from Prof. D. Bundle (University of Alberta); the GM1 pentasaccharide **L3** (MW 998.3 Da) was purchased from HyTest Ltd. (Turku, Finland) and the tetrasaccharide **L4** (MW 854.6 Da) was purchased from IsoSep AB (Tullinge, Sweden). Stock solutions of each protein (in 200 mM ammonium acetate) and each oligosaccharide (in deionized water) were prepared and stored at -20 °C until needed.

3.2.2 Mass spectrometry

A Synapt G2 quadrupole-ion mobility separation-time-of-flight (Q-IMS-TOF) mass

spectrometer (Waters UK Ltd., Manchester, UK) with an 8k quadrupole mass filter and a Synapt G2S Q-IMS-TOF mass spectrometer (Waters, Manchester, UK) with a 32k quadrupole mass filter were used for ESI-MS and liquid sample DESI-MS measurements. Both instruments were equipped with nanoflow ESI (nanoESI) sources, which were operated in positive ion mode. NanoESI tips (~5 μm i.d.) were produced from borosilicate capillaries (1.0 mm o.d., 0.68 mm i.d.), using a P-1000 micropipette puller (Sutter Instruments, Novato, CA, USA). A capillary voltage of 1.0 - 1.3 kV was applied to a platinum wire to initiate the spray on the Synapt G2 instrument, where the platinum wire was inserted into the nanoESI tip, and a Capillary voltage of between 0.8 and 1.0 kV applied to the Synapt G2S instrument. In both instruments, the Cone voltage was maintained at 30 V and the source block temperature was 60 °C. The Trap and Transfer collision energies were 5 V and 2 V, respectively, and the argon pressures in the Trap and Transfer regions were 8.56×10^{-3} mbar and 8.62×10^{-3} mbar, respectively, for the Synapt G2S and 9.17×10^{-3} mbar and 9.28×10^{-3} mbar, respectively, for the Synapt G2. For the liquid sample DESI-MS measurements, a modified OMNI SPRAY Ion Sources 2-D OS-6205 (Prosolia Inc., Indianapolis, IN) was used. Details of the experimental setup can be found elsewhere.³⁴ Briefly, the liquid sample solution was delivered through a silica capillary (360 μm o.d., 100 μm i.d.) at a flow rate of 15 $\mu\text{L h}^{-1}$ using a syringe pump. The outlet of the sample capillary was located between ESI spray tip and the inlet to the mass spectrometer. The ESI solution flow rate was 2-3 $\mu\text{L min}^{-1}$. Capillary and Cone voltages of 3.5 kV and 30 V, respectively, were used and the pressure of the N_2 nebulizing gas was 65 psi. The source block temperature was the same as for the ESI-MS binding measurements. All data were processed using MassLynx software (v4.1).

3.2.3 Isothermal titration calorimetry

The ITC affinity measurements performed on the Lyz-L1 interaction were carried out using a VP-ITC (MicroCal, Inc., Northampton, MA). For each ITC experiment, the Lyz solution (0.2 mM) in the sample cell was titrated with a solution of L1 (2 mM); both the Lyz and L1 solutions were aqueous ammonium acetate (50 mM, pH 6.8, 25 °C) containing varying percentages of sulfolane (2%, 5% or 10%).

3.2.4 Circular dichroism

Circular dichroism (CD) spectra were recorded at 25 °C on an OLIS DSM CARY-17 spectrophotometer conversion and circular dichroism module (On-line Instrument Systems Inc.) using a 0.2 mm path length quartz cuvette. Protein solutions (56 μM) were prepared in phosphate buffer (20 mM, pH 7.0) and varying percentages of sulfolane (0 to 20%). Data were collected in scanning mode from 250 to 190 nm and the average value of five repetitions was reported. Data were analyzed with OLIS Spectral Works (v4.3) and converted into molar ellipticity units. For each solution, the CD spectrum of the solvent alone was subtracted from the sample spectrum.

3.2.5 NMR spectroscopy

All NMR spectra were acquired at 27 °C on a 700 MHz Agilent/Varian spectrometer equipped with a cold probe (Agilent Technologies Inc., CA). 1D ¹H and TROESY³⁵ NMR spectra were obtained for L1 in D₂O and in 2% (v/v) sulfolane–D₂O. The spectra were referenced to an external standard of acetone (2.22 ppm for ¹H), and the intensity of the residual HOD peak was decreased using a presaturation pulse sequence, irradiating at 4.76 ppm. The spectral window was 8389 Hz (from 10.76 to –1.22 ppm). The 1D ¹H spectra were acquired in 16 transients, and no window functions were applied in the Fourier

transformation. The TROESY spectra were acquired with 8 transients in F2, 256 increments in F1, and a mixing time of 0.4 s. Sine-bell functions were applied interactively to improve signal-to-noise in the TROESY, but no line-broadening was used.

Natural abundance ^1H - ^{15}N gHSQC NMR spectra were obtained for Lyz and Lyz-L1 complex in 10% (v/v) D_2O - H_2O with varying concentrations of sulfolane – 0, 2, 5, and 10% (v/v). The Lyz concentration was 5 mM, and the L1 concentration was 20 mM. The spectra were acquired in a 5 mm D_2O -matched Shigemi tube at 27 °C on a 700 MHz Agilent/Varian spectrometer equipped with a cold probe and referenced using the default parameters in the VNMR software. The spectral window for ^1H was 8389 Hz (from 10.71 to -1.26 ppm), and the spectral window for ^{15}N was 3545 Hz (139.8 to 90.2 ppm). The spectra were acquired with 16 transients in F2, 64 increments in F1 – except for Lyz in 10% D_2O - H_2O , which was acquired with 76 increments in F1. The proton signals were decoupled during acquisition, and a $^1J_{\text{N,H}}$ value of 90 Hz was used. Sine-bell functions were applied interactively to improve signal-to-noise, but no line-broadening was used. An additional ^1H - ^{15}N gHSQC NMR spectrum was acquired for denatured Lyz in 8M urea and 10% (v/v) D_2O - H_2O . This spectrum was acquired in a 3 mm NMR tube, with 128 transients in F2 and 64 increments in F1. The remaining parameters were the same as for the folded protein.

3.2.6 Data analysis

3.2.6.1 Average charge state calculation

The average charge state (*ACS*) of the protein-ligand complexes ions was calculated from the ESI mass spectrum using eq 1:

$$ACS = \frac{\sum [Ab(PL^{n+}) \times n]}{\sum_n Ab(PL^{n+})} \quad (1)$$

where $Ab(PL^{n+})$ is the abundance of the protein-ligand complex ions and n is the charge state. The ACS of the protein ions was calculated in the same way.

3.2.6.2 Association constants from ESI mass spectra

The general procedure for determining association constants (K_a) for protein-ligand interactions from ESI mass spectra has been described in detail elsewhere^{34, 36-38} and only a brief description is given for the case where the protein has single ligand binding site. The assay relies on the detection and quantification of the gas-phase ions of the free and ligand-bound protein. Following correction of the mass spectrum for the occurrence of nonspecific ligand-protein binding during the ESI process using the reference protein method,³⁷⁻³⁸ the ratio (R) of the total abundance (Ab) of ligand-bound protein (PL) to free protein (P) ions is taken to be equal to the concentration ratio of PL to P, eq 2:

$$R = \frac{\sum Ab(PL)}{\sum Ab(P)} = \frac{[PL]}{[P]} \quad (2)$$

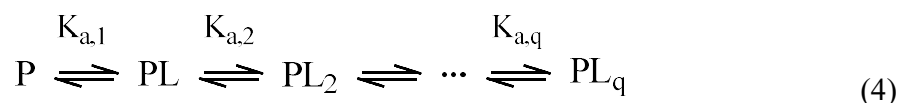
and K_a calculated from eq 3:

$$K_a = \frac{R}{[L]_0 - \frac{R}{1+R}[P]_0} \quad (3)$$

where $[P]_0$ and $[L]_0$ are the initial protein and ligand concentrations, respectively. Details on the determination of K_a for the stepwise binding of **L3** to **CTB₅**³⁹⁻⁴⁰ are given below.

3.2.6.3 Determination of association constants for stepwise binding of L3 to CTB₅

A general expression for the association constants ($K_{a,q}$) for the stepwise binding of ligand (L) to protein (P) (eq 4) is given by eq 5 [1]:



$$K_{a,q} = \frac{R_q}{R_{q-1} \left([L]_0 - \frac{(R_1 + 2R_2 + \dots + qR_q)[P]_0}{1 + R_1 + R_2 + \dots + R_q} \right)} \quad (5)$$

where $[L]_0$ and $[P]_0$ are the initial concentrations of L and P, respectively. R_q is the concentration ratio of ligand-bound (to q molecules of L) to free P, which is taken to be equal to the total ion abundance ratio of the corresponding gas-phase ions as determined from the ESI mass spectrum, eq 6:

$$R_q = \frac{\sum Ab(PL_q)}{\sum Ab(P)} = \frac{[PL_q]_{eq}}{[P]_{eq}} \quad (6)$$

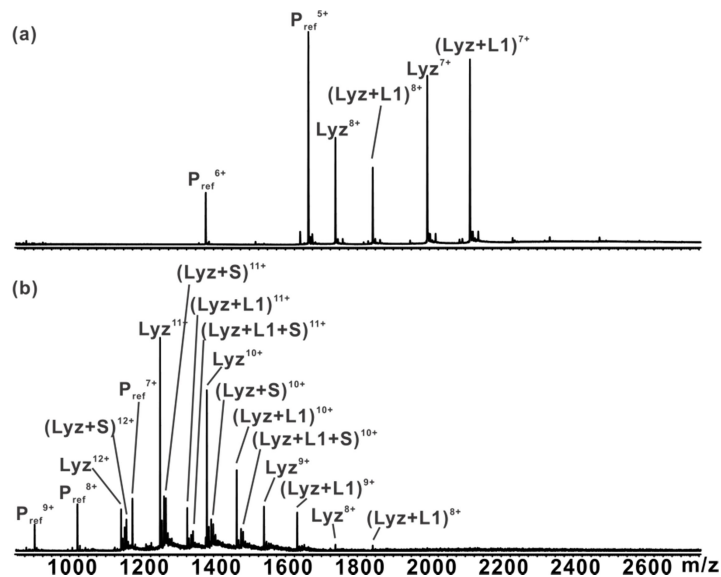
3.3 Results and discussion

3.3.1 Influence of sulfolane on protein-carbohydrate affinities

Direct ESI-MS binding measurements. ESI-MS binding measurements were carried out on four protein-carbohydrate complexes to assess whether protein-ligand interactions are generally influenced by the presence of sulfolane in solution. Shown in Figures 3.1 and 3.2 are representative ESI mass spectra acquired in positive ion mode for aqueous ammonium acetate solutions (50 mM, pH 6.8 and 25 °C) containing each protein/carbohydrate ligand pair in the absence and presence of sulfolane (H₂O:sulfolane 98:2 v/v). A reference protein (P_{ref}) was added to each solution in order to identify the occurrence of nonspecific carbohydrate-protein binding during the ESI process.³⁷⁻³⁸

Inspection of the mass spectrum measured for a solution of Lyz (10 μM), L1 (15 μM)

and $P_{\text{ref}}(\text{Ubq}, 5 \mu\text{M})$ reveals the presence of protonated Lyz^{n+} and $(\text{Lyz} + \text{L1})^{n+}$ ions, at $n = 7$ and 8 , together with Ubq^{n+} ions at $n = 5$ and 6 (Figure 3.1a). The absence of $(P_{\text{ref}} + \text{L1})^{n+}$ ions indicates that nonspecific binding was negligible under these experimental conditions. From the ratio of the total abundance of $(\text{Lyz} + \text{L1})^{n+}$ to Lyz^{n+} ions and the known initial concentrations, a K_a value of $(7.6 \pm 0.2) \times 10^4 \text{ M}^{-1}$ was determined from the mass spectrum (eqs 2 and 3). This value is in reasonable agreement with previously reported values, $0.8\text{-}1.1 \times 10^5 \text{ M}^{-1}$.^{34, 41-42} Upon addition of 2% sulfolane to the solution, the charge states of the Lyz^{n+} and $(\text{Lyz} + \text{L1})^{n+}$ ions shifted to $n = 8 - 12$ (Figure 3.1b). This shift corresponds to an increase of 35% in *ACS* for the $(\text{Lyz} + \text{L1})^{n+}$ ions; the Lyz^{n+} ions exhibited a similar increase in *ACS* (~40% increase). The P_{ref}^{n+} ions also shifted to higher charges states, $n = 6$ to 10 , which corresponds to a 50% increase in *ACS*. Also evident in the mass spectrum are Lyz^{n+} and $(\text{Lyz} + \text{L1})^{n+}$ ions bound to one or more sulfolane molecules.



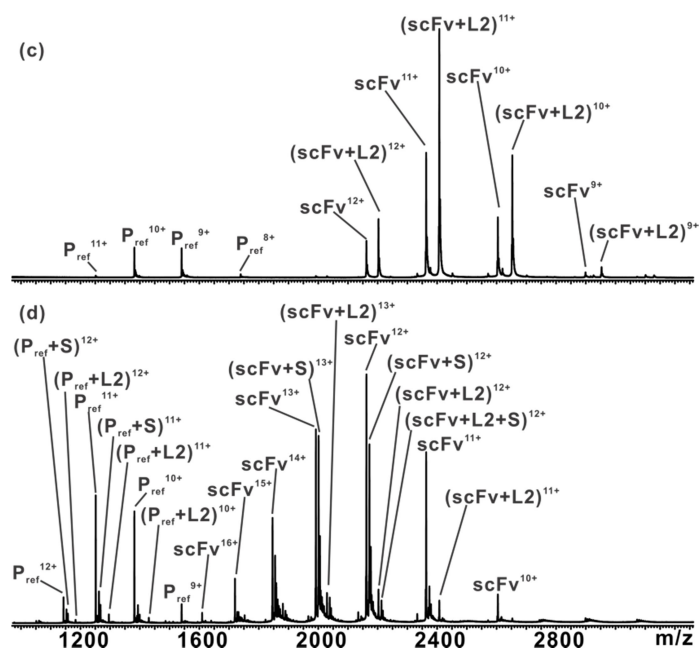


Figure 3.1 Representative ESI mass spectra acquired in positive ion mode for aqueous ammonium acetate (50 mM) solutions of Lyz (10 μ M), **L1** (15 μ M) and P_{ref} (Ubq, 5 μ M) with (a) 0% sulfolane and (b) 2% sulfolane, or scFv (10 μ M), **L2** (15 μ M) and P_{ref} (Lyz, 5 μ M), with (c) 0% sulfolane and (d) 2% sulfolane. Nonspecific sulfolane adducts are labelled as “S”.

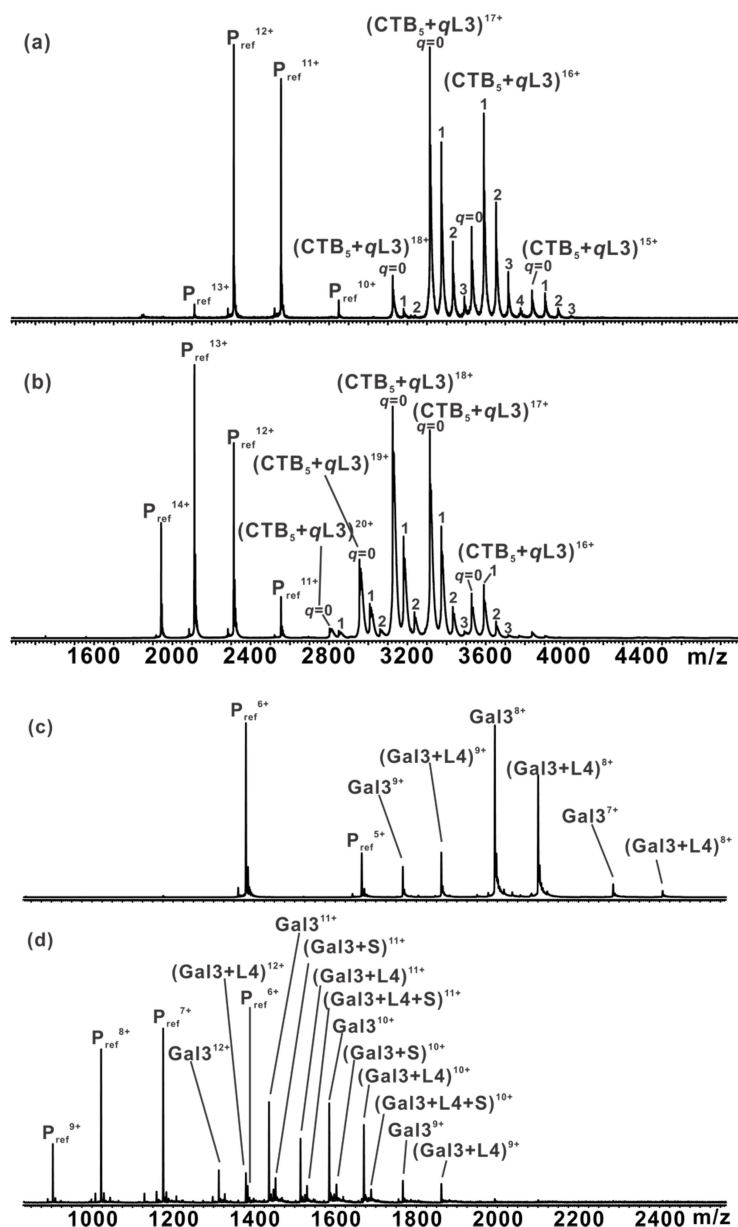


Figure 3.2 Representative ESI mass spectra acquired in positive ion mode for aqueous ammonium acetate (50 mM) solutions of CTB₅ (5 μM), L3 (5 μM) and P_{ref} (scFv, 3 μM) with (a) 0% sulfolane and (b) 2% sulfolane, or Gal3-C (10 μM), L4 (10 μM) and P_{ref} (Ubq, 5 μM) with (c) 0% sulfolane and (d) 2% sulfolane. Nonspecific sulfolane adducts are labelled as “S”.

Similar observations have been reported for other proteins analyzed in the presence of sulfolane by ESI-MS.⁴³ Notably, there is a significant reduction in the abundance of (Lyz + L1)ⁿ⁺ ions, relative to Lyzⁿ⁺ ions; the measured K_a is $(4.1 \pm 0.1) \times 10^4 \text{ M}^{-1}$, which corresponds to a 46% decrease in affinity compared to the value measured for the same solution but in the absence of sulfolane.

Analogous measurements were carried out on solutions with up to 10% sulfolane. Plotted in Figure 3.3 are the *ACS* values determined for the (Lyz + L1)ⁿ⁺ ions and the corresponding K_a values measured for the solutions at different percentages of sulfolane.

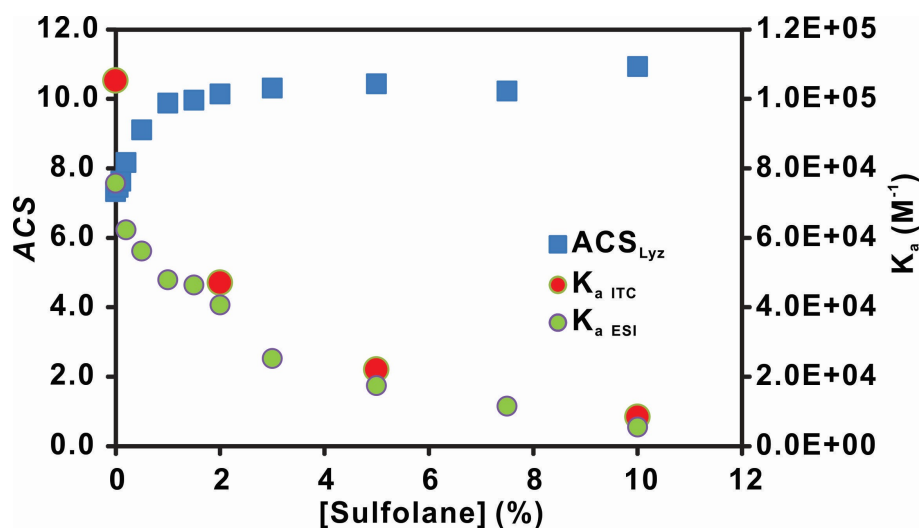


Figure 3.3 Plot of average charge state (*ACS*) of the (Lyz + L1) ions observed from ESI mass spectra acquired for aqueous ammonium acetate (50 mM) solutions of Lyz (10 μM), L1 (15 μM) and Ubq (5 μM) with 0 – 10% sulfolane. Also shown are the association constants (K_a) for the (Lyz + L1) interaction measured by ESI-MS and isothermal titration calorimetry (ITC).

It can be seen that the dependence of *ACS* on sulfolane concentration is most pronounced up to ~2% sulfolane; at higher concentrations only a slight increase in *ACS* was observed, reaching a value of (10.93±0.01) at 10% sulfolane. The dependence of K_a is also most pronounced at the lower concentrations of sulfolane, but the affinity continues to decrease with increasing sulfolane concentrations, dropping to (5.5±0.3) x 10³ M⁻¹ at 10% sulfolane. This change in K_a corresponds to a 93% decrease in affinity.

The results obtained for the scFv-**L2**, CTB₅-**L3** and Gal3C-**L4** interactions are qualitatively similar to those described above for the Lyz-**L1** system. Shown in Figures 3.1c and 3.1d are the ESI mass spectra for a solution of scFv (10 μM), **L2** (10 μM) and P_{ref} (Lyz, 5 μM), in the absence and presence of sulfolane, respectively. In the absence of sulfolane, protonated scFvⁿ⁺ and (scFv + **L2**)ⁿ⁺ ions, at n = 9 to 12, together with P_{ref}ⁿ⁺ ions at n = 8 to 11, were detected. The measured K_a value for the (scFv + **L2**) complex, (8.2±0.1) x 10⁴ M⁻¹, is in good agreement with the reported values, which are in the 0.66-1.2 x 10⁵ M⁻¹ range.^{34,44} Upon addition of sulfolane, the *ACS* of the scFvⁿ⁺ and (scFv + **L2**)ⁿ⁺ ions increased by ~14% and the presence of sulfolane adducts was evident. The measured K_a , (2.9±0.1) x 10³ M⁻¹, is 96% smaller than the value ((8.2±0.1) x 10⁴ M⁻¹) measured in the absence of sulfolane. Shown in Figures 3.2a and 3.2b are representative ESI mass spectra for a solution of CTB₅ (5 μM), **L3** (5 μM) and P_{ref}(scFv, 3 μM) in the absence and presence of sulfolane, respectively. In the absence of sulfolane, protonated CTB₅ⁿ⁺ and (CTB₅ + *q***L3**)ⁿ⁺ ions, where *q* = 1 – 4, at n = 15 to 18 are detected, along with P_{ref}ⁿ⁺ ions at n = 10 to 13. The association constants for the stepwise binding (i.e., $K_{a,q}$) of three molecules of **L3** to CTB₅ ((1.5±0.1) x 10⁷ M⁻¹ ($K_{a,1}$), (8.1±0.1) x 10⁶ M⁻¹ ($K_{a,2}$) and (5.4±0.1) x 10⁶ M⁻¹ ($K_{a,3}$)) are consistent with reported values ($K_{a,1}$ = 1.6 x 10⁷ M⁻¹, $K_{a,2}$ = 7.3 x 10⁶ M⁻¹ and $K_{a,3}$ = 3.8

$\times 10^6 \text{ M}^{-1}$).⁴⁰ Upon addition of sulfolane, the *ACS* of the $\text{CTB}_5^{\text{n}+}$ and $(\text{CTB}_5 + q\text{L3})^{\text{n}+}$ ions increased by $\sim 6\%$, while the $K_{\text{a},q}$ values decreased by 98% ($(2.6 \pm 0.1) \times 10^5 \text{ M}^{-1}$ ($K_{\text{a},1}$), $(1.3 \pm 0.1) \times 10^5 \text{ M}^{-1}$ ($K_{\text{a},2}$) and $(1.1 \pm 0.1) \times 10^5 \text{ M}^{-1}$ ($K_{\text{a},3}$)). ESI mass spectra measured for a solution of Gal3C (10 μM), **L4** (10 μM) and P_{ref} (Ubq, 6 μM), in the absence and presence of sulfolane are shown in Figures 3.2c and 3.2d, respectively. In the absence of sulfolane, protonated Gal3Cⁿ⁺ and (Gal3C + **L4**)ⁿ⁺ ions, at $n = 7$ to 9, together with P_{ref} ⁿ⁺ ions at $n = 5$ to 6, were detected. The measured K_{a} , $(1.45 \pm 0.02) \times 10^5 \text{ M}^{-1}$, is similar to the reported value, $2 \times 10^5 \text{ M}^{-1}$.⁴⁵ The introduction of sulfolane to the solution resulted in an increase of 28% in the *ACS* of the Gal3Cⁿ⁺ and (Gal3C + **L4**)ⁿ⁺ ions; sulfolane adducts were also observed. The K_{a} , $(1.25 \pm 0.02) \times 10^5 \text{ M}^{-1}$, is $\sim 14\%$ lower than the value measured in the absence of sulfolane ($(1.45 \pm 0.02) \times 10^5 \text{ M}^{-1}$).

The present results suggest that protein-carbohydrate affinities measured by ESI-MS are generally sensitive to the presence of sulfolane, and that the magnitude of the reduction in affinity (at a given sulfolane concentration) is dependent on the nature of the protein-carbohydrate interactions. However, it is not clear from the ESI-MS data alone whether this effect occurs in bulk solution, during the ESI process or as a result of in-source (gas-phase) dissociation. With the goal of establishing the origin(s) of the reduced affinity (as measured by ESI-MS), ITC measurements, CD spectroscopy and NMR spectroscopy experiments were used to quantify the Lyz-**L1** interaction in the absence and presence of sulfolane and to establish whether the sulfolane influences the higher order structure of Lyz or the Lyz-**L1** complex in solution, or interacts strongly with **L1** or Lyz.

3.3.2 Influence of sulfolane on the (Lyz + L1) complex in solution.

Isothermal titration calorimetry was used to quantify the effect of sulfolane on the stability of the (Lyz + L1) complex in solution. Binding measurements were carried out for aqueous solutions of Lyz (0.2 mM) and L1 (2.0 mM) with 2%, 5%, and 10% sulfolane, respectively (Figures 3.4, 3.5 and 3.6). Plotted in Figure 3.3 are the corresponding K_a values, as well as the reported value measured in the absence of sulfolane,³⁴ together with the values measured by ESI-MS. Notably, the ITC data reveal that sulfolane reduces the thermodynamic stability of the Lyz-L1 interaction in solution. Moreover, the K_a values measured by ESI-MS are in good agreement with the values determined by ITC. This finding confirms that ESI-MS provides an accurate measure of the distribution of free and L1-bound Lyz in the sulfolane-containing solutions, which implies that the (Lyz + L1) complex does not dissociate during the ESI process or in the gas phase (i.e., in-source dissociation).

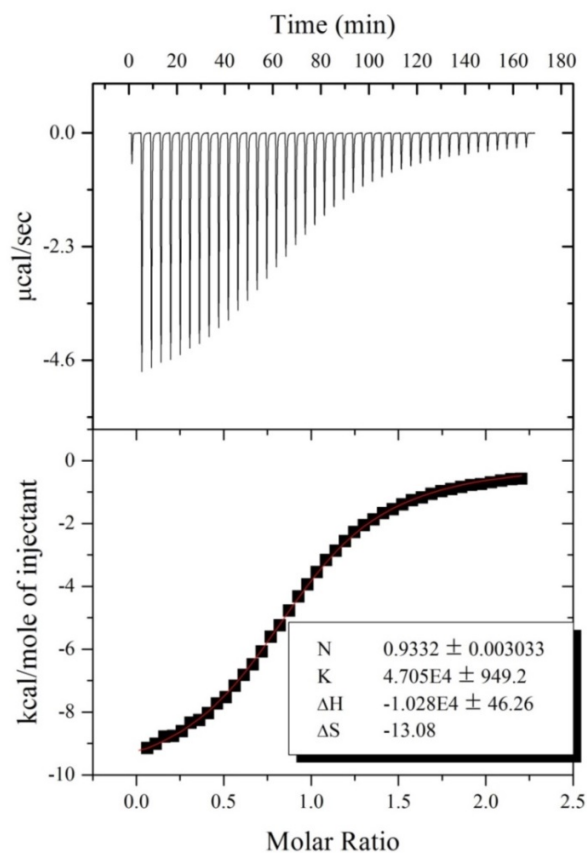


Figure 3.4 ITC profiles obtained for the binding of Lyz (0.2 mM) to L1 (2.0 mM) in aqueous ammonium acetate (50 mM, pH 6.8 and 25 °C) solution containing 2% (v/v) sulfolane. Raw data are shown in the top panel, in the lower panel integrated data (black squares) and fitting curve (solid red line) obtained using Origin 8.0 and a single site binding model, are presented. The inset in the lower panel shows best fit parameters: stoichiometry (N), association constant ($K \equiv K_a$) and enthalpy of association (ΔH). The entropy of association (ΔS) was calculated from the free energy ($\Delta G = -RT \ln K$) and enthalpy values ($\Delta G = \Delta H - T\Delta S$).

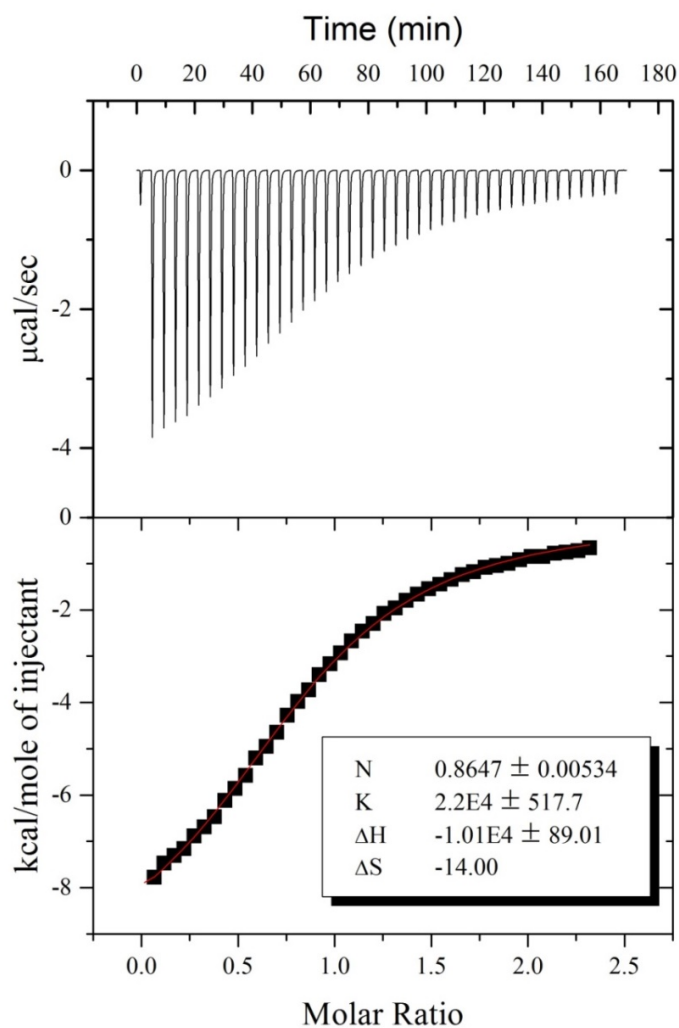


Figure 3.5 ITC profiles obtained for the binding of Lyz (0.2 mM) to L1 (2.0 mM) in aqueous ammonium acetate (50 mM, pH 6.8 and 25 °C) solution containing 5% (v/v) sulfolane. Raw data are shown in the top panel, in the lower panel integrated data (black squares) and fitting curve (solid red line) obtained using Origin 8.0 and a single site binding model, are presented. The inset in the lower panel shows best fit parameters as described in **Figure 3.4**.

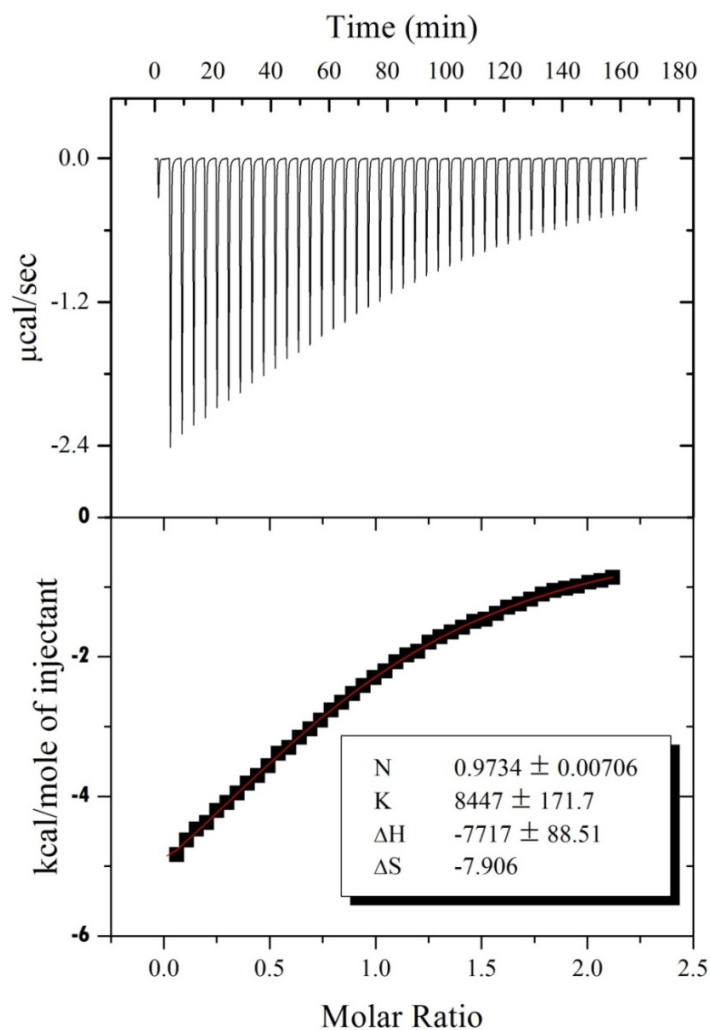


Figure 3.6 ITC profiles obtained for the binding of Lyz (0.2 mM) to L1 (2.0 mM) in aqueous ammonium acetate (50 mM, pH 6.8 and 25 °C) solution containing 10% (v/v) sulfolane. Raw data are shown in the top panel, in the lower panel integrated data (black squares) and fitting curve (solid red line) obtained using Origin 8.0 and a single site binding model, are presented. The inset in the lower panel shows best fit parameters as described in **Figure 3.4**.

The decrease in K_a upon introduction of sulfolane to solution could be due to changes in higher-order structure of Lyz or due to general or specific solvent effects. CD spectroscopy was employed to assess whether the addition of sulfolane alters the secondary structure of Lyz, which contains five standard alpha helical regions, five β -pleated sheet regions and four disulfide bonds.⁴⁶ Shown in Figure 3.7 are CD spectra measured for solutions of Lyz (56 μ M) and sulfolane (0-20%) in phosphate buffer (20 mM, pH 7, 25 °C). CD spectra of Lyz in solutions with different concentrations of sulfolane did not show significant change in the 190 – 250 nm region.⁴⁷⁻⁴⁹ The results from CD experiments suggested that sulfolane does not significantly influence the secondary structure of Lyz in bulk solution. This is consistent with the findings of Alexander and co-workers, who previously reported that Lyz is resistant to significant structural changes in the presence of high concentrations (up to 60% (v/v)) of organic solvents (e.g., acetonitrile, tetrahydrofuran and 1-propanol).⁵⁰

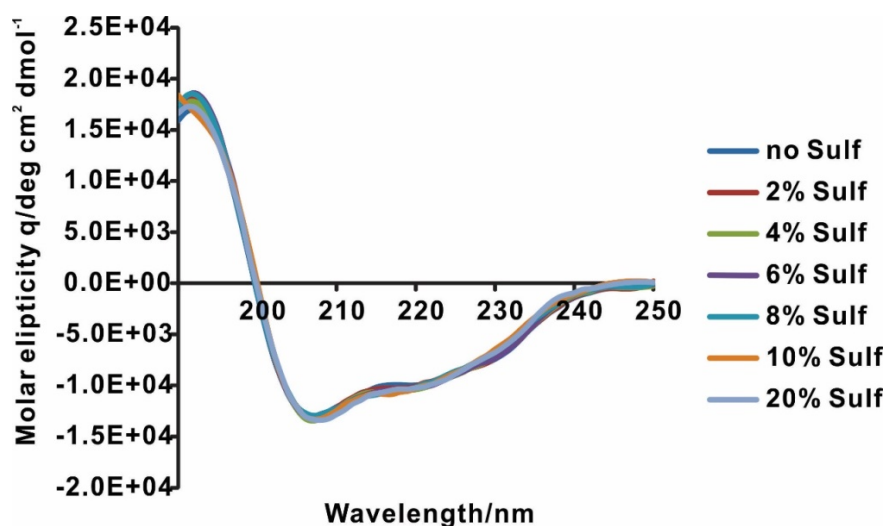


Figure 3.7 CD spectra acquired for an aqueous phosphate buffer (20 mM, pH 7.0) solutions of Lyz (56 μ M) and sulfolane (0-20%).

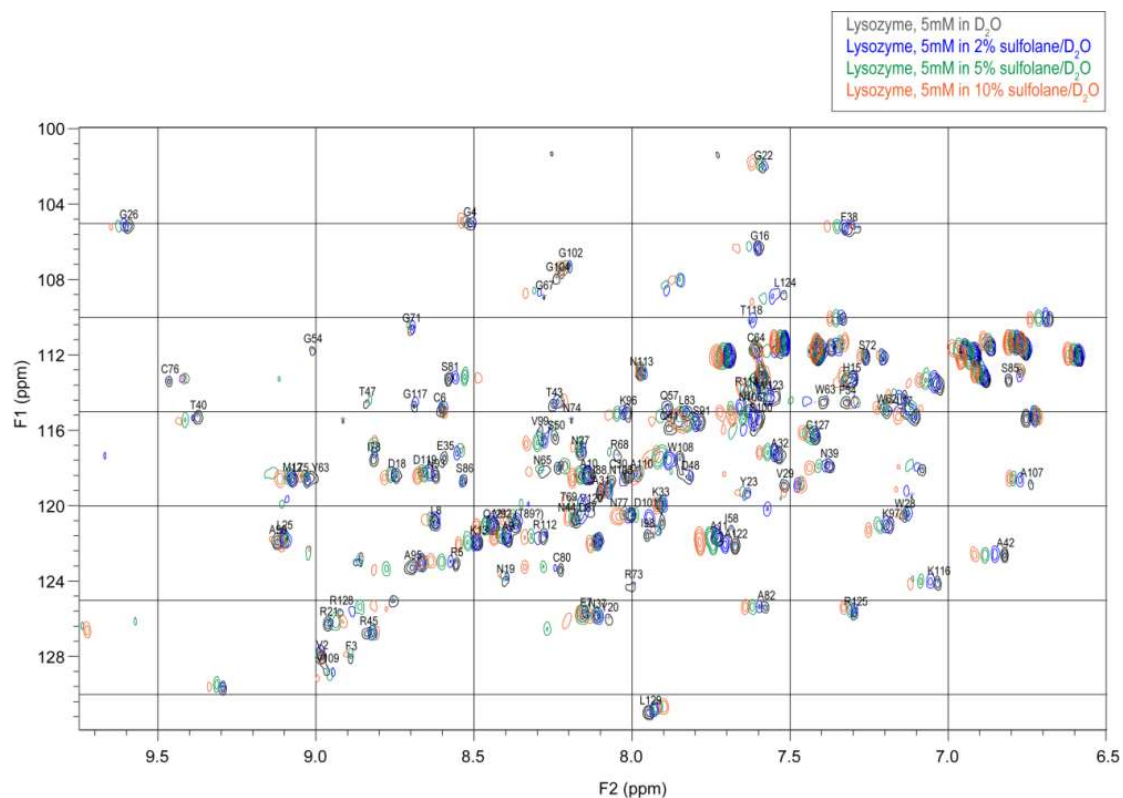


Figure 3.9 Natural abundance ^1H - ^{15}N gHSQC NMR spectra were obtained for lysozyme in 10% (v/v) D_2O - H_2O with varying concentrations of sulfolane – 0, 2, 5, and 10% (v/v). Backbone NH signals for lysozyme in 10% (v/v) D_2O - H_2O were assigned based on comparisons with literature values (reference 51 and 52).

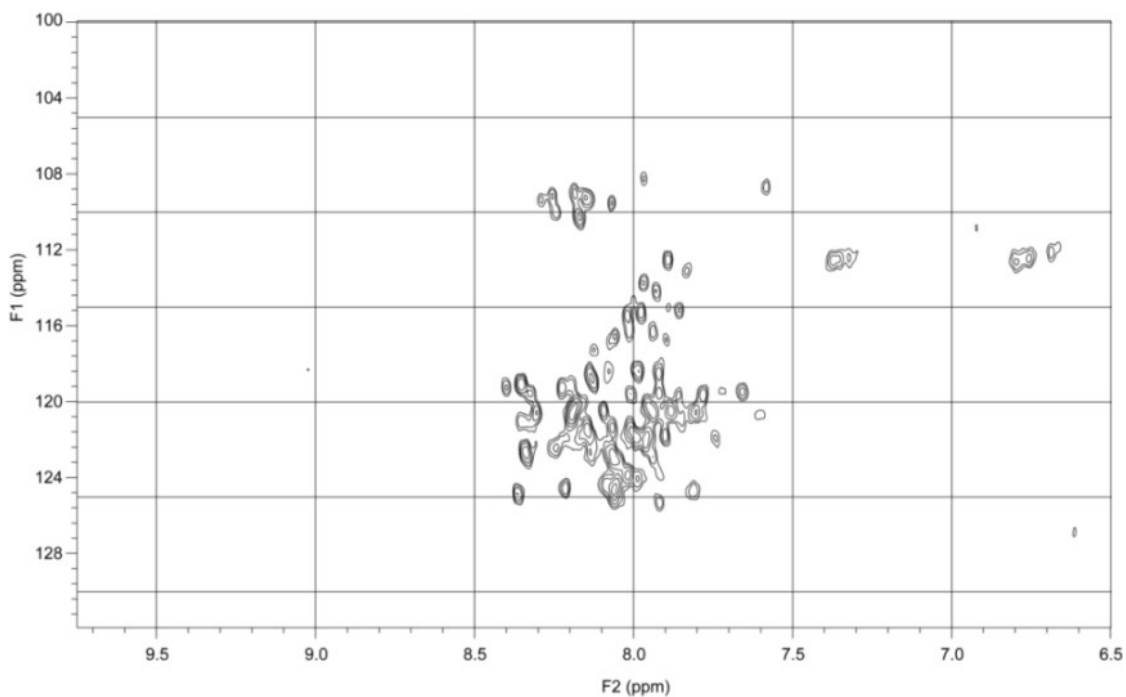


Figure 3.10 Natural abundance ^1H - ^{15}N gHSQC NMR spectrum for denatured lysozyme in 8M urea and 10% (v/v) D_2O - H_2O .

Backbone NH signals for Lyz were assigned based on comparisons with literature values.⁵¹⁻⁵² The addition of sulfolane does not cause major changes in the ^{15}N chemical shifts of the backbone NH peaks (Figure 3.9), and Lyz remains folded at sulfolane concentrations of up to 10% (Figures 3.9 and 3.10). Notably, the resonances with the largest ^1H chemical shift changes – R5, A42, S50, C80, S81, S100, N106, W108, K116, A122, L124, R128 – are not part of the **L1** binding site.⁵³⁻⁵⁵

Alternatively, the reduced affinity could be due to interactions between sulfolane and **L1** or the (Lyz + **L1**) complex. ^1H NMR spectra of **L1** in D_2O and in 2% (v/v) sulfolane- D_2O are shown in Figure 3.11.

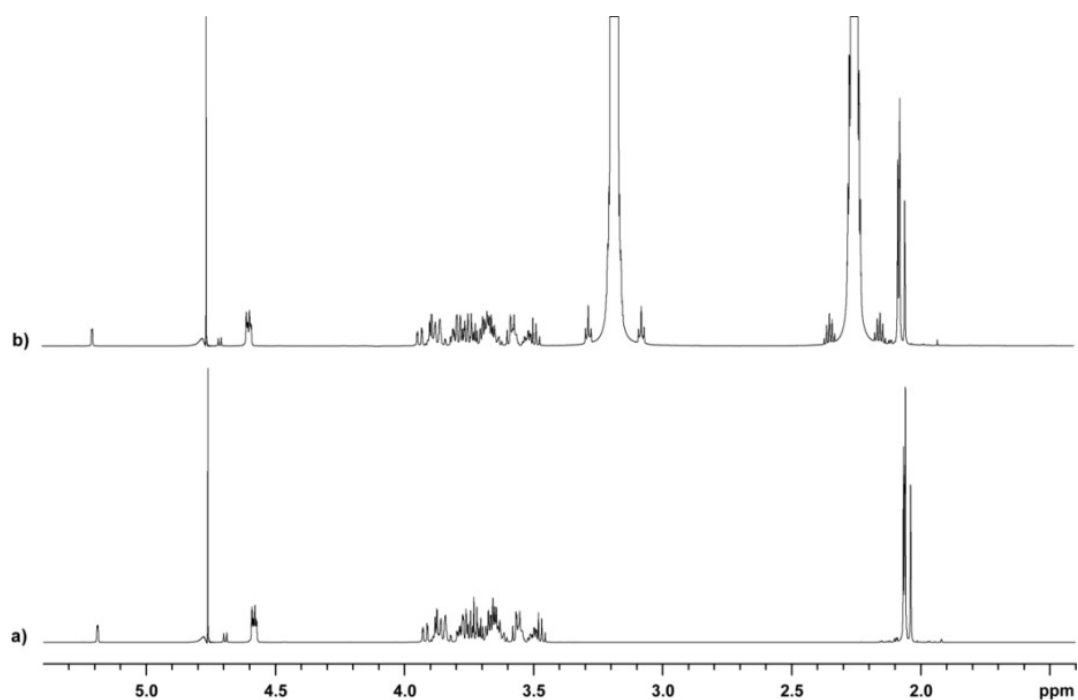


Figure 3.11 a) ^1H NMR spectrum of **L1** in D_2O . b) ^1H NMR spectrum of **L1** in 2% (v/v) sulfolane- D_2O .

None of the chemical shifts or coupling constants for the **L1** change with the addition of sulfolane, which indicates sulfolane does not form any strong interactions with **L1**. To determine whether the addition of sulfolane affects the conformation of **L1**, TROESY spectra³⁵ were acquired in both solvent systems. The signals for **L1** are unchanged in both spectra (Figure 3.12), and there are no cross peaks between **L1** and sulfolane, which means sulfolane does not change the conformation of **L1** in solution.

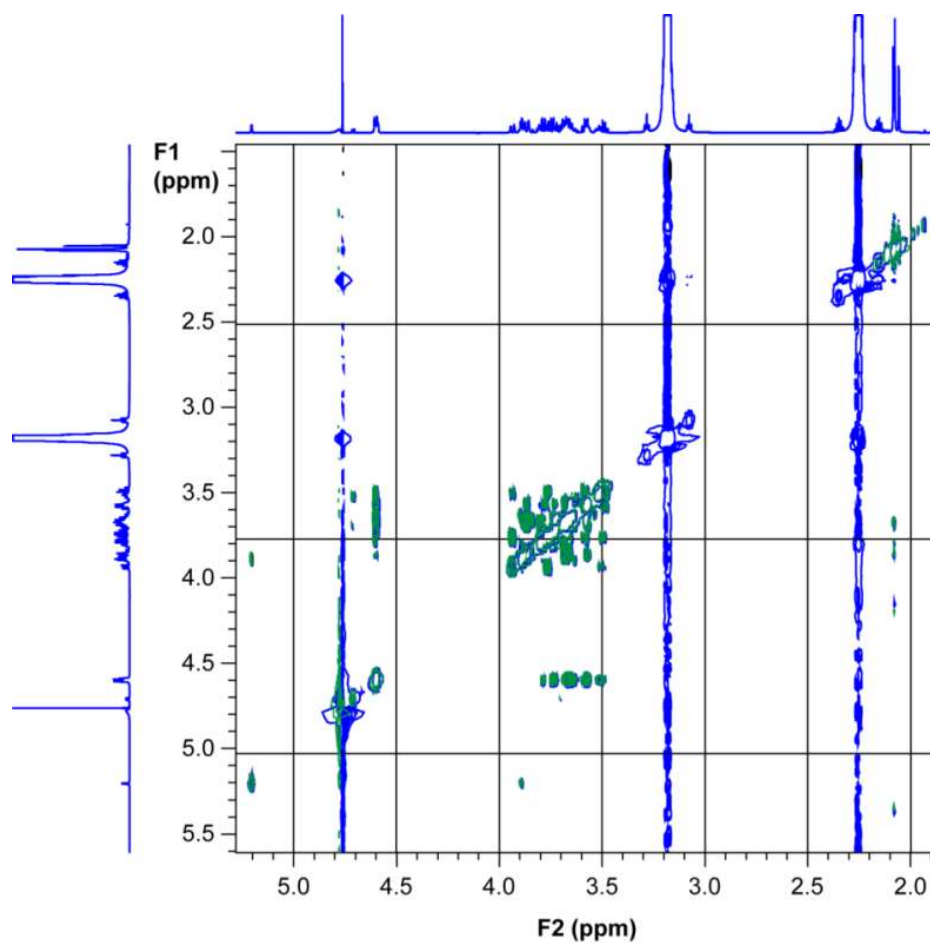


Figure 3.12 TROESY spectra of **L1** in D₂O (green) and **L1** in 2 % (v/v) sulfolane-D₂O (blue).

Natural abundance ^1H - ^{15}N gHSQC NMR spectra for the (Lyz + **L1**) complex in 10% (v/v) D₂O-H₂O and with varying concentrations of sulfolane (0, 2, 5, and 10% (v/v)) are shown in Figures 3.13 and 3.14, respectively. The spectra for Lyz with and without **L1** are very similar (Figure 3.13), as expected because the structure of Lyz changes very little upon ligand binding.⁵⁶ Three new signals are observed for the amide groups in **L1**.⁵⁷ The addition of sulfolane to the (Lyz + **L1**) complex causes similar changes in the spectra to those observed for Lyz alone (compare Figures 3.9 and 3.14).

affects the hydrogen bonding network of water provides indirect support for this hypothesis.⁵⁸

3.3.3 Supercharging and liquid sample DESI-MS

Recently, it was shown that liquid sample and reactive liquid sample DESI-MS can be used to quantify protein-ligand affinities in solution.^{31, 34} An attractive feature of the liquid sample DESI-MS assay is that it is significantly more tolerant to non-volatile buffers, such as PBS, than ESI-MS.^{31, 34} With this feature in mind, the application of liquid sample DESI-MS for protein-ligand affinity measurements carried out in the presence of supercharging reagents was investigated. In these experiments, the “sample solution” contained Lyz, **L1** and P_{ref}, in 50 mM aqueous ammonium acetate, while the “ESI solution” contained either ACN:H₂O (50:50, v/v) or ACN:H₂O:sulfolane (49.75:49.75:0.5, v/v). Shown in Figures 3.15a and 3.15b are representative liquid sample DESI mass spectra for a sample solution of Lyz (10 μM), **L1** (15 μM), and P_{ref} (Ubq, 5 μM), measured in the absence and presence of sulfolane, respectively.

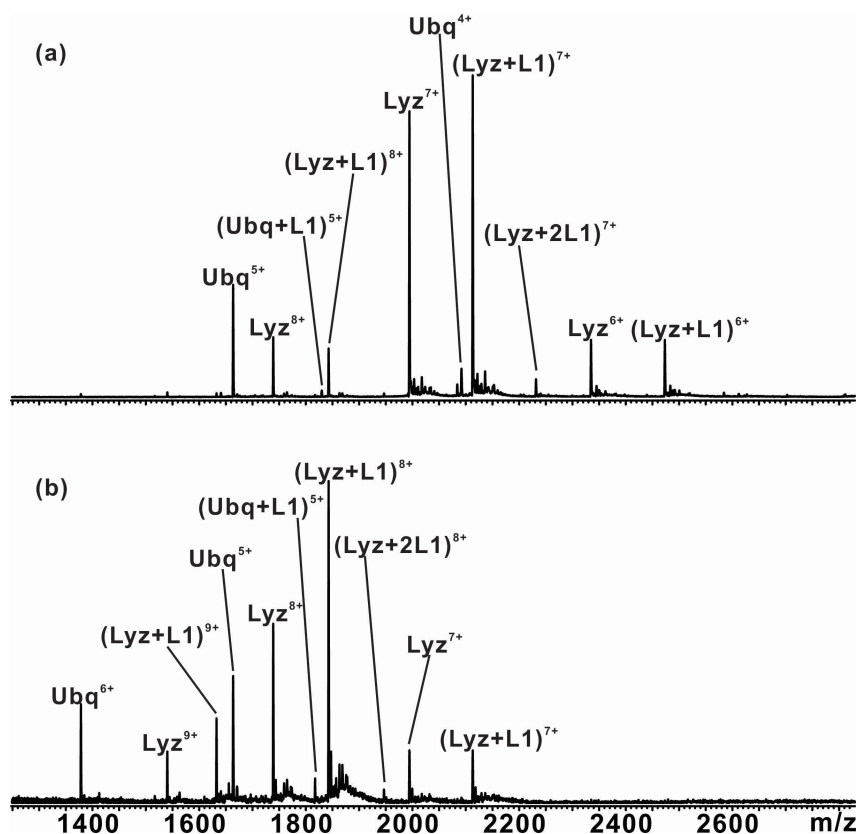


Figure 3.15 Liquid sample DESI mass spectra acquired in positive ion mode for aqueous ammonium acetate (20 mM) solutions of Lyz (10 μ M), L1 (15 μ M) and Ubq (5 μ M) using an ESI spray solvent (ACN:H₂O=50:50, v/v) containing (a) 0% sulfolane and (b) 0.5% sulfolane.

It can be seen that the *ACS* for Lyzⁿ⁺ and (Lyz + L1)ⁿ⁺ ions increased by ~20% in the presence of sulfolane, which is similar to ~24% increase of ESI-MS measurements acquired using 0.5% sulfolane. Overall, however, the *ACS* of Lyz and (Lyz + L1) complex in the presence and absence of sulfolane on liquid sample DESI spectra were lower than the *ACS* observed on their corresponding ESI spectra when the same solutions were sprayed. The lower *ACS* observed in the DESI spectra, which is consistent with the results of

previous studies,⁵⁸⁻⁶⁰ may be due to the presence of ACN vapour in the source region. Acetonitrile has a higher gas phase basicity (178.8 kcal mol⁻¹) than H₂O (157.9 kcal mol⁻¹),⁶¹ and would more efficiently deprotonate the Lyz ions in the source compared to H₂O vapour.

Notably, and in contrast to what was observed with ESI-MS, there is no measurable change in the K_a value for this interaction upon addition of sulfolane ((1.1±0.1) x 10⁵ M⁻¹ (0% sulfolane) and (1.4±0.1) x 10⁵ M⁻¹ (0.5% sulfolane)). This finding, which is consistent with observations made by Loo and coworkers,³¹ is significant in that it reveals that protein supercharging and the reduction in the K_a of the (Lyz + **L1**) complex caused by sulfolane are independent processes. The absence of a change in the distribution of bound and unbound Lyz in liquid sample DESI-MS can reasonably be explained on the basis of the limited time available for re-equilibration of the Lyz-**L1** interaction upon introduction of sulfolane into the droplet. In fact, it was reported recently that, using liquid sample DESI-MS implemented with **L1** in the ESI spray solution and Lyz in the sample solution, the lifetime of the resulting droplets (containing sample) was too short for the Lyz-**L1** interaction to reach equilibrium.³⁴ That supercharging is observed in the liquid sample DESI-MS measurements carried out with sulfolane demonstrates that the process involved in supercharging occur on a much shorter timescale than the relaxation kinetics for the Lyz-**L1** interaction.

3.4 Conclusions

The results of quantitative ESI-MS binding measurements performed on four protein-carbohydrate interactions (Lyz-**L1**, scFv-**L2**, CTB₅-**L3** and Gal3C-**L4**) revealed

that using sulfolane to supercharge protein ions is generally accompanied by a reduction in ligand affinity, although the magnitude of the effect (at a given sulfolane concentration) is dependent on the nature of the interaction. The affinities measured by ESI-MS for the Lyz-**L1** interaction in the presence of sulfolane agree with values measured by ITC. This finding indicates that there is no dissociation of the complex during the ESI process (i.e., in the droplets) or in the gas phase (i.e., in-source dissociation). Moreover, the results of CD and NMR spectroscopy measurements reveal that sulfolane does not cause any significant change in the higher order structure of Lyz, nor does it interact strongly with **L1** or the Lyz residues that make up the binding pocket in solution. It is proposed that sulfolane weakens the protein-ligand interactions through a general solvent effect. Taken together, the present findings suggest that supercharging of the (Lyz + **L1**) complex by sulfolane is not related to changes to protein structure in bulk solution or during the ESI process. It must be stressed, though, that the possibility of sulfolane-induced protein unfolding in the ESI droplets can't be definitively ruled out based on the current results. However, if protein unfolding does take place during the ESI process, the unfolding kinetics must be significantly faster than the dissociation kinetics. Finally, binding measurements performed on the Lyz-**L1** interaction using liquid sample DESI-MS revealed that the introduction of sulfolane into the ESI solution results in protein supercharging; however, this effect is not accompanied by any loss in affinity. This finding, in addition to having mechanistic implications, suggests an inherent advantage of liquid sample DESI-MS over direct ESI-MS for protein-ligand affinity measurements in cases where supercharging is desirable.

3.5 Literature cited

1. Cubrilovic, D., et al., *J Am Soc Mass Spectrom.* **2012**, *23*, 1768-1777.
2. El-Hawiet, A., et al., *Anal Chem.* **2012**, *84*, 50-58.
3. Han, L., et al., *Glycobiology.* **2013**, *23*, 276-285.
4. Kitova, E.N., et al., *J Am Soc Mass Spectrom.* **2014**, *25*, 1908-1916.
5. Kitova, E.N., et al., *J Am Chem Soc.* **2002**, *124*, 5902-5913.
6. Kitova, E.N., et al., *Angew Chem.* **2004**, *43*, 4183-4186.
7. Liu, L., et al., *J Am Chem Soc.* **2009**, *131*, 15980-15981.
8. Liu, L., et al., *J Am Chem Soc.* **2010**, *132*, 17658-17660.
9. Liu, L., et al., *J Am Chem Soc.* **2012**, *134*, 3054-3060.
10. Deng, L., et al., *J Am Chem Soc.* **2012**, *134*, 16586-16596.
11. Haselmann, K.F., et al., *Rapid Commun Mass Spectrom.* **2002**, *16*, 2260-2265.
12. Yin, S., Loo, J.A., *Int J Mass Spectrom.* **2011**, *300*, 118-122.
13. Jackson, S.N., et al., *J Am Soc Mass Spectrom.* **2009**, *20*, 176-179.
14. Luebert, F., et al., *Ecology and evolution.* **2014**, *4*, 266-275.
15. Xie, Y., et al., *J Am Chem Soc.* **2006**, *128*, 14432-14433.
16. Yin, S., Loo, J.A., *J Am Soc Mass Spectrom.* **2010**, *21*, 899-907.
17. Clarke, D.J., et al., *J Am Soc Mass Spectrom.* **2011**, *22*, 1432-1440.
18. Ledvina, A.R., et al., *Angew Chem.* **2009**, *48*, 8526-8528.
19. Swaney, D.L., et al., *Anal Chem.* **2007**, *79*, 477-485.
20. Horn, D.M., et al., *J Am Chem Soc.* **2001**, *123*, 9792-9799.
21. Gorshkov, M.V., et al., *Int J Mass Spectrom.* **2004**, *234*, 131-136.
22. Zenaidee, M.A., Donald, W.A., *Analyst.* **2015**, *140*, 1894-1905.

23. Iavarone, A.T., et al., *Anal Chem.* **2001**, *73*, 1455-1460.
24. Lomeli, S.H., et al., *J Am Soc Mass Spectrom.* **2009**, *20*, 593-596.
25. Sterling, H.J., Williams, E.R., *J Am Soc Mass Spectrom.* **2009**, *20*, 1933-1943.
26. Lomeli, S.H., et al., *J Am Soc Mass Spectrom.* **2010**, *21*, 127-131.
27. Sterling, H.J., et al., *J Am Soc Mass Spectrom.* **2010**, *21*, 1762-1774.
28. Iavarone, A.T., Williams, E.R., *J Am Chem Soc.* **2003**, *125*, 2319-2327.
29. Hogan, C.J., Jr., et al., *Phys Chem Chem Phys.* **2010**, *12*, 13476-13483.
30. Ogorzalek Loo, R.R., et al., *J Am Soc Mass Spectrom.* **2014**, *25*, 1675-1693.
31. Liu, P., et al., *Anal Chem.* **2013**, *85*, 11966-11972.
32. Zdanov, A., et al., *Proc Natl Acad Sci U S A.* **1994**, *91*, 6423-6427.
33. Rademacher, C., et al., *J Am Chem Soc.* **2007**, *129*, 10489-10502.
34. Yao, Y., et al., *J Am Soc Mass Spectrom.* **2015**, *26*, 98-106.
35. Hwang, T.L., Shaka, A.J., *J Am Chem Soc.* **1992**, *114*, 3157-3159.
36. Wang, W., et al., *Anal Chem.* **2003**, *75*, 4945-4955.
37. Wang, W., Kitova, E.N., Klassen, J.S., *Anal Chem.* **2005**, *77*, 3060-3071.
38. Sun, J., et al., *Anal Chem.* **2006**, *78*, 3010-3018.
39. Turnbull, W.B., Precious, B.L., Homans, S.W., *J Am Chem Soc.* **2004**, *126*, 1047-1054.
40. Lin, H., Kitova, E.N., Klassen, J.S., *J Am Soc Mass Spectrom.* **2014**, *25*, 104-110.
41. Schindler, M., et al., *Biochemistry.* **1977**, *16*, 423-431.
42. Veros, C.T., Oldham, N.J., *Rapid Commun Mass Spectrom.* **2007**, *21*, 3505-3510.
43. Douglass, K.A., Venter, A.R., *J Am Soc Mass Spectrom.* **2012**, *23*, 489-497.
44. Daneshfar, R., Kitova, E.N., Klassen, J.S., *J Am Chem Soc.* **2004**, *126*, 4786-4787.

45. Hirabayashi, J., et al., *Biochim Biophys Acta*. **2002**, *1572*, 232-254.
46. Phillips, D.C., *Proc Natl Acad Sci U S A*. **1967**, *57*, 483-495.
47. Holzwarth, G., Doty, P., *J Am Chem Soc*. **1965**, *87*, 218-228.
48. Greenfield, N., Fasman, G.D., *Biochemistry*. **1969**, *8*, 4108-4116.
49. Venyaminov, S., et al., *Anal Biochem*. **1993**, *214*, 17-24.
50. Griebenow, K., Klibanov, A.M., *J Am Chem Soc*. **1996**, *118*, 11695-11700.
51. Redfield, C., Dobson, C.M., *Biochemistry*. **1988**, *27*, 122-136.
52. Buck, M., et al., *Biochemistry*. **1995**, *34*, 4041-4055.
53. Strynadka, N.C., James, M.N., *Journal of molecular biology*. **1991**, *220*, 401-424.
54. Cheetham, J.C., Artymiuk, P.J., Phillips, D.C., *J Mol Biol*. **1992**, *224*, 613-628.
55. Hadfield, A.T., et al., *Journal of molecular biology*. **1994**, *243*, 856-872.
56. Moorman, V.R., Valentine, K.G., Wand, A.J., *Protein Sci*. **2012**, *21*, 1066-1073.
57. Blundell, C.D., et al., *Glycobiology*. **2004**, *14*, 999-1009.
58. Bates, R.G., Pawlak, Z., *J Solution Chem*. **1976**, *5*, 213-222.
59. DeMuth, J.C., McLuckey, S.A., *Anal Chem*. **2015**, *87*, 1210-1218.
60. Hopper, J.T., Sokratous, K., Oldham, N.J., *Anal Biochem*. **2012**, *421*, 788-790.
61. Hunter, E.P.L., Lias, S.G., *J Phys Chem Ref Data*. **1998**, *27*, 413-656.

Chapter 4

Conclusions and Future Work

The work describes the development of mass spectrometry methods to study protein-glycan interactions. The first research project focuses on quantifying protein-carbohydrate interactions using liquid sample desorption electrospray ionization mass spectrometry. The second research project studies influence of sulfolane on ESI-MS measurements of protein-ligand affinities. The third research project compares effects of amino acids and imidazole on ESI-MS measurements on protein-carbohydrate interactions.

In Chapter 2, the application of liquid sample DESI-MS for quantifying protein-carbohydrate interactions in aqueous solutions is described. Notably, the affinities of tri- and tetrasaccharide ligands for Lyz and scFv measured using liquid sample DESI-MS are found to be in good agreement with values measured by ITC and the direct ESI-MS assay. It is also found that the reference protein method, which was originally developed to correct ESI mass spectra for the occurrence of nonspecific ligand-protein binding, can be used to correct liquid sample DESI mass spectra for nonspecific carbohydrate binding. The tolerance of liquid sample DESI-MS for quantitative binding measurements carried out using solutions containing high concentrations of PBS was also explored. The binding between Lyz and a trisaccharide ligand was successfully measured with liquid sample DESI-MS at concentrations up to 1x PBS. In contrast, direct ESI-MS binding measurements were limited to PBS concentrations less than ~ 0.02 x PBS.

One of the attractive features of liquid sample DESI is the short time scale (< 2 ms) from ionization to detection, which is not enough time to allow the protein-ligand

solution to reach the new equilibrium after picked-up and diluted into secondary droplets. If liquid sample DESI was coupled with time-resolved reaction setups,¹⁻³ it is possible to extend applications to perform kinetic study of protein-ligand interactions in biological buffers (e.g., PBS).

In Chapter 3, the results of quantitative ESI-MS binding measurements performed on four protein-carbohydrate interactions (Lyz-**L1**, scFv-**L2**, CTB₅-**L3** and Gal3C-**L4**) revealed that using sulfolane to supercharge protein ions is generally accompanied by a reduction in ligand affinity, although the magnitude of the effect (at a given sulfolane concentration) is dependent on the nature of the interaction. The affinities measured by ESI-MS for the Lyz-**L1** interaction in the presence of sulfolane agree with values measured by ITC. This finding indicates that there is no dissociation of the complex during the ESI process (i.e., in the droplets) or in the gas phase (i.e., in-source dissociation). Moreover, the results of CD and NMR spectroscopy measurements reveal that sulfolane does not cause any significant change in the higher order structure of Lyz, nor does it interact strongly with **L1** or the Lyz residues that make up the binding pocket in solution. It is proposed that sulfolane weakens the protein-ligand interactions through a general solvent effect. Taken together, the present findings suggest that supercharging of the (Lyz + **L1**) complex by sulfolane is not related to changes to protein structure in bulk solution or during the ESI process. It must be stressed, though, that the possibility of sulfolane-induced protein unfolding in the ESI droplets can't be definitively ruled out based on the current results. However, if protein unfolding does take place during the ESI process, the unfolding kinetics must be significantly faster than the dissociation kinetics. Finally, binding measurements performed on the Lyz-**L1** interaction using liquid sample DESI-MS

revealed that the introduction of sulfolane into the ESI solution results in protein supercharging; however, this effect is not accompanied by any loss in affinity. This finding, in addition to having mechanistic implications, suggests an inherent advantage of liquid sample DESI-MS over direct ESI-MS for protein-ligand affinity measurements in cases where supercharging is desirable.

The possible extension is to add sulfolane into spray solvent on liquid sample DESI and increase the charge states of protein-ligand complex ions during ionization. With utilizing ECD/ETD techniques, it is very useful to study and localize binding pocket of ligand-bound heavy proteins using liquid sample DESI-MS.

4.1 References

1. Chen, Y.C., Urban, P.L., *Trends in Anal Chem* **2013**, *44*, 106-120.
2. Vahidi, S., et al., *Anal Chem* **2013**, *85*, 8618-8625.
3. Miao, Z., et al., *Anal Chem* **2011**, *83*, 3994-3997.
4. Liu, P.Y., et al., *Anal Chem.* **2013**, *85*, 11966-11972.
5. Yao, Y., et al., *J Am Soc Mass Spectrom.* **2015**, *26*, 98-106.

Bibliography

- Ahadi, E., Konermann, L., *J Phys Chem B*. **2012**, *116*, 104-112.
- Badu-Tawiah, A., et al., *J Am Soc Mass Spectrom*. **2010**, *21*, 572-579.
- Bagal, D., et al., *Anal Chem*. **2009**, *81*, 7801-7806.
- Banerjee, S., Mazumdar, S., *Int J Anal Chem*. **2012**, *2012*, 282574.
- Bates, R.G., Pawlak, Z., *J Solution Chem*. **1976**, *5*, 213-222.
- Bewley, C.A., *Protein-carbohydrate Interactions in Infectious Diseases*. RSC Publishing: Cambridge, UK, **2006**
- Blundell, C.D., et al., *Glycobiology*. **2004**, *14*, 999-1009.
- Buck, M., et al., *Biochemistry*. **1995**, *34*, 4041-4055.
- Cech, N.B., Enke, C.G., *Mass Spectrom Rev*. **2001**, *20*, 362-387.
- Cheetham, J.C., Artymiuk, P.J., Phillips, D.C., *J Mol Biol*. **1992**, *224*, 613-628.
- Chen, Y.C., Urban, P.L., *Trends in Anal Chem* **2013**, *44*, 106-120.
- Chiodo, F., et al., *PloS one*. **2013**, *8*, e73027.
- Chitta, R.K., et al., *J Am Soc Mass Spectrom*. **2005**, *16*, 1031-1038.
- Clark, S.M., Konermann, L., *Anal Chem*. **2004**, *76*, 7077-7083.
- Clarke, D.J., et al., *J Am Soc Mass Spectrom*. **2011**, *22*, 1432-1440.
- Cole, R.B., *J Mass Spectrom*. **2000**, *35*, 763-772.
- Costa, A.B., Cooks, R.G., *Chem Commun*. **2007**, 3915-3917.
- Cubrilovic, D., et al., *J Am Soc Mass Spectrom*. **2012**, *23*, 1768-1777.
- Daghestani, H.N., Day, B.W., *Sensors*. **2010**, *10*, 9630-9646.
- Daneshfar, R., Kitova, E.N., Klassen, J.S., *J Am Chem Soc*. **2004**, *126*, 4786-4787.
- Daniel, J.M., et al., *Int J Mass Spectrom*. **2002**, *216*, 1-27.

De Crescenzo, G., et al., *Cell Mol Bioeng.* **2008**, *1*, 204-215.

De La Mora, J.F., *Anal Chim Acta.* **2000**, *406*, 93-104.

DeMuth, J.C., et al., *Rapid Commun Mass Spectrom.* **2015**, *29*, 973-981.

DeMuth, J.C., McLuckey, S.A., *Anal Chem.* **2015**, *87*, 1210-1218.

Deng, L., et al., *Anal Chem.* **2010**, *82*, 2170-2174.

Deng, L., et al., *J Am Chem Soc.* **2012**, *134*, 16586-16596.

Dennis, J.W., Granovsky, M., Warren, C.E., *Bioessays.* **1999**, *21*, 412-421.

Disney, M.D., Seeberger, P.H., *Chem Biol.* **2004**, *11*, 1701-1707.

Dole, M., et al., *J Chem Phys.* **1968**, *49*, 2240-2249.

Douglass, K.A., Venter, A.R., *J Am Soc Mass Spectrom.* **2012**, *23*, 489-497.

Douglass, K.A., Venter, A.R., *J Mass Spectrom.* **2013**, *48*, 553-560.

Dwek, R.A., *Biochem Soc T.* **1995**, *23*, 1-25.

El-Hawiet, A., et al., *Anal Chem.* **2012**, *84*, 3867-3870.

El-Hawiet, A., et al., *Anal Chem.* **2012**, *84*, 50-58.

El-Hawiet, A., et al., *Anal Chem.* **2013**, *85*, 7637-7644.

El-Hawiet, A., et al., *Biochemistry.* **2012**, *51*, 4244-4253.

El-Hawiet, A., et al., *Glycobiology.* **2011**, *21*, 1217-1227.

El-Hawiet, A., et al., *J Am Soc Mass Spectrom.* **2010**, *21*, 1893-1899.

Fenn, J.B., et al., *Science.* **1989**, *246*, 64-71.

Ferguson, C.N., et al., *Anal Chem.* **2011**, *83*, 6468-6473.

Fernandez-Alonso, M.D., et al., *Curr Protein Pept Sc.* **2012**, *13*, 816-830.

Frostell, Å., et al., *Methods in molecular biology.* **2013**, *1008*, 139-165.

Gabelica, V., et al., *J Mass Spectrom.* **2003**, *38*, 491-501.

- Gorshkov, M.V., et al., *Int J Mass Spectrom.* **2004**, *234*, 131-136.
- Green, F.M., et al., *Analyst.* **2010**, *135*, 731-737.
- Greenfield, N., Fasman, G.D., *Biochemistry.* **1969**, *8*, 4108-4116.
- Griebenow, K., Klibanov, A.M., *J Am Chem Soc.* **1996**, *118*, 11695-11700.
- Guilhaus, M., et al., *Mass Spectrom Rev.* **2000**, *19*, 65-107.
- Hadfield, A.T., et al., *Journal of molecular biology.* **1994**, *243*, 856-872.
- Han, L., et al., *Glycobiology.* **2013**, *23*, 276-285.
- Haselmann, K.F., et al., *Rapid Commun Mass Spectrom.* **2002**, *16*, 2260-2265.
- Heaton, K., et al., *J Archaeol Sci.* **2009**, *36*, 2145-2154.
- Hirabayashi, J., et al., *Biochim Biophys Acta.* **2002**, *1572*, 232-254.
- Ho, J.G.S., et al., *Proc Natl Acad Sci U S A.* **2005**, *102*, 18373-18378.
- Hoffmann, E. d., Stroobant, V., *Mass Spectrometry : Principles and Applications. 3rd ed.*, Wiley: 2007.
- Hogan, C.J., Jr., et al., *Phys Chem Chem Phys.* **2010**, *12*, 13476-13483.
- Holzwarth, G., Doty, P., *J Am Chem Soc.* **1965**, *87*, 218-228.
- Homola, J., *Anal Bioanal Chem.* **2003**, *377*, 528-539.
- Hopper, J.T., et al., *Anal Biochem.* **2012**, *421*, 788-790.
- Hopper, J.T., Oldham, N.J., *Anal Chem.* **2011**, *83*, 7472-7479.
- Hopper, J.T., Sokratous, K., Oldham, N.J., *Anal Biochem.* **2012**, *421*, 788-790.
- Horn, D.M., et al., *J Am Chem Soc.* **2001**, *123*, 9792-9799.
- Hunter, E.P.L., Lias, S.G., *J Phys Chem Ref Data.* **1998**, *27*, 413-656.
- Hwang, T.L., Shaka, A.J., *J Am Chem Soc.* **1992**, *114*, 3157-3159.
- Iavarone, A.T., et al., *Anal Chem.* **2001**, *73*, 1455-1460.

Iavarone, A.T., Williams, E.R., *J Am Chem Soc.* **2003**, *125*, 2319-2327.

Ifa, D.R., et al., *Analyst.* **2010**, *135*, 669-681.

Iribarne, J.V., Thomson, B.A., *J Chem Phys.* **1976**, *64*, 2287-2294.

Jackson, S.N., et al., *J Am Soc Mass Spectrom.* **2009**, *20*, 176-179.

Jecklin, M.C., et al., *Anal Chem.* **2009**, *81*, 408-419.

Jecklin, M.C., et al., *J Am Soc Mass Spectrom.* **2008**, *19*, 332-343.

Joensson, H.N., et al., *Angew Chem.* **2009**, *48*, 2518-2521.

Juraschek, R., Dulcks, T., Karas, M., *J Am Soc Mass Spectrom.* **1999**, *10*, 300-308.

Karas, M., Bahr, U., Dulcks, T., *Fresenius J Anal Chem.* **2000**, *366*, 669-676.

Karlsson, R., *J Mol Recognit.* **2004**, *17*, 151-161.

Kebarle, P., *J Mass Spectrom.* **2000**, *35*, 804-817.

Kebarle, P., Tang, L., *Anal Chem.* **1993**, *65*, 972A-986A.

Kebarle, P., Verkerk, U.H., *Mass Spectrom Rev.* **2009**, *28*, 898-917.

Kitova, E.N., Bundle, D.R., Klassen, J.S., *J Am Chem Soc.* **2002**, *124*, 9340-9341.

Kitova, E.N., et al., *Anal Chem.* **2011**, *83*, 5160-5167.

Kitova, E.N., et al., *Angew Chem.* **2004**, *43*, 4183-4186.

Kitova, E.N., et al., *Glycobiology.* **2007**, *17*, 1127-1137.

Kitova, E.N., et al., *J Am Chem Soc.* **2002**, *124*, 5902-5913.

Kitova, E.N., et al., *J Am Soc Mass Spectrom.* **2012**, *23*, 431-441.

Kitova, E.N., et al., *J Am Soc Mass Spectrom.* **2014**, *25*, 1908-1916.

Konermann, L., et al., *Anal Chem.* **2013**, *85*, 2-9.

Konermann, L., Rodriguez, A.D., Liu, J., *Anal Chem.* **2012**, *84*, 6798-6804.

Larsen, K., et al., *Carbohydr Res.* **2006**, *341*, 1209-1234.

Leavitt, S., Freire, E., *Curr Opin Struct Biol.* **2001**, *11*, 560-566.

Ledvina, A.R., et al., *Angew Chem.* **2009**, *48*, 8526-8528.

Lin, H., et al., *J Am Soc Mass Spectrom.* **2014**, *25*, 104-110.

Lin, H., Kitova, E.N., Klassen, J.S., *J Am Soc Mass Spectrom.* **2014**, *25*, 104-110.

Liu, L., et al., *J Am Chem Soc.* **2012**, *134*, 3054-3060.

Liu, P.Y., et al., *Anal Chem.* **2013**, *85*, 11966-11972.

Lomeli, S.H., et al., *J Am Soc Mass Spectrom.* **2009**, *20*, 593-596.

Lomeli, S.H., et al., *J Am Soc Mass Spectrom.* **2010**, *21*, 127-131.

Loo, J.A., *Mass Spectrom Rev.* **1997**, *16*, 1-23.

Lu, X., et al., *J Am Soc Mass Spectrom.* **2014**, *25*, 454-463.

Luebert, F., et al., *Ecology and evolution.* **2014**, *4*, 266-275.

Mack, L.L., et al., *J Chem Phys.* **1970**, *52*, 4977-4986.

Marshall, A.G., et al., *Mass Spectrom Rev.* **1998**, *17*, 1-35.

Marshall, A.G., Hendrickson, C.L., *Int J Mass Spectrom.* **2002**, *215*, 59-75.

Mathur, S., et al., *Phys Chem Chem Phys.* **2007**, *9*, 6187-6198.

Miao, Z., Chen, H., *J Am Soc Mass Spectrom.* **2009**, *20*, 10-19.

Miao, Z., et al., *Anal Chem* **2011**. *83*, 3994-3997.

Miao, Z., et al., *J Am Soc Mass Spectrom.* **2010**, *21*, 1730-1736.

Moore, B.N., Hamdy, O., Julian, R.R., *Int J Mass Spectrom.* **2012**, *330-332*, 220-225.

Moorman, V.R., Valentine, K.G., Wand, A.J., *Protein Sci.* **2012**, *21*, 1066-1073.

Myung, S., et al., *J Phys Chem B.* **2006**, *110*, 5045-5051.

Nguyen, S., Fenn, J.B., *Proc Natl Acad Sci U S A.* **2007**, *104*, 1111-1117.

Ogorzalek Loo, R.R., et al., *J Am Soc Mass Spectrom.* **2014**, *25*, 1675-1693.

Olumee, Z., Callahan, J.H., Vertes, A., *J Phys Chem A*. **1998**, *102*, 9154-9160.

Orosz, F., Ovadi, J., *J Immunol Methods*. **2002**, *270*, 155-162.

Patching, S.G., *Biochim Biophys Acta*. **2014**, *1838*, 43-55.

Phillips, D.C., *Proc Natl Acad Sci U S A*. **1967**, *57*, 483-495.

Przybylski, M., Glocker, M.O., *Angew Chem*. **1996**, *35*, 807-826.

Rademacher, C., et al., *J Am Chem Soc*. **2007**, *129*, 10489-10502.

Rayleigh, L., *Phil Mag*. **1882**, *14*, 184-186.

Redfield, C., Dobson, C.M., *Biochemistry*. **1988**, *27*, 122-136.

Saboury, A.A., *J Iran Chem Soc*. **2006**, *3*, 1-21.

Saxon, E., Bertozzi, C.R., *Annu Rev Cell Dev Bi*. **2001**, *17*, 1-23.

Schindler, M., et al., *Biochemistry*. **1977**, *16*, 423-431.

Schuck, P., *Annu Rev Bioph Biom*. **1997**, *26*, 541-566.

Shin, Y.S., et al., *Anal Chem*. **2007**, *79*, 3514-3518.

Shuker, S.B., et al., *Science*. **1996**, *274*, 1531-1534.

Soya, N., et al., *Glycobiology*. **2009**, *19*, 1224-1234.

Sterling, H.J., et al., *J Am Soc Mass Spectrom*. **2010**, *21*, 1045-1049.

Sterling, H.J., et al., *J Am Soc Mass Spectrom*. **2010**, *21*, 1762-1774.

Sterling, H.J., Williams, E.R., *J Am Soc Mass Spectrom*. **2009**, *20*, 1933-1943.

Strynadka, N.C., James, M.N., *Journal of molecular biology*. **1991**, *220*, 401-424.

Sun, J., et al., *Anal Chem*. **2006**, *78*, 3010-3018.

Sun, J., et al., *Anal Chem*. **2007**, *79*, 8301-8311.

Sun, J.X., Kitova, E.N., Klassen, J.S., *Anal Chem*. **2007**, *79*, 416-425.

Sun, N., et al., *J Am Soc Mass Spectrom*. **2010**, *21*, 472-481.

Swaney, D.L., et al., *Anal Chem.* **2007**, *79*, 477-485.

Takats, Z., et al., *J Mass Spectrom.* **2005**, *40*, 1261-1275.

Takats, Z., et al., *Science.* **2004**, *306*, 471-473.

Taniguchi, N., et al., *Curr Opin Struct Biol.* **2006**, *16*, 561-566.

Thomson, B., Iribarne, J., *J Chem Phys.* **1979**, *71*, 4451-4463.

Turnbull, W.B., Precious, B.L., Homans, S.W., *J Am Chem Soc.* **2004**, *126*, 1047-1054.

Utsuno, K., Uludag, H., *Biophys J.* **2010**, *99*, 201-207.

Vahidi, S., et al., *Anal Chem* **2013**, *85*, 8618-8625.

Varki, A., *Glycobiology.* **1993**, *3*, 97-130.

Venter, A., et al., *Anal Chem.* **2006**, *78*, 8549-8555.

Venjaminov, S., et al., *Anal Biochem.* **1993**, *214*, 17-24.

Veros, C.T., Oldham, N.J., *Rapid Commun Mass Spectrom.* **2007**, *21*, 3505-3510.

Wang, W., et al., *Anal Chem.* **2003**, *75*, 4945-4955.

Wang, W., et al., *Anal Chem.* **2005**, *77*, 3060-3071.

Wang, W., et al., *Methods in enzymology.* **2003**, *362*, 376-397.

Wang, W., Kitova, E.N., Klassen, J.S., *Anal Chem.* **2005**, *77*, 3060-3071.

Wilcox, J.M., Rempel, D.L., Gross, M.L., *Anal Chem.* **2008**, *80*, 2365-2371.

Wilm, M., Mann, M., *Anal Chem.* **1996**, *68*, 1-8.

Wishart, D., *Curr Pharm Biotechno.* **2005**, *6*, 105-120.

Wu, X., Oleschuk, R.D., Cann, N.M., *Analyst.* **2012**, *137*, 4150-4161.

Xie, Y., et al., *J Am Chem Soc.* **2006**, *128*, 14432-14433.

Yanes, O., et al., *Mol Cell Proteomics.* **2005**, *4*, 1602-1613.

Yanes, O., et al., *Nat Protoc.* **2007**, *2*, 119-130.

- Yang, P., et al., *Anal Chem.* **2005**, *77*, 6174-6183.
- Yao, Y., et al., *J Am Soc Mass Spectrom.* **2015**, *26*, 98-106.
- Yin, S., Loo, J.A., *Int J Mass Spectrom.* **2011**, *300*, 118-122.
- Yin, S., Loo, J.A., *J Am Soc Mass Spectrom.* **2010**, *21*, 899-907.
- Yue, X., Vahidi, S., Konermann, L., *J Am Soc Mass Spectrom.* **2014**, *25*, 1322-1331.
- Zdanov, A., et al., *Proc Natl Acad Sci U S A.* **1994**, *91*, 6423-6427.
- Zech, S.G., et al., *J Am Chem Soc.* **2004**, *126*, 13948-13953.
- Zenaidee, M.A., Donald, W.A., *Analyst.* **2015**, *140*, 1894-1905.
- Zhang, H., et al., *Anal Chem.* **2015**, *87*, 7433-7438.
- Zhao, Y.Y., et al., *Cancer Sci.* **2008**, *99*, 1304-1310.
- Zivolic, F., et al., *J Mass Spectrom.* **2010**, *45*, 411-420.